Andreas Öchsner

Elements of Classical Plasticity Theory

Springer

Elements of Classical Plasticity Theory

Andreas Öchsner

Elements of Classical Plasticity Theory

Springer

Andreas Öchsner
Faculty of Mechanical and Systems
Engineering
Esslingen University of Applied Sciences
Esslingen am Neckar
Baden-Württemberg, Germany

ISBN 978-3-031-14200-0 ISBN 978-3-031-14201-7 (eBook)
https://doi.org/10.1007/978-3-031-14201-7

This Springer imprint is published by the registered company Springer Nature Switzerland AG
The registered company address is: Gewerbestrasse 11, 6330 Cham, Switzerland

Preface

This monograph provides a compact introduction into the classical, i.e., rate-independent, plasticity theory. Starting from the engineering stress–strain diagram, the concept of elastic and elasto-plastic material behavior is introduced, as well as the concept of uniaxial and multiaxial stress states. Continuum mechanical modeling in the elasto-plastic range requires, in regard to the constitutive equation, in addition to the elastic law (e.g., Hooke's law), a yield condition, a flow rule and a hardening rule. These basic equations are thoroughly introduced and explained for one-dimensional stress states. Considering three-dimensional plasticity, different sets of stress invariants to characterize the stress matrix and the decomposition of the stress matrix in its hydrostatic and deviatoric part are introduced. Furthermore, the concept of the yield condition, flow rule and hardening rule is generalized for multiaxial stress states. Some typical yield conditions are introduced, and their graphical representation in different stress spaces is discussed in detail. The book concludes with an introduction in the elasto-plastic finite element simulation of mechanical structures. In the context of numerical approximation methods, the so-called predictor–corrector methods are used to integrate the constitutive equations. This is again introduced in detail based on one-dimensional stress states and afterward generalized to the three-dimensional case.

Esslingen, Germany
June 2022

Andreas Öchsner

Contents

Symbols and Abbreviations

Latin Symbols (Capital Letters)

A	Area
$\boldsymbol{C}$	Elasticity matrix
D^{pl}	Generalized plastic modulus
$\boldsymbol{D}$	Compliance matrix
E	Modulus of elasticity
$\tilde{E}$	Modulus
E^{elpl}	Elastic–plastic modulus
E^{pl}	Plastic modulus (isotropic hardening)
F	Force, Yield condition
G	Shear modulus
H	Kinematic hardening modulus
I	Principal invariant, Second moment of area
I°	Principal invariant of hydrostatic stress matrix
I'	Principal invariant of deviatoric stress matrix
$\mathbf{I}$	Identity matrix (diagonal matrix), $\mathbf{I} = \lceil 1\,1\,1\ldots\rfloor$
J	Basic invariant
J°	Basic invariant of hydrostatic stress matrix
J'	Basic invariant of deviatoric stress matrix
K	Bulk modulus
$\boldsymbol{K}$	Stiffness matrix
L	Length
$\mathbf{L}$	Scaling matrix (diagonal matrix), $\mathbf{L} = \lceil 1\,1\,1\,2\,2\,2\rfloor$
$\boldsymbol{M}$	Mass matrix
$\mathbf{O}$	Zero matrix (diagonal matrix), $\mathbf{O} = \lceil 0\,0\,0\,0\,0\,0\rfloor$
Q	Plastic potential function (plastic potential)

R	Radius of curvature, Stress ratio
T_{mt}	Melting temperature

Latin Symbols (Small Letters)

a	Factor (kinematic hardening)
d	Diameter
f	Stress fraction
$\boldsymbol{f}$	Column matrix of external forces
h	Evolution function of hardening parameter
$\boldsymbol{h}$	Evolution function matrix of hardening parameters
j	Cycle index
k	Yield stress
k_{c}	Compressive yield stress
k_{s}	Shear yield stress
k_{t}	Tensile yield stress
$k_{\mathrm{c}}^{\mathrm{init}}$	Initial compressive yield stress
$k_{\mathrm{t}}^{\mathrm{init}}$	Initial tensile yield stress
$\boldsymbol{m}$	Vector function
$\tilde{m}$	Element of the Jacobian matrix
n	Increment number
p	Pressure
q	Internal variable (hardening)
$\boldsymbol{q}$	Column matrix of hardening variables
r	Plastic flow direction, Radius, Residual
$\boldsymbol{r}$	Matrix of plastic flow direction, Residuum matrix
s_{ij}	Deviatoric stress matrix
$\boldsymbol{s}$	Deviatoric stress matrix
t	Time
u	Displacement
$\boldsymbol{u}$	Column matrix of displacements
$\boldsymbol{v}$	Argument matrix
w	Volume-specific work
w^{pl}	Volume-specific plastic work
w^{s}	Volume-specific distortional deformation energy
x	Cartesian coordinate
$\boldsymbol{x}$	Column matrix of arguments

y Cartesian coordinate
z Cartesian coordinate

Greek Symbols (Capital Letters)

$\boldsymbol{\Phi}$ Modal matrix

Greek Symbols (Small Letters)

α Back stress/kinematic hardening parameter, Factor
$\boldsymbol{\alpha}$ Column matrix of kinematic hardening parameter
γ Shear strain (engineering definition)
ε Normal strain
$\varepsilon^{\mathrm{el}}$ Elastic strain
$\varepsilon^{\mathrm{pl}}$ Plastic strain
$\varepsilon^{\mathrm{pl}}_{\mathrm{eff}}$ Effective plastic strain
$\varepsilon^{\mathrm{f}}_{\mathrm{t}}$ Tensile strain at fracture
$\varepsilon^{\mathrm{init}}_{\mathrm{t}}$ Initial tensile yield strain
$\varepsilon_{\mathrm{tr}}$ True strain
$\varepsilon^{\mathrm{el}}_{\mathrm{tr}}$ True elastic strain
$\varepsilon^{\mathrm{pl}}_{\mathrm{tr}}$ True plastic strain
ε_{ij} Strain matrix
$\boldsymbol{\varepsilon}$ Strain matrix
η Parameter
θ Lode angle
κ Isotropic hardening parameter
λ Lamé's constant, Consistency parameter
μ Lamé's constant, Proportionality factor (kinematic hardening)
ν Poisson's ratio
ξ Haigh–Westergaard coordinate
π Volume-specific energy
$\bar{\pi}$ Volume-specific complementary energy
ρ Haigh–Westergaard coordinate
σ Normal stress
σ_{a} Stress amplitude
σ_{eff} Effective stress
σ_{m} Hydrostatic stress

$\sigma_{\mathrm{t}}^{\mathrm{f}}$	Tensile fracture stress
$\sigma_{\mathrm{t}}^{\max}$	Ultimate tensile strength
σ_{tr}	True stress
σ_{ij}	Stress matrix
σ_{ij}°	Hydrostatic stress matrix
$\boldsymbol{\sigma}$	Stress matrix
τ	Shear stress
ω	Eigenfrequency

Mathematical Symbols

$\det(\dots)$	Determinant
$[\dots]^{\mathrm{T}}$	Transpose
$\lvert\dots\rvert$	Absolute value
$\otimes$	Dyadic product of two column matrices, $\boldsymbol{a} \otimes \boldsymbol{b} = \boldsymbol{a}\boldsymbol{b}^{\mathrm{T}}$
$\mathcal{L}(\dots)$	Lagrange function
$\mathrm{sgn}(\dots)$	Signum (sign) function
$\partial \dots$	Partial derivative symbol (rounded d)
IR	Set of real numbers
$\Delta \dots$	Change in a variable

Special Matrices

1	Unit column matrix, $\mathbf{1} = \{1\,1\,1\,0\,0\,0\}^{\mathrm{T}}$
I	Identity matrix (diagonal matrix), $\mathbf{I} = \lceil 1\,1\,1\,1\,1\,1 \rfloor$
L	Scaling matrix (diagonal matrix), $\mathbf{L} = \lceil 1\,1\,1\,2\,2\,2 \rfloor$
O	Zero matrix (diagonal matrix), $\mathbf{O} = \lceil 0\,0\,0\,0\,0\,0 \rfloor$

Indices, Superscripted

$\dots^{\mathrm{el}}$	Elastic
$\dots^{\mathrm{init}}$	Init
$\dots^{\mathrm{pl}}$	Plastic
$\dots^{\mathrm{trial}}$	Trial state (return mapping)
$\dots^{\mathrm{upper}}$	Upper bound

Indices, Subscripted

$\ldots_0$	Initial
$\ldots_{\text{eff}}$	Effective
$\ldots_{\max}$	Maximum
$\ldots_{\min}$	Minimum

Abbreviations

BEM	Boundary element method
CPP	Closest point projection
FDM	Finite difference method
FVM	Finite volume method
PAT	Principal axis transformation

Chapter 1
Introduction

Abstract The first chapter introduces the concept of elasto-plastic material behavior based on the uniaxial stress-strain diagram. A universal testing machine is commonly used to perform the fundamental tensile test based on round or flat specimens. Based on the recorded force and displacement or strain signals, the classical stress-strain diagram can be plotted. This diagram allows to introduce the concept of elastic or elasto-plastic material behavior, as well as the uniaxial and multiaxial stress states. In addition, the concept of engineering or true quantities is explained. The chapter closes with a general systematic on how to model structural elements in the context of classical continuum mechanics.

1.1 Uniaxial Tensile Testing

Let us consider in the following a uniaxial tensile test whose idealized specimen is schematically shown in Fig. 1.1. The original dimensions of the specimens are characterized by the initial cross-sectional area A_0 and length L_0. This specimen is now elongated in a universal testing machine and its length increases to $L_0 + \Delta L$. In the case of a specimen made of a classical engineering material, the cross-sectional area reduces to $A = A_0 - \Delta A$. This phenomenon can be described based on Poissson's ratio. Thus, we have a uniaxial stress state, i.e. just the stress component in the loading direction, and a multiaxial strain state due to the specimen's contraction.

During the tensile test, the force F is normally recorded by a load cell attached to the movable or fixed cross-head of the machine. If this force is divided by the *initial* cross-sectional area A_0, the engineering stress is obtained as:

$$\sigma = \frac{F}{A_0}. \tag{1.1}$$

The deformation or elongation of the specimen can be measured, for example, by an external extensometer (see Fig. 1.2 for an application example) which should be directly attached to the specimen. These devices are either realized based on strain

A. Öchsner, *Elements of Classical Plasticity Theory*,
https://doi.org/10.1007/978-3-031-14201-7_1

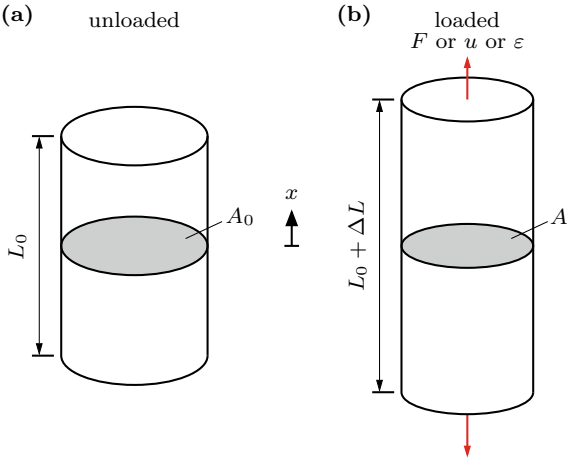

Fig. 1.1 Schematic representation of a round tensile specimen: **a** unloaded initial state and **b** deformed shape. The deformation is controlled either by a force F, a displacement u, or a strain ε (the grip ends and the corresponding geometrical modifications are not shown for simplicity)

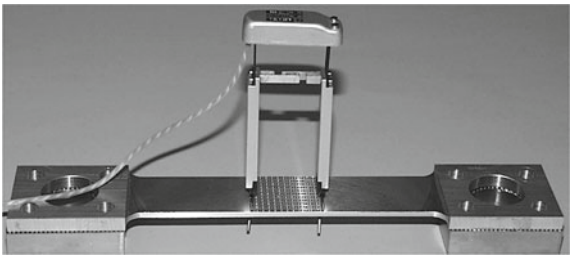

Fig. 1.2 Flat tensile specimen with extensometer (SANDNER Messtechnik GmbH, Germany) [1]

gauges or inductive extensometers.[1] Any measurements based on the movement of the machine's cross-head must be avoided since they do not guarantee an accurate determination of the specimen's behavior. The definition of strain is given in its simplest form as elongation over initial length and the engineering strain can be calculated as:

$$\varepsilon = \frac{\Delta L}{L_0}. \tag{1.2}$$

The value of ε is often provided in % or ‰ to avoid very small numbers.

One can distinguish for metallic materials two different types of stress-strain curves, see Fig. 1.3. In the case of a ductile material (see Fig. 1.3a), a distinct non-linear course can be observed after the initial linear, i.e. elastic, range. Contrary to this, a brittle behavior practically ends after the initial elastic course, see Fig. 1.3b. Common theories to describe such a behavior in the plastic range are summarized in Table 1.1. The following introduction into plastic material behavior will focus on the ductile behavior since it is much easier for this type of material to predict the failure (e.g. plasticity or fracture).

[1] More modern devises are contactless laser or video based extensometers.

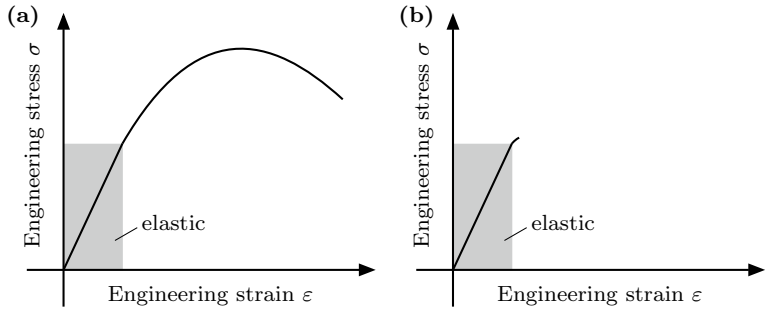

Fig. 1.3 Schematic representations of typical engineering stress-strain diagrams for metals: **a** ductile and **b** brittle behavior

Table 1.1 Summary of some typical plastic yield or failure criteria for classical metals

Ductile	Brittle
Maximum shear stress theory (Tresca theory), see Sect. 3.3.2	Maximum principal stress theory (Rankine theory)
Maximum shear shear strain theory (von Mises theory), see Sect. 3.3.1	

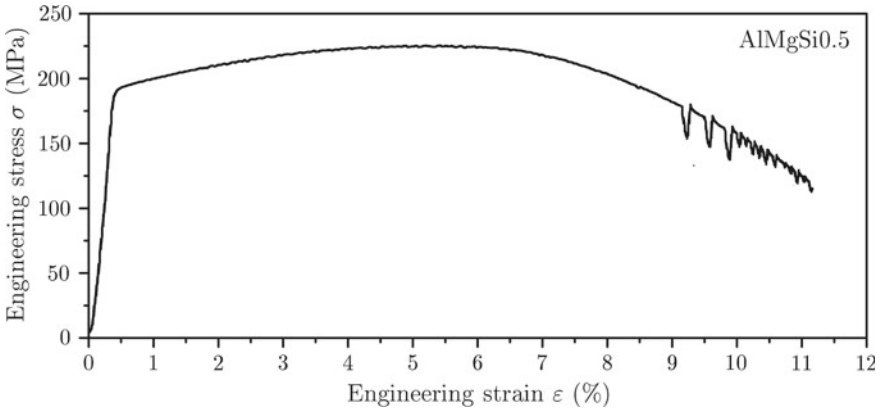

Fig. 1.4 Typical engineering stress-strain diagram of a ductile aluminium alloy (AlMgSi0.5). Adapted from [2]

A typical engineering stress-strain diagram of a ductile aluminium alloy is shown in Fig. 1.4. Such a diagram for a ductile alloy is characterized by its distinct elasto-plastic region.

A closer look on the engineering stress-strain diagram allows to identify different regions, see Fig. 1.5.

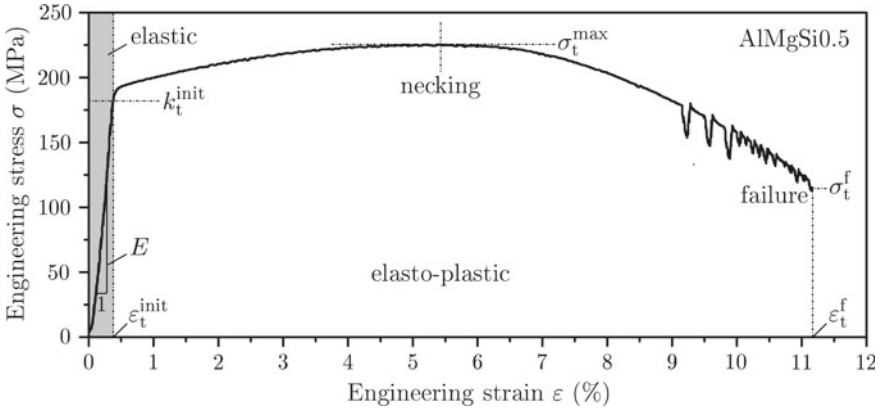

Fig. 1.5 Typical engineering stress-strain diagram of a ductile aluminium alloy (AlMgSi0.5). Several characteristic material parameters and regions are indicated. Adapted from [2]

This diagram allows to extract several characteristic material parameters such as:

- Young's modulus E,
- initial tensile yield stress k_t^{init},
- ultimate tensile strength σ_t^{max},
- tensile fracture stress σ_t^f,
- initial tensile yield strain ε_t^{init},
- tensile strain at fracture ε_t^f.

Looking at the microstructure of a material and its evolution during the tensile test (see Fig. 1.6), different stages can be distinguished. The evaluation of micrographs of a ductile aluminium alloy (AlMgSi0.5) obtained from a scanning electron microscope (SEM) shows that the ductile damage occurs simultaneously with plastic deformation larger than a certain threshold. In the initial state or at deformations before necking, a classical micrograph is obtained which shows the matrix and precipitates as smaller light regions, see Fig. 1.6a. At larger strains after necking, it can be observed that the usually brittle precipitates can break or separate from the matrix, both resulting in the formation of pores. These voids join together under tensile load and grow, see Fig. 1.6b. This mechanism leads to microcracking and subsequently to the formation of a macro-crack which ultimately results in the failure of the material, see Fig. 1.6c.

Let us have a look on the different theories that occur in literature (see Fig. 1.7). Classical continuum mechanics which treats a material continuously distributed and filling the entire space it occupies. The material is considered homogeneous without—at the considered length scale—any microstructure, defects, pores, etc. Continuum damage mechanics considers the effect of pores, voids and microcracks on the mechanical properties but still considers the material as homogeneous. Fracture mechanics considers discontinuities in the material in the form of cracks and their influence on the mechanical properties and final failure.

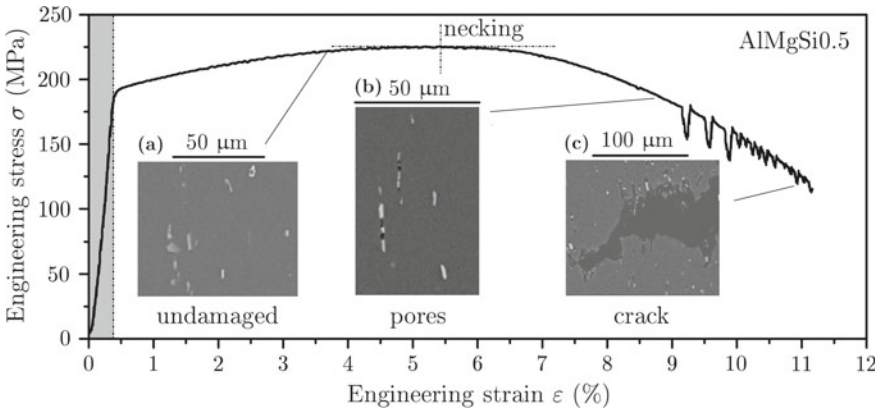

Fig. 1.6 Typical engineering stress-strain diagram of a ductile aluminium alloy and corresponding SEM micrographs: **a** region of uniform deformation showing precipitates, **b** after necking with formation of pores near the precipitates, **c** close to fracture with internal crack. Adapted from [2]

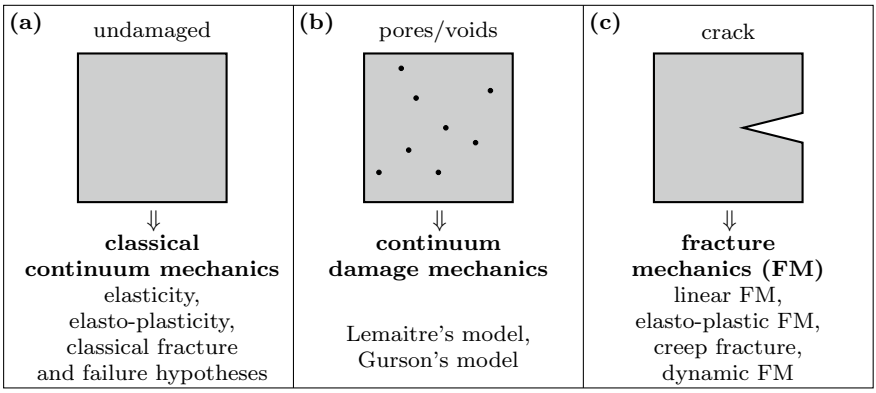

Fig. 1.7 Differentiation of the various theories in continuum mechanics: **a** classical continuum mechanics, **b** continuum damage mechanics, and **c** fracture mechanics

Let us look again on the engineering stress-strain diagram of a ductile aluminum alloy as shown in Fig. 1.8. Before necking, the stress state is uniaxial and from a practical point of view, damage effects can be disregarded. Only after necking, a three-dimensional stress state is acting (see Fig. 1.9).

After the necking phenomenon (see Fig. 1.10), the stress state in the grey shaded region is multiaxial (see also Fig. 1.9b). For a first approximation, it can be assumed that there are no voids, pores (damage) or microcracks (fracture) in the material present.

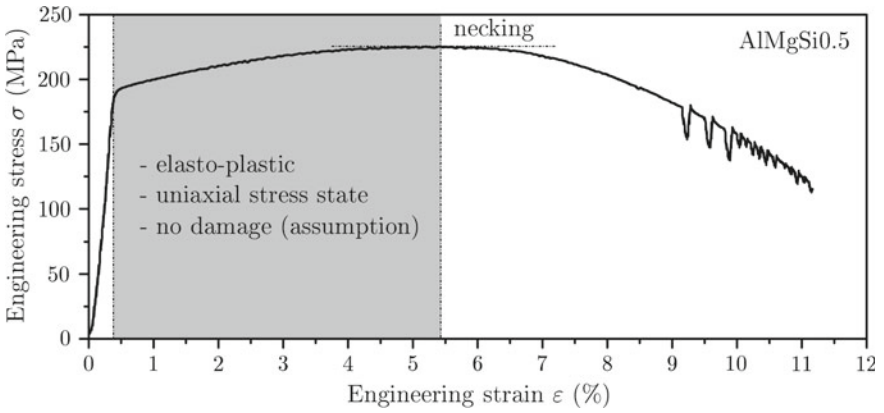

Fig. 1.8 Engineering stress-strain diagram highlighting the region of uniaxial stress during the elasto-plastic deformation

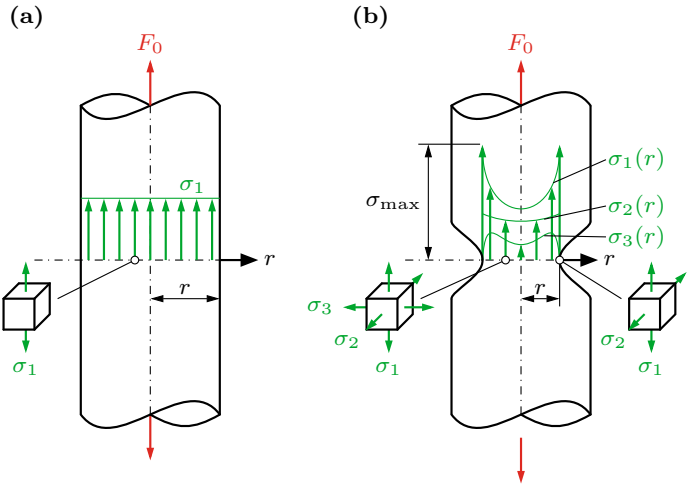

Fig. 1.9 Stress distribution in a round tensile specimen: **a** before and **b** after necking

In the case of larger deformations and strains, particularly after necking point, it is common to calculate the so-called true stress, i.e.

$$\sigma_{\mathrm{tr}} = \frac{F}{A}, \tag{1.3}$$

where the force F is divided by the actual cross-sectional area A. The so-called true strain is the natural logarithm of the actual length $L_0 + \Delta L$ over the initial length L_0:

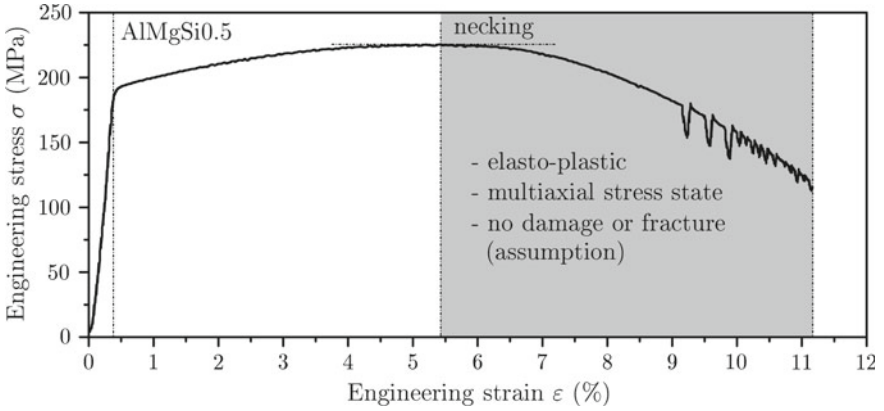

Fig. 1.10 Engineering stress-strain diagram highlighting the region of multiaxial stress during the elasto-plastic deformation

$$\varepsilon_{\mathrm{tr}} = \ln\left(\frac{L_0 + \Delta L}{L_0}\right) = \ln(1+\varepsilon). \tag{1.4}$$

The true plastic strain is obtained by subtracting the elastic strain part from the total value as follows:

$$\varepsilon_{\mathrm{tr}}^{\mathrm{pl}} = \ln(1+\varepsilon) - \varepsilon_{\mathrm{tr}}^{\mathrm{el}} = \ln(1+\varepsilon) - \frac{\sigma_{\mathrm{tr}}}{E}. \tag{1.5}$$

Let us have here a closer look on the stress state in the specimen after necking, see Fig. 1.9b. Three stress components are acting and the sole calculation of the uniaxial true stress does not sufficiently characterize the stress state.

An approximation to convert this multiaxial stress state ($\sigma_1, \sigma_2, \sigma_3$) in an effective or equivalent stress σ_{eff} (scalar value) was proposed by Bridgman [3, 4] and is based on a correction of the uniaxial true stress σ_{tr} due to the actual geometry of the neck region, i.e. the radius of curvature R and the diameter d (see Fig. 1.11b):

$$\sigma_{\mathrm{eff}} = \frac{\sigma_{\mathrm{tr}}}{\left(1 + \frac{4R}{d}\right) \times \ln\left(1 + \frac{d}{4R}\right)}. \tag{1.6}$$

It should be noted here that the actual geometry (radius of curvature R and the diameter d) can be obtained from image analyses as indicated in Fig. 1.11.

Not only the stress state is multiaxial after necking but also the strain state. After necking, the flow curve is given in engineering practice[2] as $\sigma_{\mathrm{eff}} = \sigma_{\mathrm{eff}}(\varepsilon_{\mathrm{eff}}^{\mathrm{pl}})$, i.e. as a function of the equivalent plastic strain. Neglecting the elastic strain and assuming that the volume remains constant, the following approximation of the true plastic strain can be derived [5]:

[2] This formulation would be expected in a finite element code.

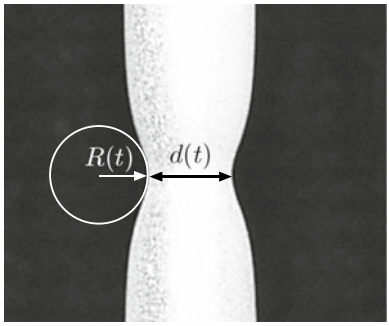

Fig. 1.11 Optical determination of minimum cross section d and radius of curvature R in the necking region. Adapted from [2]

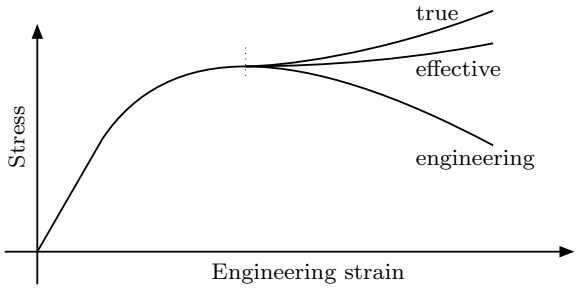

Fig. 1.12 Schematic difference between engineering, true, and effective stress

$$\varepsilon_{\mathrm{tr}}^{\mathrm{pl}} = 2 \times \ln\left(\frac{d_0}{d}\right), \tag{1.7}$$

where d is the actual (see Fig. 1.11) and d_0 the initial diameter of the round tensile sample. Equation (1.7) can be easily derived from Eq. (1.4), i.e. $\varepsilon_{\mathrm{tr}} = \ln(1+\varepsilon)$. Assuming that the elastic strain can be disregarded, one obtains that $\varepsilon_{\mathrm{tr}}^{\mathrm{pl}} \approx \varepsilon_{\mathrm{tr}}$. Under the additional assumption that the material is incompressible (i.e. no volume change: $A_0 L_0 = AL \;\Leftrightarrow\; \frac{L}{L_0} = \frac{A_0}{A}$), one can write that:

$$\varepsilon_{\mathrm{tr}}^{\mathrm{pl}} = \ln\left(1 + \frac{\Delta L}{L_0}\right) = \ln\left(\frac{L}{L_0}\right) = \ln\left(\frac{A_0}{A}\right) = \ln\left(\frac{\frac{\pi}{4}d_0^2}{\frac{\pi}{4}d^2}\right) = \ln\left(\frac{d_0}{d}\right)^2. \tag{1.8}$$

It should be noted here that this true plastic strain is often equated to the equivalent plastic strain in engineering practice: $\varepsilon_{\mathrm{tr}}^{\mathrm{pl}} \approx \varepsilon_{\mathrm{eff}}^{\mathrm{pl}}$.

The difference between the engineering stress, the true stress, and the effective stress is schematically shown in Fig. 1.12. It can be seen that a significant difference occurs after the necking point, i.e the true stress and the effective stress is monotonically increasing whereas the engineering stress is decreasing.

1.2 Continuum Mechanical Modelling

A common approach to model structural members (e.g. bars, beams or plates) in the context of continuum mechanics is provided in Fig. 1.13, see [6] for further details.

A combination of the kinematics equation (i.e., the relation between the strains and deformations) with the constitutive equation (i.e., the relation between the stresses and strains) and the equilibrium equation (i.e., the equilibrium between the internal reactions and the external loads) results in a partial differential equation, or a corresponding system of differential equations. Limited to simple problems and configurations, *analytical* solutions are possible. These analytical solutions are then exact in the frame of the assumptions made. However, the solution of complex problems requires the application of numerical methods such as the finite element method (FEM), see [7, 8]. Other classical approximation methods are the finite difference method (FDM), the finite volume method (FVM), and the boundary element method (BEM).

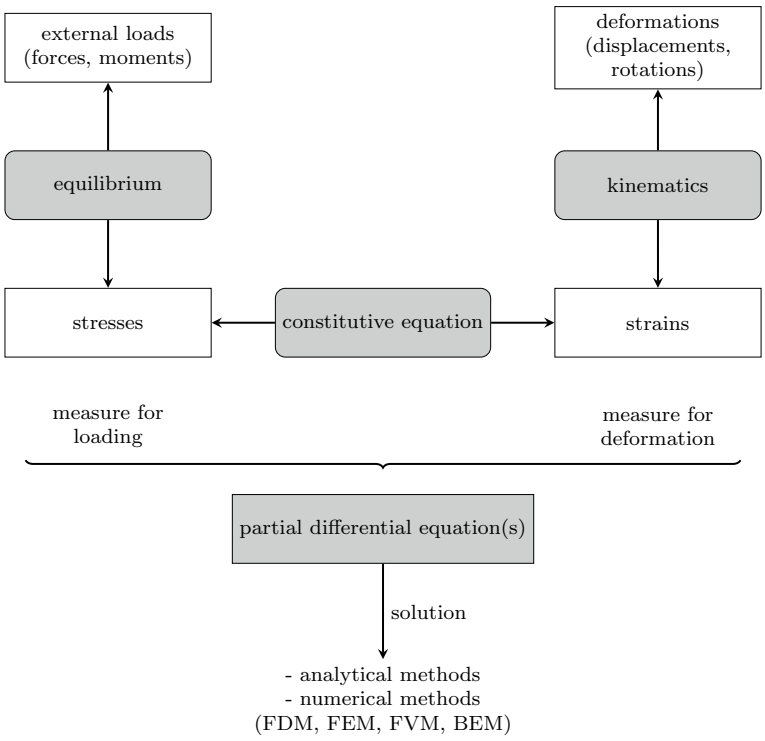

Fig. 1.13 Continuum mechanical modeling of structural members

Let us look at the end of this section on the constitutive equation in the elastic range. For most of the engineering materials, a straight line is observed in the stress-strain diagram (see Fig. 1.5) and its slope is equal to Young's modulus:

$$E = \frac{\mathrm{d}\sigma_x}{\mathrm{d}\varepsilon_x} = \frac{\Delta\sigma_x}{\Delta\varepsilon_x}. \tag{1.9}$$

If the specimen is elongated, the cross-sectional area of all classical engineering materials is reduced and the transversal strain is defined based on the original diameter d_0 as:

$$\varepsilon_y = \frac{\Delta d}{d_0}. \tag{1.10}$$

Relating the transversal to the longitudinal strain defines Poisson's ratio:

$$\nu = -\frac{\varepsilon_y}{\varepsilon_x}. \tag{1.11}$$

The generalized Hooke's law for a linear-elastic isotropic material based on the Young's modulus E and Poisson's ratio ν can be written for a constant temperature with all six stress and strain components as

$$\begin{bmatrix} \sigma_x \\ \sigma_y \\ \sigma_z \\ \sigma_{xy} \\ \sigma_{yz} \\ \sigma_{xz} \end{bmatrix} = \frac{E}{(1+\nu)(1-2\nu)} \begin{bmatrix} 1-\nu & \nu & \nu & 0 & 0 & 0 \\ \nu & 1-\nu & \nu & 0 & 0 & 0 \\ \nu & \nu & 1-\nu & 0 & 0 & 0 \\ 0 & 0 & 0 & \frac{1-2\nu}{2} & 0 & 0 \\ 0 & 0 & 0 & 0 & \frac{1-2\nu}{2} & 0 \\ 0 & 0 & 0 & 0 & 0 & \frac{1-2\nu}{2} \end{bmatrix} \begin{bmatrix} \varepsilon_x \\ \varepsilon_y \\ \varepsilon_z \\ 2\,\varepsilon_{xy} \\ 2\,\varepsilon_{yz} \\ 2\,\varepsilon_{xz} \end{bmatrix}, \tag{1.12}$$

or in matrix notation as

$$\boldsymbol{\sigma} = \boldsymbol{C}\boldsymbol{\epsilon}, \tag{1.13}$$

where $\boldsymbol{C}$ is the so-called elasticity matrix. It should be noted here that the engineering shear strain $\gamma_{ij} = 2\varepsilon_{ij}$ (for $i \neq j$) is used in the formulation of Eq. (1.12). Rearranging the elastic stiffness form given in Eq. (1.12) for the strains gives the elastic compliance form

$$\begin{bmatrix} \varepsilon_x \\ \varepsilon_y \\ \varepsilon_z \\ 2\,\varepsilon_{xy} \\ 2\,\varepsilon_{yz} \\ 2\,\varepsilon_{xz} \end{bmatrix} = \frac{1}{E} \begin{bmatrix} 1 & -\nu & -\nu & 0 & 0 & 0 \\ -\nu & 1 & -\nu & 0 & 0 & 0 \\ -\nu & -\nu & 1 & 0 & 0 & 0 \\ 0 & 0 & 0 & 2(1+\nu) & 0 & 0 \\ 0 & 0 & 0 & 0 & 2(1+\nu) & 0 \\ 0 & 0 & 0 & 0 & 0 & 2(1+\nu) \end{bmatrix} \begin{bmatrix} \sigma_x \\ \sigma_y \\ \sigma_z \\ \sigma_{xy} \\ \sigma_{yz} \\ \sigma_{xz} \end{bmatrix}, \tag{1.14}$$

Table 1.2 Conversion of elastic constants: λ, μ: Lamé's constants; K: bulk modulus; G: shear modulus; E: Young's modulus; ν: Poisson's ratio [9]

	λ, μ	E, ν	μ, ν	E, μ	K, ν	G, ν	K, G
λ	λ	$\frac{\nu E}{(1+\nu)(1-2\nu)}$	$\frac{2\mu\nu}{1-2\nu}$	$\frac{\mu(E-2\mu)}{3\mu-E}$	$\frac{3K\nu}{1+\nu}$	$\frac{2G\nu}{1-2\nu}$	$K-\frac{2G}{3}$
μ	μ	$\frac{E}{2(1+\nu)}$	μ	μ	$\frac{3K(1-2\nu)}{2(1+\nu)}$	μ	μ
K	$\lambda+\frac{2}{3}\mu$	$\frac{E}{3(1-2\nu)}$	$\frac{2\mu(1+\nu)}{3(1-2\nu)}$	$\frac{\mu E}{3(3\mu-E)}$	K	$\frac{2G(1+\nu)}{3(1-2\nu)}$	K
E	$\frac{\mu(3\lambda+2\mu)}{\lambda+\mu}$	E	$2\mu(1+\nu)$	E	$3K(1-2\nu)$	$2G(1+\nu)$	$\frac{9KG}{3K+G}$
ν	$\frac{\lambda}{2(\lambda+\mu)}$	ν	ν	$\frac{E}{2\mu}-1$	ν	ν	$\frac{3K-2G}{2(3K+G)}$
G	μ	$\frac{E}{2(1+\nu)}$	μ	G	$\frac{3K(1-2\nu)}{2(1+\nu)}$	G	G

or in matrix notation as

$$\boldsymbol{\epsilon} = \boldsymbol{D}\boldsymbol{\sigma}\,, \tag{1.15}$$

where $\boldsymbol{D} = \boldsymbol{C}^{-1}$ is the so-called elastic compliance matrix. The general characteristic of Hooke's law in the form of Eqs. (1.13) and (1.15) is that two independent material parameters are used. In addition to Young's modulus E and Poisson's ratio ν, other elastic parameters can be used to form the set of two independent material parameters and the following Table 1.2 summarizes the conversion between the common material parameters.

References

1. Öchsner A (2003) Experimentelle und numerische Untersuchung des elastoplastischen verhaltens zellularer modellwerkstoffe. VDI-Verlag, Düsseldorf
2. Öchsner A, Gegner J, Winter W, Kuhn G (2001) Experimental and numerical investigations of ductile damage in aluminium alloys. Mat Sci Eng A-Struct 318:328–333
3. Bridgman PW (1952) Studies in large plastic flow and fracture. McGraw Hill, New York
4. Gromada M, Mishuris G, Öchsner A (2011) Correction formulae for the stress distribution in round tensile specimens at neck presence. Springer, Heidelberg
5. Davis JR (2004) Tensile testing. ASM International, Ohio
6. Altenbach H, Öchsner A (eds) (2020) Encyclopedia of continuum mechanics. Springer, Berlin
7. Öchsner A, Öchsner M (2018) A first introduction to the finite element analysis program MSC Marc/Mentat. Springer, Cham

8. Öchsner A (2020) Computational statics and dynamics: an introduction based on the finite element method. Springer, Singapore
9. Chen WF, Saleeb AF (1982) Constitutive equations for engineering materials. Vol. 1: Elasticity and modelling. Wiley, New York

Chapter 2
Theory of One-Dimensional Plasticity

Abstract This chapter introduces the theory of one-dimensional plasticity. This concept can easily be illustrated based on the engineering stress-strain diagram. The fundamental concept of the yield condition, flow rule and hardening rule is introduced. These three equations are required in addition to, for example, Hooke's law to complement the entire constitutive law. For hardening, the concepts of isotropic, kinematic and combined hardening are treated. The chapter concludes with some remarks on the elasto-plastic modulus and changing loading directions, i.e. unloading, reversed and cyclic loading.

2.1 Initial Remarks

Let us look again on the engineering stress-strain diagram of a ductile aluminum alloy as shown in Fig. 1.8. Before necking, the stress state is uniaxial and from a practical point of view, damage effects can be disregarded. Only after necking, a three-dimensional stress state is acting (see Fig. 1.9b), which is covered in Chap. 3.

The characteristic feature of plastic material behavior is that a remaining strain $\varepsilon^{\mathrm{pl}}$ occurs after complete unloading, see Fig. 2.1a. Only the elastic strains $\varepsilon^{\mathrm{el}}$ returns to zero at complete unloading. An additive composition of the strains by their elastic and plastic parts [1]

$$\varepsilon = \varepsilon^{\mathrm{el}} + \varepsilon^{\mathrm{pl}} \tag{2.1}$$

is permitted when restricted to small strains. The elastic strains $\varepsilon^{\mathrm{el}}$ can hereby be determined via Hooke's law, whereby ε in Eq. (1.9) has to be substituted by $\varepsilon^{\mathrm{el}}$.

Furthermore, no explicit correlation is given anymore for plastic material behavior in general between stress and strain, since the strain state is also dependent on the loading history. Due to this, rate equations are necessary and need to be integrated throughout the entire load history. Within the framework of the time-independent plasticity investigated here, the rate equations can be simplified to incremental relations. From Eq. (2.1) the additive composition of the strain increments results in:

A. Öchsner, *Elements of Classical Plasticity Theory*,
https://doi.org/10.1007/978-3-031-14201-7_2

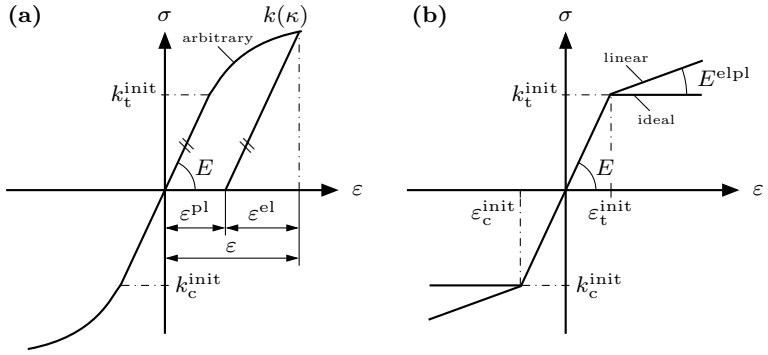

Fig. 2.1 Uniaxial engineering stress-strain diagrams for different isotropic hardening laws: **a** arbitrary hardening; **b** linear hardening and ideal plasticity

$$\Delta\varepsilon = \Delta\varepsilon^{\mathrm{el}} + \Delta\varepsilon^{\mathrm{pl}}. \tag{2.2}$$

The constitutive description of plastic material behavior includes (in addition to a relationship for the pure elastic part, e.g. Hooke's law) [2]:

- a yield condition,
- a flow rule, and
- a hardening law.

In the following, the case of the monotonic loading is considered first, so that isotropic hardening is explained first in the case of material hardening. This important case, for example, occurs in experimental mechanics at the uniaxial tensile test with monotonic loading. Furthermore, it is assumed that the yield stress is identical in the tensile and compressive regime: $k_{\mathrm{t}} = k_{\mathrm{c}} = k$.

2.2 Yield Condition

The yield condition enables one to determine whether the relevant material suffers only elastic or also plastic strains at a certain stress state at a point of the relevant body. In the uniaxial tensile test, plastic flow begins when reaching the initial yield stress k^{init}, see Fig. 2.1. The yield condition in its general one-dimensional form can be set as follows ($\mathbb{R} \times \mathbb{R} \to \mathbb{R}$):

$$F = F(\sigma, \kappa), \tag{2.3}$$

where κ represents the inner variable of isotropic hardening. In the case of ideal plasticity, see Fig. 2.1b, the following is valid: $F = F(\sigma)$. The values of F have the following mechanical meaning, see Fig. 2.2:

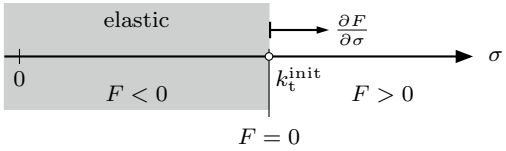

Fig. 2.2 Schematic representation of the values of the yield condition and the direction of the stress gradient in the uniaxial stress space

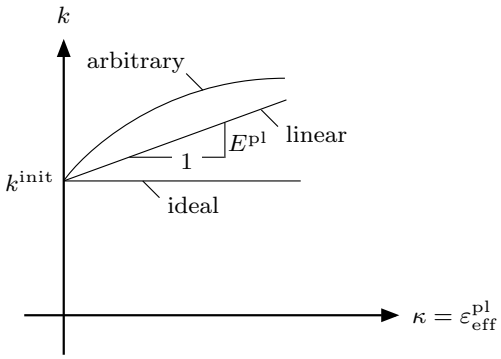

Fig. 2.3 Flow curve for different isotropic hardening laws. The abscissa is drawn for the case of strain hardening

$$F(\sigma, \kappa) < 0 \quad \rightarrow \quad \text{elastic material behavior,} \tag{2.4}$$

$$F(\sigma, \kappa) = 0 \quad \rightarrow \quad \text{plastic material behavior,} \tag{2.5}$$

$$F(\sigma, \kappa) > 0 \quad \rightarrow \quad \text{invalid.} \tag{2.6}$$

A further simplification results under the assumption that the yield condition can be split into a pure stress fraction $f(\sigma)$, the so-called yield criterion,[1] and into an experimental material parameter $k(\kappa)$, the so-called flow stress:

$$F(\sigma, \kappa) = f(\sigma) - k(\kappa). \tag{2.7}$$

For a uniaxial tensile test (see Fig. 2.1) the yield condition can be noted in the following form:

$$F(\sigma, \kappa) = \underbrace{|\sigma|}_{\sigma_{\mathrm{eff}}} - k(\kappa) \leq 0. \tag{2.8}$$

If one considers the idealized case of linear hardening (see Fig. 2.1b), Eq. (2.8) can be written as

$$F(\sigma, \kappa) = |\sigma| - (k^{\mathrm{init}} + E^{\mathrm{pl}}\kappa) \leq 0. \tag{2.9}$$

[1] If the unit of the yield criterion equals the stress, $f(\sigma)$ represents the equivalent stress or effective stress (σ_{eff}). In the general three-dimensional case the following is valid under consideration of the symmetry of the stress tensor $\sigma_{\mathrm{eff}} : (\mathbb{R}^6 \rightarrow \mathbb{R}_+)$.

The parameter E^{pl} is the plastic modulus (see Fig. 2.3), which becomes zero in the case of ideal plasticity:

$$F(\sigma, \kappa) = |\sigma| - k^{\mathrm{init}} \leq 0. \tag{2.10}$$

2.3 Flow Rule

The flow rule serves as a mathematical description of the evolution of the infinitesimal increments of the plastic strain $\mathrm{d}\varepsilon^{\mathrm{pl}}$ in the course of the load history of the body. In its most general one-dimensional form, the flow rule can be set up as follows [3]:

$$\mathrm{d}\varepsilon^{\mathrm{pl}} = \mathrm{d}\lambda\, r(\sigma, \kappa), \tag{2.11}$$

whereupon the factor $\mathrm{d}\lambda$ is described as the consistency parameter ($\mathrm{d}\lambda \geq 0$) and $r : (\mathbb{R} \times \mathbb{R} \to \mathbb{R})$ as the function of the flow direction.[2] One considers that solely for $\mathrm{d}\varepsilon^{\mathrm{pl}} = 0$ then $\mathrm{d}\lambda = 0$ results. Based on the stability postulate of Drucker [4] the following flow rule can be derived[3]:

$$\mathrm{d}\varepsilon^{\mathrm{pl}} = \mathrm{d}\lambda \frac{\partial F(\sigma, \kappa)}{\partial \sigma}. \tag{2.12}$$

Such a flow rule is referred to as the normal rule[4] (see Fig. 2.2a) or due to $r = \partial F(\sigma, \kappa)/\partial\sigma$ as the *associated* flow rule.

Experimental results, among other things from the area of granular materials [6] can however be approximated better if the stress gradient is substituted through a different function, the so-called plastic potential Q. The resulting flow rule is then referred to as the *non-associated* flow rule:

$$\mathrm{d}\varepsilon^{\mathrm{pl}} = \mathrm{d}\lambda \frac{\partial Q(\sigma, \kappa)}{\partial \sigma}. \tag{2.13}$$

In the case of quite complicated yield conditions, often it occurs that a more simple yield condition is used for Q in the first approximation, for which the gradient can easily be determined.

The application of the associated flow rule (2.12) to the yield conditions according to Eqs. (2.8)–(2.10) yields for all three types of yield conditions (meaning arbitrary hardening, linear hardening and ideal plasticity):

---

[2] In the general three-dimensional case $\boldsymbol{r}$ hereby defines the direction of the vector $\mathrm{d}\boldsymbol{\varepsilon}^{\mathrm{pl}}$, while the scalar factor defines the absolute value.

[3] A formal alternative derivation of the associated flow rule can occur via the Lagrange multiplier method as extreme value with side-conditions from the principle of maximum plastic work [5].

[4] In the general three-dimensional case the image vector of the plastic strain increment has to be positioned upright and outside oriented to the yield surface, see Fig. 2.2b.

$$\mathrm{d}\varepsilon^{\mathrm{pl}} = \mathrm{d}\lambda\, \mathrm{sgn}(\sigma), \tag{2.14}$$

where $\mathrm{sgn}(\sigma)$ represents the so-called sign function,[5] which can adopt the following values:

$$\mathrm{sgn}(\sigma) = \begin{cases} -1 \text{ for } \sigma < 0 \\ 0 \text{ for } \sigma = 0 \\ +1 \text{ for } \sigma > 0 \end{cases}. \tag{2.15}$$

2.4 Hardening Rule

The hardening law allows the consideration of the influence of material hardening on the yield condition and the flow rule.

2.4.1 Isotropic Hardening

In the case of isotropic hardening, the yield stress is expressed as being dependent on an inner variable κ:

$$k = k(\kappa). \tag{2.16}$$

If the equivalent plastic strain[6] is used for the hardening variable ($\kappa = |\varepsilon^{\mathrm{pl}}|$), then one talks about strain hardening.

Another possibility is to describe the hardening being dependent on the specific[7] plastic work ($\kappa = w^{\mathrm{pl}} = \int \sigma\, \mathrm{d}\varepsilon^{\mathrm{pl}}$). Then one talks about work hardening. If Eq. (3.85) is combined with the flow rule according to (2.14), the evolution equation for the isotropic hardening variable results in:

$$\mathrm{d}\kappa = \mathrm{d}|\varepsilon^{\mathrm{pl}}| = \mathrm{d}\lambda. \tag{2.17}$$

Figure 2.3 shows the flow curve, meaning the graphical illustration of the yield stress being dependent on the inner variable for different hardening approaches.

---

[5] Also signum function; from the Latin 'signum' for 'sign'.

[6] The effective plastic strain is in the general three-dimensional case the function $\varepsilon^{\mathrm{pl}}_{\mathrm{eff}} : (\mathbb{R}^6 \rightarrow \mathbb{R}_+)$. In the one-dimensional case, the following is valid: $\varepsilon^{\mathrm{pl}}_{\mathrm{eff}} = \sqrt{\varepsilon^{\mathrm{pl}}\varepsilon^{\mathrm{pl}}} = |\varepsilon^{\mathrm{pl}}|$. Attention: Finite element programs optionally use the more general definition for the illustration in the post processor, this means $\varepsilon^{\mathrm{pl}}_{\mathrm{eff}} = \sqrt{\frac{2}{3} \sum \Delta\varepsilon^{\mathrm{pl}}_{ij} \sum \Delta\varepsilon^{\mathrm{pl}}_{ij}}$, which considers the lateral contraction at uniaxial stress problems in the plastic area via the factor $\frac{2}{3}$. However in pure one-dimensional problems *without* lateral contraction, this formula leads to an illustration of the effective plastic strain, which is reduced by the factor $\sqrt{\frac{2}{3}} \approx 0.816$.

[7] This is the volume-specific definition, meaning $\left[w^{\mathrm{pl}}\right] = \frac{\mathrm{N}}{\mathrm{m}^2}\frac{\mathrm{m}}{\mathrm{m}} = \frac{\mathrm{kg\,m}}{\mathrm{s}^2\mathrm{m}^2}\frac{\mathrm{m}}{\mathrm{m}} = \frac{\mathrm{kg\,m}^2}{\mathrm{s}^2\mathrm{m}^3} = \frac{\mathrm{J}}{\mathrm{m}^3}$.

The yield condition which was expressed in Eq. (2.3) can be generalized to the formulation

$$F = F(\sigma, q) = 0, \tag{2.18}$$

where the internal variable q considers the influence of the material hardening on the yield condition. The evolution equation for this internal variable can be stated in its most general form based on Eq. (2.18) as

$$\mathrm{d}q = \mathrm{d}\lambda \times h(\sigma, q), \tag{2.19}$$

where the function h defines the evolution of the hardening parameter. Assigning for the internal variable $q = \kappa$ (in the case that κ equals the effective plastic strain, one speaks of a strain space formulation) and considering the case of associated plasticity, a more specific rule for the evolution of the internal variable is given as

$$\begin{aligned} \mathrm{d}\kappa &= -\mathrm{d}\lambda \times \left(D^{\mathrm{pl}}\right)^{-1} \frac{\partial F(\sigma, \kappa)}{\partial \kappa} = -\mathrm{d}\lambda \times \frac{\partial \kappa}{\partial k(\kappa)} \frac{\partial F(\sigma, \kappa)}{\partial \kappa} \\ &= -\mathrm{d}\lambda \times \frac{1}{E^{\mathrm{pl}}} \frac{\partial F(\sigma, \kappa)}{\partial \kappa}, \end{aligned} \tag{2.20}$$

where D^{pl} is the generalized plastic modulus. Considering the yield stress k as the internal variable, one obtains a stress space formulation as $F = F(\sigma, k)$ and the corresponding evolution equation for the internal variable is given by:

$$\mathrm{d}k = -\mathrm{d}\lambda \times D^{\mathrm{pl}} \frac{\partial F(\sigma, k)}{\partial k} = -\mathrm{d}\lambda \times E^{\mathrm{pl}} \frac{\partial F(\sigma, k)}{\partial k}, \tag{2.21}$$

where $\mathrm{d}k$ can be written as $E^{\mathrm{pl}}\mathrm{d}\kappa$. Thus, one may alternatively formulate:

$$\mathrm{d}\kappa = -\mathrm{d}\lambda \times \frac{\partial F(\sigma, k)}{\partial k}. \tag{2.22}$$

Application of the instruction for the evolution of the internal variable according to Eq. (2.20) or (2.22) to the yield condition with $k_{\mathrm{t}} = k_{\mathrm{t}}(\kappa)$ (cf. Eqs. (2.9) and (2.7)) gives:

$$\mathrm{d}\kappa = \mathrm{d}\lambda. \tag{2.23}$$

Thus, it turned out that h, i.e. the evolution equation for the hardening parameter in Eq. (2.19), is simplified to $h = 1$. However, in the case of more complex yield conditions, the function h may take a more complex form. This is the case if, for example, damage models (e.g. Lemaitre [7, 8] or Gurson [9]) are introduced.

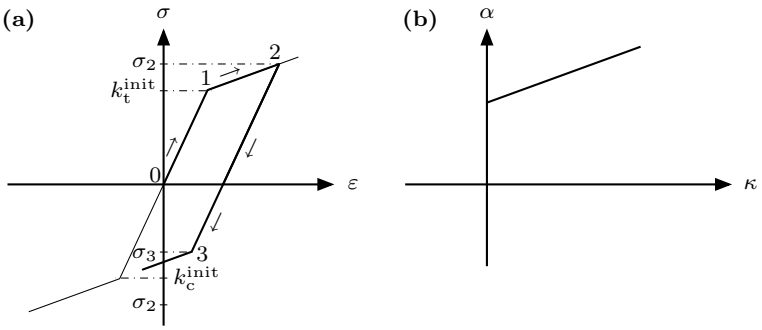

Fig. 2.4 Uniaxial kinematic hardening: **a** idealized stress-strain curve with Bauschinger effect and **b** kinematic hardening parameter as a function of the internal variable (linear hardening)

2.4.2 Kinematic Hardening

In the case of pure monotonic loading, i.e. pure tensile or pure compression, it is not possible to distinguish the cases of isotropic or kinematic hardening from the stress-strain diagram. Let us look in the following at a uniaxial test with plastic deformation and stress reversal as schematically shown in Fig. 2.4a. The test starts without any initial stress or strain in the origin of the stress-strain diagram (point '0') and a tensile load is continuously increased. The first part of the path, i.e. as long as the stress is below the yield stress k, is in the pure linear-elastic range and Hooke's law describes the stress-strain behavior. Reaching the yield stress k (point '1'), the slope of the diagram changes and plastic deformation occurs. With ongoing increasing load, the plastic deformation and the plastic strain increases in this part of the diagram. Let us assume now that the load is reversed at point '2'. The unloading is completely elastic and compressive stress develops as soon as the load path passes the strain axis. The interesting question is now when the subsequent plastic deformations starts in the compressive regime. This plastic deformation occurs now in the case of kinematic hardening at a stress level σ_3 which is lower than the initial yield stress k or the subsequent stress σ_2. This behavior is known as the Bauschinger effect [10] and requires plastic pre-straining with subsequent load reversal.

The behavior shown in Fig. 2.4a can be described based on the following yield condition

$$F = |\sigma - \alpha(\kappa)| - k = 0, \tag{2.24}$$

where the initial yield stress k is constant and the kinematic hardening parameter[8] α is a function of an internal variable κ. Figure 2.4b shows the case of linear hardening where a linear relationship between kinematic hardening parameter and internal variable is obtained.

[8] An alternative expression for the kinematic hardening parameter is back-stress.

The simplest relation between the kinematic hardening parameter and the internal variable was proposed in [11] as

$$\alpha = H\varepsilon^{\mathrm{pl}} \quad \text{or} \quad \mathrm{d}\alpha = H\mathrm{d}\varepsilon^{\mathrm{pl}}, \tag{2.25}$$

where H is a constant called the kinematic hardening modulus and the plastic strain is assigned as the internal variable. Thus, Eq. (2.25) describes the case of linear hardening. A more general formulation of Eq. (2.25) is known as Prager's hardening rule [12, 13]:

$$\mathrm{d}\alpha = H(\sigma, \kappa)\mathrm{d}\varepsilon^{\mathrm{pl}}, \tag{2.26}$$

where the kinematic hardening modulus is now a scalar function which depends on the state variables (σ, κ). One suggestion is to use the effective plastic strain $\varepsilon^{\mathrm{pl}}_{\mathrm{eff}}$ as the internal variable [14]. A further extension is proposed in [15] where the hardening modulus is formulated as a tensor.

Another formulation was proposed by Ziegler [16, 17] as

$$\mathrm{d}\alpha = \mathrm{d}\mu(\sigma - \alpha), \tag{2.27}$$

where the proportionality factor $\mathrm{d}\mu$ can be expressed as:

$$\mathrm{d}\mu = a\mathrm{d}\varepsilon^{\mathrm{pl}}, \tag{2.28}$$

or in a more general way as $a = a(\sigma, \kappa_i)$. The rule given in Eq. (2.27) is known in the literature as Ziegler's hardening rule. It should be noted here that the plastic strain increments in Eqs. (2.28) and (2.26) can be calculated based on the flow rules given in Sect. 2.3. Thus, the kinematic hardening rule can be expressed in a more general way as:

$$\mathrm{d}\alpha = \mathrm{d}\lambda h(\sigma, \alpha). \tag{2.29}$$

2.4.3 Combined Hardening

The isotropic and kinematic hardening rules presented in Sects. 3.5.1 and 3.5.2 can simply be joined together to obtain a combined hardening rule for the one-dimensional yield condition as:

$$F(\sigma, \boldsymbol{q}) = |\sigma - \alpha| - k(\kappa), \tag{2.30}$$

or for the special case of isotropic linear hardening as

$$F = |\sigma - \alpha| - (k^{\mathrm{init}} + E^{\mathrm{pl}}\varepsilon^{\mathrm{pl}}_{\mathrm{eff}}), \tag{2.31}$$

where the back-stress α can be a function as indicated in Eqs. (2.25)–(2.27). The associated flow rule is then obtained according to Eq. (2.12) as:

$$\mathrm{d}\varepsilon^{\mathrm{pl}} = \mathrm{d}\lambda \frac{\partial F}{\partial \sigma} = \mathrm{d}\lambda \, \mathrm{sgn}(\sigma - \alpha) \tag{2.32}$$

and the isotropic and kinematic hardening (Prager) laws can be written as:

$$\mathrm{d}\kappa = \mathrm{d}|\varepsilon^{\mathrm{pl}}| = |\mathrm{d}\lambda \, \mathrm{sgn}(\sigma - \alpha)| = \mathrm{d}\lambda, \tag{2.33}$$

$$\mathrm{d}\alpha = H \mathrm{d}\varepsilon^{\mathrm{pl}} = H \, \mathrm{d}\lambda \, \mathrm{sgn}(\sigma - \alpha). \tag{2.34}$$

The last two equations can be combined and generally expressed as:

$$\mathrm{d}\boldsymbol{q} = \mathrm{d}\lambda \boldsymbol{h}(\sigma, \boldsymbol{q}), \tag{2.35}$$

or

$$\begin{bmatrix} \mathrm{d}\kappa \\ \mathrm{d}\alpha \end{bmatrix} = \mathrm{d}\lambda \begin{bmatrix} 1 \\ H \, \mathrm{sgn}(\sigma - \alpha) \end{bmatrix}. \tag{2.36}$$

2.5 Elasto-plastic Modulus

The stiffness of a material changes during plastic deformation and the strain state is dependent on the loading history. Therefore, Hooke's law, which is valid for the linear-elastic material behavior according to Eq. (1.9), must be replaced by the following infinitesimal incremental relation:

$$\mathrm{d}\sigma = E^{\mathrm{elpl}} \mathrm{d}\varepsilon, \tag{2.37}$$

where E^{elpl} is the elasto-plastic modulus. The algebraic expression for this modulus can be obtained in the following manner. The total differential of a yield condition $F = F(\sigma, \boldsymbol{q})$, see Eq. (2.30), is given by:

$$\mathrm{d}F(\sigma, \boldsymbol{q}) = \left(\frac{\partial F}{\partial \sigma} \right) \mathrm{d}\sigma + \left(\frac{\partial F}{\partial \boldsymbol{q}} \right)^{\mathrm{T}} \mathrm{d}\boldsymbol{q} = 0. \tag{2.38}$$

If Hooke's law (1.9) and the flow rule (2.11) are introduced in the relation for the additive composition of the elastic and plastic strain according to Eq. (2.2), one obtains:

$$\mathrm{d}\varepsilon = \frac{1}{E} \mathrm{d}\sigma + \mathrm{d}\lambda r. \tag{2.39}$$

Multiplication of Eq. (2.39) from the left-hand side with $\left(\frac{\partial F}{\partial \sigma}\right) E$ and inserting in Eq. (2.38) gives, under the consideration of the evolution equation of the hardening variables (2.35), the consistence parameter as:

$$\mathrm{d}\lambda = \frac{\left(\frac{\partial F}{\partial \sigma}\right) E}{\left(\frac{\partial F}{\partial \sigma}\right) Er - \left(\frac{\partial F}{\partial \boldsymbol{q}}\right)^{\mathrm{T}} \boldsymbol{h}} \mathrm{d}\varepsilon. \tag{2.40}$$

This equation for the consistency parameter can be inserted into Eq. (2.39) and solving for $\frac{\mathrm{d}\sigma}{\mathrm{d}\varepsilon}$ gives the elasto-plastic modulus as:

$$E^{\mathrm{elpl}} = E - \frac{E\left(\frac{\partial F}{\partial \sigma}\right) Er}{\left(\frac{\partial F}{\partial \sigma}\right) Er - \left(\frac{\partial F}{\partial \boldsymbol{q}}\right)^{\mathrm{T}} \boldsymbol{h}}. \tag{2.41}$$

Let us consider now the case of combined linear kinematic and isotropic hardening (see Eq. (2.31)) where the kinematic hardening modulus H (Prager) and the plastic modulus E^{pl} are constant. Furthermore, the flow rule is assumed to be associated. We assume in the following that the yield condition is a function of the following internal variables: $F = F(\sigma, \boldsymbol{q}) = F(\sigma, \varepsilon^{\mathrm{pl}}, \varepsilon^{\mathrm{pl}}_{\mathrm{eff}})$. The corresponding terms in the expression for the elasto-plastic modulus are as follows:

- $$\left(\frac{\partial F}{\partial \sigma}\right) = \operatorname{sgn}\left|\sigma - H\varepsilon^{\mathrm{pl}}\right|, \tag{2.42}$$
- $$r = \frac{\partial F}{\partial \sigma} = \operatorname{sgn}\left|\sigma - H\varepsilon^{\mathrm{pl}}\right|, \tag{2.43}$$
- $$\left(\frac{\partial F}{\partial \boldsymbol{q}}\right) = \begin{bmatrix} -E^{\mathrm{pl}} \\ -\operatorname{sgn}\left(\sigma - H\varepsilon^{\mathrm{pl}}\right) H \end{bmatrix}, \tag{2.44}$$
- $$\boldsymbol{h} = \begin{bmatrix} 1 \\ \operatorname{sgn}\left(\sigma - H\varepsilon^{\mathrm{pl}}\right) \end{bmatrix}. \tag{2.45}$$

Introducing these four expressions in Eq. (2.41) finally gives:

$$E^{\mathrm{elpl}} = \frac{\mathrm{d}\sigma}{\mathrm{d}\varepsilon} = \frac{E(H + E^{\mathrm{pl}})}{E + (H + E^{\mathrm{pl}})}. \tag{2.46}$$

Table 2.1 Comparison of the different definitions of the stress-strain characteristics (moduli) in the case of the one-dimensional σ-ε space

Range	Definition	Graphical representation
Elastic	$E = \dfrac{\mathrm{d}\sigma}{\mathrm{d}\varepsilon^{\mathrm{el}}}$	Fig. 2.1
Plastic	$E^{\mathrm{elpl}} = \dfrac{\mathrm{d}\sigma}{\mathrm{d}\varepsilon}$ for $\varepsilon > \varepsilon^{\mathrm{init}}$	Fig. 2.1b
	$E^{\mathrm{pl}} = \dfrac{\mathrm{d}k}{\mathrm{d}\lvert\varepsilon^{\mathrm{pl}}\rvert}$	Fig. 2.3

A slightly different derivation is obtained by considering the yield condition depending on the following internal variables: $F = F(\sigma, \boldsymbol{q}) = F(\sigma, \alpha, \varepsilon^{\mathrm{pl}}_{\mathrm{eff}})$. Then, the following different expressions are obtained:

Table 2.2 Comparison between the 1D plasticity formulations for linear (E^{pl} and H are assumed constant) general hardening approaches

1D *Linear* hardening plasticity	1D *Arbitrary* hardening plasticity
Yield condition	
$F = (\sigma, \boldsymbol{q}) \leq 0$	
$F = \lvert\sigma - \alpha\rvert - (k^{\mathrm{init}} + E^{\mathrm{pl}}\varepsilon^{\mathrm{pl}}_{\mathrm{eff}}) \leq 0$	$F = \sigma_{\mathrm{eff}}(\sigma, \alpha) - k(\kappa)$
Flow rule	
$\mathrm{d}\varepsilon^{\mathrm{pl}} = \mathrm{d}\lambda \times r(\sigma, \boldsymbol{q})$	
$\mathrm{d}\varepsilon^{\mathrm{pl}} = \mathrm{d}\lambda \times \mathrm{sgn}(\sigma - \alpha)$	
Hardening law	
$\mathrm{d}\boldsymbol{q} = \mathrm{d}\lambda \times \boldsymbol{h}(\sigma, \boldsymbol{q})$	
$\boldsymbol{q} = [\mathrm{d}\varepsilon^{\mathrm{pl}}_{\mathrm{eff}}, \alpha]^{\mathrm{T}}$	$\boldsymbol{q} = [\kappa, \alpha]^{\mathrm{T}}$
$\mathrm{d}\varepsilon^{\mathrm{pl}}_{\mathrm{eff}} = \mathrm{d}\lambda, \mathrm{d}\alpha = \mathrm{d}\lambda H \mathrm{sgn}(\sigma - \alpha)$	
Elasto-plastic modulus	
$E^{\mathrm{elpl}} = \dfrac{E \times (H + E^{\mathrm{pl}})}{E + (H + E^{\mathrm{pl}})}$	$E^{\mathrm{elpl}} = E - \dfrac{E\left(\frac{\partial F}{\partial \sigma}\right) Er}{\left(\frac{\partial F}{\partial \sigma}\right) Er - \left(\frac{\partial F}{\partial \boldsymbol{q}}\right)^{\mathrm{T}} \boldsymbol{h}}$

$$\bullet \quad \left(\frac{\partial F}{\partial \boldsymbol{q}}\right) = \begin{bmatrix} -E^{\mathrm{pl}} \\ -\mathrm{sgn}\left(\sigma - H\varepsilon^{\mathrm{pl}}\right) \end{bmatrix}, \tag{2.47}$$

$$\bullet \quad \boldsymbol{h} = \begin{bmatrix} 1 \\ H\,\mathrm{sgn}\left(\sigma - H\varepsilon^{\mathrm{pl}}\right) \end{bmatrix}, \tag{2.48}$$

which result again in Eq. (2.46). The different general definitions of the moduli used in this derivation are summarized in Table 2.1.

At the end of this section, Table 2.2 compares the different equations and formulations for linear and arbitrary hardening of one-dimensional plasticity.

2.6 Consideration of Unloading, Reversed Loading and Cyclic Loading

The previous sections considered only monotonic loading either in the tensile or compressive regimes. We will now briefly look at the cases where the loading direction can change. Figure 2.5a shows the case of loading in the elastic ($0 \rightarrow 1$) and elasto-plastic ($1 \rightarrow 2$) range, followed by elastic unloading ($2 \rightarrow 3$) and elastic reloading ($3 \rightarrow 2$).

In the case of Fig. 2.5b, the elastic unloading ($2 \rightarrow 3$) is followed by reversed loading ($3 \rightarrow 4$). The important feature which should be highlighted here is that the unloading phase ($2 \rightarrow 3$) can be described based on Hooke's law, cf. Eq. (1.9). Figure 2.6 shows the case of cyclic loading where a specimen is exposed to fluctuating loads $F(t)$.

Some characteristic stress quantities are indicated in Fig. 2.6b: The stress range $\Delta\sigma$ is the difference between the maximum and minimum stress:

$$\Delta\sigma = \sigma_{\max} - \sigma_{\min}. \tag{2.49}$$

The stress amplitude σ_{a} is half the value of the stress range:

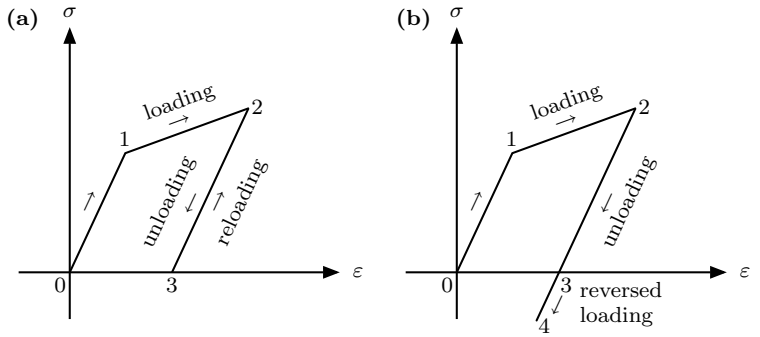

Fig. 2.5 Idealized stress-strain curve with **a** loading–unloading–reloading and **b** loading–unloading–reversed loading

$$\sigma_{\mathrm{a}} = \frac{\Delta\sigma}{2} = \frac{\sigma_{\max} - \sigma_{\min}}{2}. \tag{2.50}$$

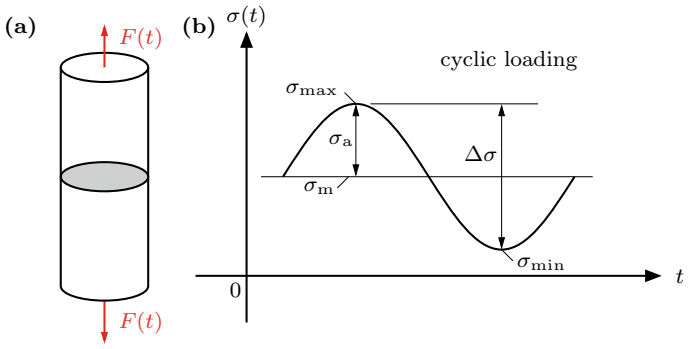

Fig. 2.6 Cyclic loading: **a** idealized specimen and **b** stress-time curve at constant amplitude

The so-called stress ratio R is often used to characterize the stress level in cyclic tests:

$$R = \frac{\sigma_{\min}}{\sigma_{\max}}, \tag{2.51}$$

where a value $R = -1$ characterizes a fully-reversed load cycle, $R = 1$ stands for static loading and $R = 0$ refers to the case where the mean stress is positive and equal to the stress amplitude. In materials testing, cyclic tests are performed to determine the fatigue life of components and structures. Further details can be found in [18, 19].

References

1. Altenbach H, Öchsner A (eds) (2020) Encyclopedia of continuum mechanics. Springer, Berlin
2. Öchsner A (2014) Elasto-plasticity of frame structure elements: modeling and simulation of rods and beams. Springer, Berlin
3. Simo JC, Hughes TJR (1998) Computational inelasticity. Springer, New York
4. Drucker DC (1952) A more fundamental approach to plastic stress-strain relations. In: Sternberg E et al (eds) Proceedings of the 1st US national congress of applied mechanics. Edward Brothers Inc, Michigan, pp 487–491
5. Betten J (2001) Kontinuumsmechanik. Springer, Berlin
6. de Borst R (1986) Non-linear analysis of frictional materials. Dissertation, Delft University of Technology
7. Lemaitre J (1985) A continuous damage mechanics model for ductile fracture. J Eng Mater-T ASME 107:83–89
8. Lemaitre J (1985) Coupled elasto-plasticity and damage constitutive equations. Comput Method Appl 51:31–49
9. Gurson AL (1977) Continuum theory of ductile rupture by void nucleation and growth: part I—yield criteria and flow rules for ductile media. J Eng Mater-T ASME 99:2–15

10. Bauschinger J (1886) Über die Veränderung der Elastizitätsgrenze und die Festigkeit des Eisens und Stahls durch Strecken und Quetschen, durch Erwärmen und Abkühlen und durch oftmals wiederholte Beanspruchungen (On the change of the elastic limit and strength of iron and steel by elongation, shortening, heating, cooling and repeated loading). Mitt Mech-Tech Lab Königl Tech Hochsch München 13:1–116
11. Melan E (1938) Zur Plastizität des räumlichen Kontinuums (On the plasticity of the spatial continuum). Ing Arch 9:116–126
12. Prager W (1955) The theory of plasticity: a survey of recent achievements (James Clayton lecture). Proc Inst Mech Eng 169:41–57
13. Prager W (1956) A new method of analyzing stress and strain in work-hardening plastic solids. J Appl Mech 23:493–496
14. Backhaus G (1968) Zur fließgrenze bei allgemeiner verfestigung (On the yield condition for general work hardening). Z Angew Math Mech 48:99–108
15. Lehmann Th (1972) Einige Bemerkungen zu einer allgemeinen Klasse von Stoffgesetzen für große elasto-plastische Formänderungen (Some remarks on a general class of yield conditions for large elasto-plastic deformations). Ing Arch 41:297–310
16. Shield RT, Ziegler H (1958) On Prager's hardening rule. Z Angew Math Phys 9a:260-276
17. Ziegler H (1959) A modification of Prager's hardening rule. Q Appl Math 17:55–65
18. Pook L (2007) Metal fatigue—what it is, why it matters. Springer, Dordrecht
19. Schijve J (2001) Fatigue of structures and materials. Kluwer Academic Pulishers, Dordrecht

Chapter 3
Theory of Three-Dimensional Plasticity

Abstract The first part of this chapter introduces the concept of the stress matrix with its six stress components. Then, different sets of stress invariants are introduced to characterize the stress matrix and the stress matrix is decomposed in its hydrostatic and deviatoric part. Afterwards, the one-dimensional concept of the previous chapter, i.e. the yield condition, the flow and hardening rule is generalized for multiaxial stress states. Some typical yield conditions are introduced and their graphical representation in different stress spaces is discussed in detail.

3.1 Comments on the Stress Matrix

Let us consider a three-dimensional body which is sufficiently supported and loaded (i.e., by any point or distributed loads) as schematically shown in Fig. 3.1a. Considering the symmetry of the stress matrix, six independent stress components, i.e., three normal and three shear stresses, can be identified, see Fig. 3.1b.

The stress components acting on a differential volume element may have, for example, the values as shown in Eq. (3.1) for the given (x, y, z) coordinate system. A coordinate transformation from the original (x, y, z) to the (x', y', z') coordinate system results in a stress matrix with different stress components, while a principal axis transformation (PAT) calculates the principal stresses σ_i, $(i = 1, 2, 3)$.

$$\sigma_{ij} = \begin{bmatrix} 50 & 0 & 20 \\ 0 & 80 & 20 \\ 20 & 20 & 90 \end{bmatrix}_{(x,y,z)} \overset{\text{rotation}}{\Rightarrow} \begin{bmatrix} 65 & 15 & 28.28 \\ 15 & 65 & 0 \\ 28.28427 & 0 & 90 \end{bmatrix}_{(x',y',z')} \overset{\text{PAT}}{\Rightarrow} \begin{bmatrix} 110 & 0 & 0 \\ 0 & 70 & 0 \\ 0 & 0 & 40 \end{bmatrix}_{(1,2,3)} . \tag{3.1}$$

A. Öchsner, *Elements of Classical Plasticity Theory*,
https://doi.org/10.1007/978-3-031-14201-7_3

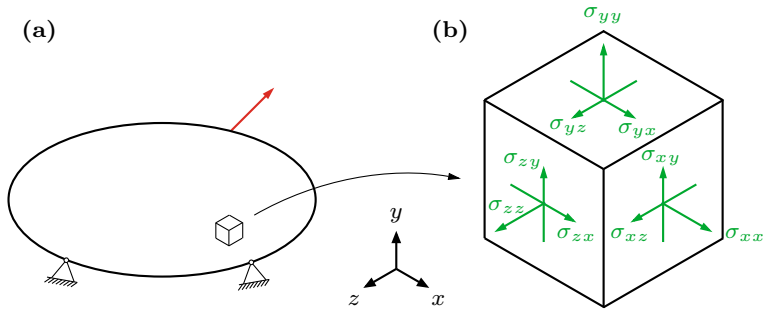

Fig. 3.1 **a** Three-dimensional body under arbitrary load and boundary conditions; **b** infinitesimal volume element with acting normal and shear stress components (see [1])

Looking at this simple example, the following characteristics of the stress matrix can be summarized:

- The components of the stress matrix depend on the orientation of the user-defined coordinate system.
- There is a specific coordinate system (1, 2, 3) where the shear stresses vanish and only normal stresses remain on the main diagonal, i.e., the so-called principal stresses $\sigma_i (i = 1, 2, 3)$.
- The six or three stress components cannot easily be compared to experimental values from uniaxial tests (e.g. the initial yield stress in tension $k_{\mathrm{t}}^{\mathrm{init}}$).
- A graphical representation of any surface is much easier in a principal stress space (1, 2, 3) with three coordinates than in a space with six coordinates (σ_i).

Further information on continuum mechanics and plasticity theory can be taken from the classical textbooks by [1–8].

Let us review in the following the determination of the principal stresses and the axes directions of the corresponding (1, 2, 3) coordinate system. From a mathematical point of view, this question can be answered by determining the eigenvalues of the stress matrix (principal stresses) and the corresponding eigenvectors (principal directions). The solution of the so-called *characteristic equation*, i.e.

$$\det\left(\sigma_{ij} - \sigma_i \mathrm{I}\right) = 0, \tag{3.2}$$

gives the three principal stresses $\sigma_i (i = 1, 2, 3)$. Equation (3.2) can be written in components as:

$$\det\left(\begin{bmatrix} \sigma_{xx} & \sigma_{xy} & \sigma_{xz} \\ \sigma_{yx} & \sigma_{yy} & \sigma_{yz} \\ \sigma_{zx} & \sigma_{zy} & \sigma_{zz} \end{bmatrix} - \sigma_i \begin{bmatrix} 1 & 0 & 0 \\ 0 & 1 & 0 \\ 0 & 0 & 1 \end{bmatrix}\right) = \det\left(\begin{bmatrix} \sigma_{xx} - \sigma_i & \sigma_{xy} & \sigma_{xz} \\ \sigma_{yx} & \sigma_{yy} - \sigma_i & \sigma_{yz} \\ \sigma_{zx} & \sigma_{zy} & \sigma_{zz} - \sigma_i \end{bmatrix}\right) = 0. \tag{3.3}$$

The calculation of the determinant ('det') results in the following cubic equation in σ_i:

$$\sigma_i^3 - \underbrace{\left(\sigma_{xx} + \sigma_{yy} + \sigma_{zz}\right)}_{I_1}\sigma_i^2 + \underbrace{\left(\sigma_{xx}\sigma_{yy} + \sigma_{xx}\sigma_{zz} + \sigma_{yy}\sigma_{zz} - \sigma_{xy}^2 - \sigma_{xz}^2 - \sigma_{yz}^2\right)}_{I_2}\sigma_i - \underbrace{\left(\sigma_{xx}\sigma_{yy}\sigma_{zz} - \sigma_{xx}\sigma_{yz}^2 - \sigma_{yy}\sigma_{xz}^2 - \sigma_{zz}\sigma_{xy}^2 + 2\sigma_{xy}\sigma_{xz}\sigma_{yz}\right)}_{I_3} = 0, \tag{3.4}$$

or in short:

$$\sigma_i^3 - I_1\sigma_i^2 + I_2\sigma_i - I_3 = 0, \tag{3.5}$$

where the three roots $(\sigma_1, \sigma_2, \sigma_3)$ of Eq. (3.5) are the principal stresses. Equation (3.4) can be used to define the three scalar so-called principal invariants I_1, I_2 and I_3. These tensor invariants are independent of the orientation of the coordinate system (objectivity) and represent the physical content of the stress matrix.

The coordinates of the ith eigenvector (x_i, y_i, z_i)—which correspond to the direction of one of the new $(1, 2, 3)$ coordinate axes—result from the following system of three equations:

$$\begin{bmatrix} \sigma_{xx} - \sigma_i & \sigma_{xy} & \sigma_{xz} \\ \sigma_{yx} & \sigma_{yy} - \sigma_i & \sigma_{yz} \\ \sigma_{zx} & \sigma_{zy} & \sigma_{zz} - \sigma_i \end{bmatrix} \begin{bmatrix} x_i \\ y_i \\ z_i \end{bmatrix} = \begin{bmatrix} 0 \\ 0 \\ 0 \end{bmatrix}. \tag{3.6}$$

Let us mention at this point that the determination of the eingenvalues and eigenvectors is also common in applied mechanics for other tensors or matrices. The second moment of the area tensor (or the moment of inertia tensor) has similar properties as the stress matrix:

$$\begin{bmatrix} I_{xx} & I_{xy} & I_{xz} \\ I_{yx} & I_{yy} & I_{yz} \\ I_{zx} & I_{zy} & I_{zz} \end{bmatrix}_{(x,y,z)} \overset{\text{PAT}}{\Rightarrow} \begin{bmatrix} I_1 & 0 & 0 \\ 0 & I_2 & 0 \\ 0 & 0 & I_3 \end{bmatrix}_{(1,2,3)}. \tag{3.7}$$

The application to the principal equation for a dynamic system results in the eigenfrequencies and eigenmodes of a vibrating system:

$$\boldsymbol{M}\ddot{\boldsymbol{u}} + \boldsymbol{K}\boldsymbol{u} = \boldsymbol{0} \quad \Rightarrow \quad \det\left(\boldsymbol{K} - \omega_i^2\boldsymbol{M}\right) = 0, \tag{3.8}$$

where the ω_i are the eigenfrequencies.

$$\left(\boldsymbol{K} - \omega_i^2\boldsymbol{M}\right)\boldsymbol{\Phi} = \boldsymbol{0}, \tag{3.9}$$

where the $\boldsymbol{\Phi}_i$ are the eigenmodes of the system.

Let us look in the following a bit closer at the stress invariants.[1] Another interpretation of the *principal* stress invariants is given by [6]:

- I_1 = sum of the diagonal terms of σ_{ij}:

$$I_1 = \sigma_{xx} + \sigma_{yy} + \sigma_{zz}. \tag{3.10}$$

- I_2 = sum of the two-row main subdeterminants:

$$I_2 = \begin{vmatrix} \sigma_{xx} & \sigma_{xy} \\ \sigma_{xy} & \sigma_{yy} \end{vmatrix} + \begin{vmatrix} \sigma_{yy} & \sigma_{yz} \\ \sigma_{yz} & \sigma_{zz} \end{vmatrix} + \begin{vmatrix} \sigma_{xx} & \sigma_{xz} \\ \sigma_{xz} & \sigma_{zz} \end{vmatrix}. \tag{3.11}$$

- I_3 = determinant of σ_{ij}:

$$I_3 = \begin{vmatrix} \sigma_{xx} & \sigma_{xy} & \sigma_{xz} \\ \sigma_{xy} & \sigma_{yy} & \sigma_{yz} \\ \sigma_{xz} & \sigma_{yz} & \sigma_{zz} \end{vmatrix}. \tag{3.12}$$

Besides these principal invariants, there is also often another set of invariants used. This set is included in the principal invariants and called *basic invariants* (see [4]):

$$J_1 = I_1, \tag{3.13}$$
$$J_2 = \tfrac{1}{2} I_1^2 - I_2, \tag{3.14}$$
$$J_3 = \tfrac{1}{3} I_1^3 - I_1 I_2 + I_3. \tag{3.15}$$

The definition of both sets of invariants is given in Table 3.1.

It is common in the framework of the plasticity theory of isotropic materials to decompose the stress matrix σ_{ij} into a pure volume changing (spherical or hydrostatic) matrix σ_{ij}^{o} and a pure shape changing (deviatoric) stress matrix s_{ij} (cf. Fig. 3.2)[2]:

$$\sigma_{ij} = \sigma_{ij}^{\mathrm{o}} + s_{ij} = \sigma_{\mathrm{m}} \mathbf{I} + s_{ij}. \tag{3.16}$$

In Eq. (3.16), $\sigma_{\mathrm{m}} = \frac{1}{3}(\sigma_{xx} + \sigma_{yy} + \sigma_{zz})$ denotes the mean normal stress[3] and $\mathbf{I}$ the identity matrix. Furthermore, Einstein's summation convention was used (see [10]).

Equation (3.16) can be written in components as

[1] It is useful for some applications (e.g. the calculation of the derivative with respect to the stresses) to *not* consider the symmetry of the shear stress components and to work with nine stress components. These invariants are denoted by $\underline{I}_i$ and $\underline{J}_i$.

[2] It should be noted that in the case of anisotropic materials, a hydrostatic stress state may result in a shape change [9].

[3] Also called the hydrostatic stress; in the context of soil mechanics, the pressure $p = -\sigma_{\mathrm{m}}$ is also used.

Table 3.1 Definition of the three principal (I_i) and basic (J_i) stress invariants of the stress matrix

First stress invariant of σ_{ij}
$I_1 = \sigma_{xx} + \sigma_{yy} + \sigma_{zz}$
$J_1 = \sigma_{xx} + \sigma_{yy} + \sigma_{zz}$
Second stress invariant of σ_{ij}
$I_2 = \sigma_{xx}\sigma_{yy} + \sigma_{xx}\sigma_{zz} + \sigma_{yy}\sigma_{zz} - \sigma_{xy}^2 - \sigma_{xz}^2 - \sigma_{yz}^2$
$J_2 = \frac{1}{2}\left(\sigma_{xx}^2 + \sigma_{yy}^2 + \sigma_{zz}^2\right) + \sigma_{xy}^2 + \sigma_{xz}^2 + \sigma_{yz}^2$
Third stress invariant of σ_{ij}
$I_3 = \sigma_{xx}\sigma_{yy}\sigma_{zz} - \sigma_{xx}\sigma_{yz}^2 - \sigma_{yy}\sigma_{xz}^2 - \sigma_{zz}\sigma_{xy}^2 + 2\sigma_{xy}\sigma_{xz}\sigma_{yz}$
$J_3 = \frac{1}{3}\left(\sigma_{xx}^3 + \sigma_{yy}^3 + \sigma_{zz}^3 + 3\sigma_{xy}^2\sigma_{xx} + 3\sigma_{xy}^2\sigma_{yy} + 3\sigma_{xz}^2\sigma_{xx} + 3\sigma_{xz}^2\sigma_{zz} + 3\sigma_{yz}^2\sigma_{yy} + 3\sigma_{yz}^2\sigma_{zz} + 6\sigma_{xy}\sigma_{xz}\sigma_{yz}\right)$

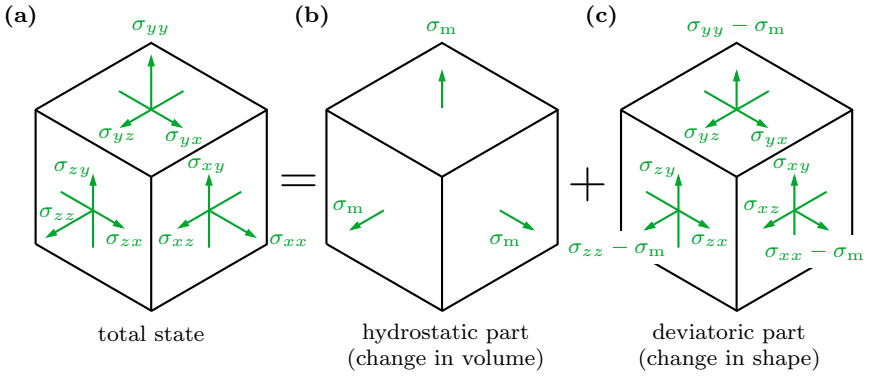

Fig. 3.2 Decomposition of the stress matrix **a** into its spherical **b** and the deviatoric **c** part

$$\underbrace{\begin{bmatrix} \sigma_{xx} & \sigma_{xy} & \sigma_{xz} \\ \sigma_{xy} & \sigma_{yy} & \sigma_{yz} \\ \sigma_{xz} & \sigma_{yz} & \sigma_{zz} \end{bmatrix}}_{\text{stress matrix } \sigma_{ij}} = \underbrace{\begin{bmatrix} \sigma_{\mathrm{m}} & 0 & 0 \\ 0 & \sigma_{\mathrm{m}} & 0 \\ 0 & 0 & \sigma_{\mathrm{m}} \end{bmatrix}}_{\text{hydrostatic matrix } \sigma_{ij}^{\mathrm{o}}} + \underbrace{\begin{bmatrix} s_{xx} & s_{xy} & s_{xz} \\ s_{xy} & s_{yy} & s_{yz} \\ s_{xz} & s_{yz} & s_{zz} \end{bmatrix}}_{\text{deviatoric matrix } s_{ij}} . \tag{3.17}$$

It can be seen that the elements outside the diagonal terms, i.e., the shear stresses, are the same for the stress and the deviatoric stress matrix

$$s_{ij} = \sigma_{ij} \quad \text{for} \quad i \neq j, \tag{3.18}$$

$$s_{ij} = \sigma_{ij} - \sigma_{\mathrm{m}} \quad \text{for} \quad i = j, \tag{3.19}$$

and it can be shown that the so-called deviator equation

$$s_{xx} + s_{yy} + s_{zz} = 0 \tag{3.20}$$

holds. The following list summarizes the calculation of the stress deviator components:

$$s_{xx} = \sigma_{xx} - \sigma_{\mathrm{m}} = \frac{2}{3}\sigma_{xx} - \frac{1}{3}(\sigma_{yy} + \sigma_{zz}), \tag{3.21}$$

$$s_{yy} = \sigma_{yy} - \sigma_{\mathrm{m}} = \frac{2}{3}\sigma_{yy} - \frac{1}{3}(\sigma_{xx} + \sigma_{zz}), \tag{3.22}$$

$$s_{zz} = \sigma_{zz} - \sigma_{\mathrm{m}} = \frac{2}{3}\sigma_{zz} - \frac{1}{3}(\sigma_{xx} + \sigma_{yy}), \tag{3.23}$$

$$s_{xy} = \sigma_{xy}, \tag{3.24}$$

$$s_{yz} = \sigma_{yz}, \tag{3.25}$$

$$s_{xz} = \sigma_{xz}. \tag{3.26}$$

The definitions of the principal and basic invariants can be applied directly to the hydrostatic and deviatoric part of the stress matrix to obtain a similar representation as provided in Table 3.1, see summary in Table 3.2 for the hydrostatic matrix and the summary in Table 3.3 for the deviatoric matrix.

The hydrostatic part of σ_{ij} has in the case of metallic materials (full dense materials) for temperatures approximately under $0.3T_{\mathrm{mt}}$ (T_{mt}: melting temperature) nearly no influence on the occurrence of inelastic strains since dislocations slip only under the influence of shear stresses (for higher temperatures from 0.3 till $0.5T_{\mathrm{mt}}$ also non-conservative climbing is possible) [11]. On the other hand, the hydrostatic stress has a considerable influence on the yielding behavior in the case of soil mechanics, cellular materials or in damage mechanics (formation of pores, e.g. [12]).

The evaluation of the basic invariants for the stress matrix, as well as the hydrostatic and deviatoric part is presented in Table 3.4, expressed in components of σ_{ij} and the principal stresses $\sigma_1, \sigma_2, \sigma_3$.

It can be seen in Table 3.4 that the spherical matrix is completely characterised by its first invariant because the second and third invariant are powers of it. The stress deviator matrix is completely characterised by its second and third invariant. Therefore, the physical contents of the stress state σ_{ij} can be described either by the three basic stress invariants J_i or if we use the decomposition in its spherical and deviatoric part by the first invariant of the spherical matrix and the second and third invariant of the stress deviator matrix. In the following, we will only use these three basic invariants to describe yield and failure conditions. Thus, the physical content of a state of stress will be described by the following set of invariants:

Table 3.2 Definition of the three principal (I_i°) and basic (J_i°) stress invariants of the hydrostatic stress matrix σ_{ij}°

First stress invariant of σ_{ij}°
$I_1^\circ = 3\sigma_\mathrm{m}$
$J_1^\circ = 3\sigma_\mathrm{m}$
Second stress invariant of σ_{ij}°
$I_2^\circ = 3\sigma_\mathrm{m}^2$
$J_2^\circ = \frac{3}{2}\sigma_\mathrm{m}^2$
Third stress invariant of σ_{ij}°
$I_3^\circ = \sigma_\mathrm{m}^3$
$J_3^\circ = \sigma_\mathrm{m}^3$

Table 3.3 Definition of the three principal (I_i') and basic (J_i') stress invariants of the deviatoric stress matrix s_{ij}

First stress invariant of s_{ij}
$I_1' = 0$
$J_1' = 0$
Second stress invariant of s_{ij}
$I_2' = s_{xx}s_{yy} + s_{xx}s_{zz} + s_{yy}s_{zz} - s_{xy}^2 - s_{xz}^2 - s_{yz}^2$
$J_2' = -I_2'$
Third stress invariant of s_{ij}
$I_3' = s_{xx}s_{yy}s_{zz} - s_{xx}s_{yz}^2 - s_{yy}s_{xz}^2 - s_{zz}s_{xy}^2 + 2s_{xy}s_{xz}s_{yz}$
$J_3' = I_3'$

Table 3.4 Basic invariants in terms of σ_{ij} and principal values

Invariants	Components of σ_{ij}	Principal stresses $\sigma_1, \sigma_2, \sigma_3$
Stress matrix		
J_1	$\sigma_{xx} + \sigma_{yy} + \sigma_{zz}$	$\sigma_1 + \sigma_2 + \sigma_3$
J_2	$\frac{1}{2}\left(\sigma_{xx}^2 + \sigma_{yy}^2 + \sigma_{zz}^2\right) + \sigma_{xy}^2 + \sigma_{xz}^2 + \sigma_{yz}^2$	$\frac{1}{2}\left(\sigma_1^2 + \sigma_2^2 + \sigma_3^2\right)$
J_3	$\frac{1}{3}\left(\sigma_{xx}^3 + \sigma_{yy}^3 + \sigma_{zz}^3 + 3\sigma_{xy}^2\sigma_{xx} + 3\sigma_{xy}^2\sigma_{yy} + 3\sigma_{xz}^2\sigma_{xx} + 3\sigma_{xz}^2\sigma_{zz} + 3\sigma_{yz}^2\sigma_{yy} + 3\sigma_{yz}^2\sigma_{zz} + 6\sigma_{xy}\sigma_{xz}\sigma_{yz}\right)$	$\frac{1}{3}\left(\sigma_1^3 + \sigma_2^3 + \sigma_3^3\right)$
Spherical matrix		
J_1^{o}	$\sigma_{xx} + \sigma_{yy} + \sigma_{zz}$	$\sigma_1 + \sigma_2 + \sigma_3$
J_2^{o}	$\frac{1}{6}\left(\sigma_{xx} + \sigma_{yy} + \sigma_{zz}\right)^2$	$\frac{1}{6}\left(\sigma_1 + \sigma_2 + \sigma_3\right)^2$
J_3^{o}	$\frac{1}{27}\left(\sigma_{xx} + \sigma_{yy} + \sigma_{zz}\right)^3$	$\frac{1}{27}\left(\sigma_1 + \sigma_2 + \sigma_3\right)^3$
Stress deviator matrix		
J_1'	0	0
J_2'	$\frac{1}{6}\left[(\sigma_{xx} - \sigma_{yy})^2 + (\sigma_{yy} - \sigma_{zz})^2 + (\sigma_{zz} - \sigma_{xx})^2\right] + \sigma_{xy}^2 + \sigma_{yz}^2 + \sigma_{zx}^2$	$\frac{1}{6}\left[(\sigma_1 - \sigma_2)^2 + (\sigma_2 - \sigma_3)^2 + (\sigma_3 - \sigma_1)^2\right]$
J_3'	$s_{xx}s_{yy}s_{zz} + 2\sigma_{xy}\sigma_{yz}\sigma_{zx} - s_{xx}\sigma_{yz}^2 - s_{yy}\sigma_{zx}^2 - s_{zz}\sigma_{xy}^2$	$s_1 s_2 s_3$
With	$s_{xx} = \frac{1}{3}(2\sigma_{xx} - \sigma_{yy} - \sigma_{zz})$	$s_1 = \frac{1}{3}(2\sigma_1 - \sigma_2 - \sigma_3)$
	$s_{yy} = \frac{1}{3}(-\sigma_{xx} + 2\sigma_{yy} - \sigma_{zz})$	$s_2 = \frac{1}{3}(-\sigma_1 + 2\sigma_2 - \sigma_3)$
	$s_{zz} = \frac{1}{3}(-\sigma_{xx} - \sigma_{yy} + 2\sigma_{zz})$	$s_3 = \frac{1}{3}(-\sigma_1 - \sigma_2 + 2\sigma_3)$
	$s_{xy} = \sigma_{xy}, s_{xz} = \sigma_{xz}, s_{yz} = \sigma_{yz}$	

Table 3.5 Basic invariants for the σ_1-σ_2 and σ-τ space

Invariants	σ_1-σ_2 space	σ-τ space
J_1^{o}	$\sigma_1 + \sigma_2$	σ
J_2'	$\frac{1}{3}\left(\sigma_1^2 + \sigma_2^2 - \sigma_1\sigma_2\right)$	$\frac{1}{3}\sigma^2 + \tau^2$
J_3'	$\frac{1}{27}\left(2\sigma_1^3 + 2\sigma_2^3 - 3\sigma_1\sigma_2(\sigma_1 + \sigma_2)\right)$	$\frac{2}{27}\sigma^3 + \frac{1}{3}\sigma\tau^2$

Table 3.6 Basic invariants for a uniaxial (normal) stress (σ) state and a pure shear stress state (τ)

Invariants	Only σ	Only τ
J_1^{o}	σ	0
J_2'	$\frac{1}{3}\sigma^2$	τ^2
J_3'	$\frac{2}{27}\sigma^3$	0

$$\sigma_{ij} \;\rightarrow\; J_1^{\mathrm{o}},\, J_2',\, J_3'. \tag{3.27}$$

To derive important special cases of yield conditions, it is also useful to specify the stress invariants for a plane stress state σ_1-σ_2 and a stress state σ-τ where only one normal and one shear stress is acting. Thus, the stress invariants reduce to the given form in Table 3.5.

Finally, Table 3.6 summarizes the stress invariants for a uniaxial or pure shear stress state.

The representation of a tress state in terms of invariants is also very useful in the context of the implementation of yield conditions into commercial finite elements codes. This significantly facilities the calculation of derivatives (see [13]).

3.2 Graphical Representation of Yield Conditions

Plastic flow starts in a uniaxial tensile test as soon as the acting tensile stress σ reaches the initial yield stress k^{init}, see [14]. In the case of a multiaxial stress state, this simple comparison is replaced by the yield condition. To this end, a scalar value is calculated from the acting six stress components and compared to an experimental

scalar value. The yield condition in stress space can be expressed in its most general form ($\mathbb{R}^6 \times \mathbb{R}^{\dim(q)} \rightarrow \mathbb{R}$) as:

$$F = F(\boldsymbol{\sigma}, \boldsymbol{q}). \tag{3.28}$$

For further characterisation, we assume in the following the special case of ideal plastic material behavior (vector of hardening variables $\boldsymbol{q} = \mathbf{0}$) so that for ($\mathbb{R}^6 \rightarrow \mathbb{R}$)

$$F = F(\boldsymbol{\sigma}) \tag{3.29}$$

depends now only on the stress state. The values of F have—as in the uniaxial case—the following mechanical meaning[4]:

$$F(\boldsymbol{\sigma}) = 0 \rightarrow \text{plastic material behavior}, \tag{3.30}$$

$$F(\boldsymbol{\sigma}) < 0 \rightarrow \text{elastic material behavior}, \tag{3.31}$$

$$F(\boldsymbol{\sigma}) > 0 \rightarrow \text{invalid}. \tag{3.32}$$

A further simplification is obtained under the assumption that the yield condition can be split in a pure stress part $f(\boldsymbol{\sigma})$ and an experimental material parameter k:

$$F(\boldsymbol{\sigma}) = f(\boldsymbol{\sigma}) - k. \tag{3.33}$$

The yield condition $F = 0$ represents in a n-dimensional space a hypersurface that is also called the yield surface or the yield loci. The number n is equal to the independent stress matrix components. A direct graphical representation of the yield surface is not possible due to its dimensionality, i.e., six variables. However, a reduction of the dimensionality is possible to achieve if a principle axis transformation (see Eq. (3.2)) is applied to the argument σ_{ij}. The components of the stress matrix reduce to the principal stresses σ_1, σ_2 and σ_3 on the principal diagonal of the stress matrix and the non-diagonal elements are equal to zero. In such a principal stress space, it is possible to graphically represent the yield condition as a three-dimensional surface. This space is also called the Haigh-Westergaard stress space (see [15]). A hydrostatic stress state lies in such a principal stress system on the space diagonal (hydrostatic axis). Any plane perpendicular to the hydrostatic axis is called an octahedral plane. The particular octahedral plane passing through the origin is called the deviatoric plane or π-plane (see [6]). Because $\sigma_1 + \sigma_2 + \sigma_3 = 0$, it follows from Eq. (3.16) that $\sigma_{ij} = s_{ij}$, i.e. any stress state on the π-plane is pure deviatoric.

The possibility of a representation of a yield condition based on a set of independent stress invariants (e.g. according to Eq. (3.27)) is the characteristic of any isotropic yield condition, regardless of the choice of coordinate system. Therefore, Eq. (3.29) can also be written as

$$F = F(J_1^{\mathrm{o}}, J_2', J_3'). \tag{3.34}$$

[4] Under the restriction of rate-independent plasticity.

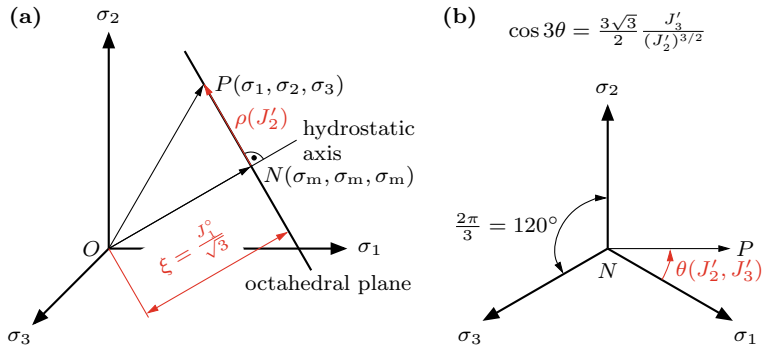

Fig. 3.3 Geometrical interpretation of basic stress invariants: **a** principal stress space; **b** octahedral plane

On the basis of the dependency of the yield condition on the invariants, a descriptive classification can be performed. Yield conditions independent of the hydrostatic stress (J_1^o) can be represented by the invariants J_2' and J_3'. Stress states with $J_2' = \text{const.}$ lie on a circle around the hydrostatic axis in an octahedral plane. A dependency of the yield condition on J_3' results in a deviation from the circle shape. The yield surface forms a prismatic body whose longitudinal axis is represented by the hydrostatic axis. A dependency on J_1^o denotes a size change of the cross-section of the yield surface along the hydrostatic axis. However, the shape of the cross-section remains similar in the mathematical sense. Therefore, a dependency on J_1^o can be represented by sectional views through planes along the hydrostatic axis.

The geometrical interpretation of stress invariants (see [6]) is given in Fig. 3.3.

It can be seen that an arbitrary stress state P can be expressed by its position along the hydrostatic axis $\xi = \frac{1}{\sqrt{3}} J_1^o$ and its polar coordinates ($\rho = \sqrt{2J_2'}$, $\theta(J_2', J_3')$) in the octahedral plane through P. For the set of polar coordinates, the so-called stress Lode angle θ is defined in the range $0 \leq \theta \leq 60°$ as (see [16]),

$$\cos(3\theta) = \frac{3\sqrt{3}}{2} \cdot \frac{J_3'}{(J_2')^{3/2}}. \tag{3.35}$$

It can be concluded from Eq. (3.35) that

$$3\theta = 3\theta(J_2', J_3'), \tag{3.36}$$

or that

$$\theta = \theta(J_2', J_3'). \tag{3.37}$$

The trigonometric identity $\cos(3\theta) = 4\cos^3(\theta) - 3\cos(\theta)$ may be used for some transformations.

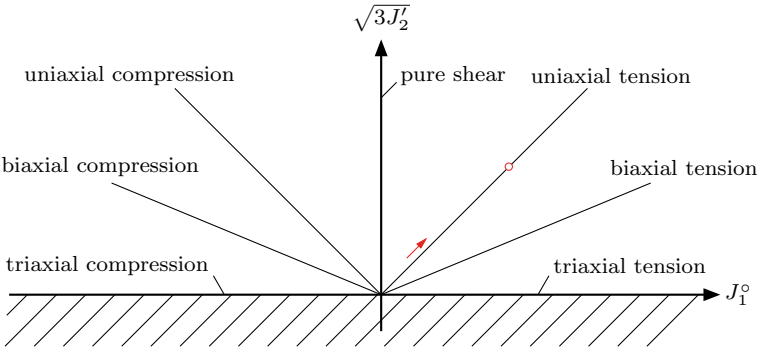

Fig. 3.4 Schematic representation of basic mechanical tests in the J_1°-$\sqrt{3J_2'}$ invariant space

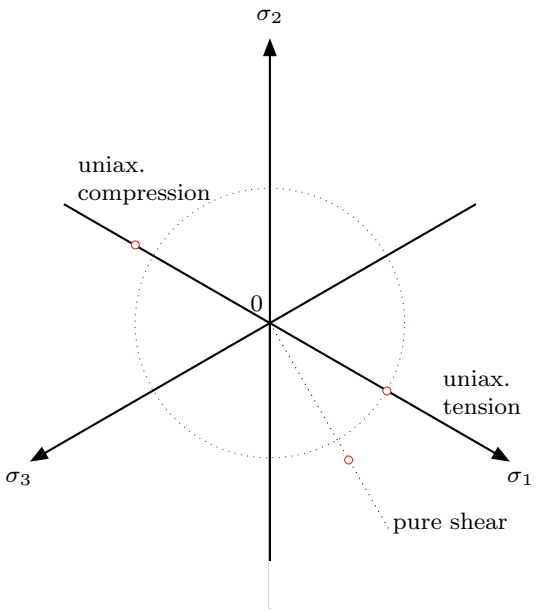

Fig. 3.5 Identification of the shape of a yield condition in an octahedral plane ($\sigma_\mathrm{m} = \text{const.}$)

The set of coordinates $(\xi, \rho, \cos(3\theta))$ is known in the literature as the Haigh-Westergaard coordinates. To investigate the shape of the yield surface, particular experiments, including multiaxial stress states, must be realized and the initial yield points marked and approximated in the Haigh-Westergaard space, the J_1°-$\sqrt{3J_2'}$ invariant space, and octahedral planes, see Figs. 3.4 and 3.5.

The loading path, for example, for the biaxial tension case in the J_1°-$\sqrt{3J_2'}$ invariant space (see Fig. 3.4) is obtained as follows (see Table 3.5 for the evaluation of the invariants) (Table 3.7):

Table 3.7 Definition of basic tests in the J_1°-$\sqrt{3J_2'}$ invariant space

Case	J_1°	$\sqrt{3J_2'}$	Comment
Uniax. tension (σ)	σ	σ	Slope: 1
Uniax. compression ($-\sigma$)	$-\sigma$	σ	Slope: -1
Biax. tension (σ)	2σ	σ	Slope: 0.5
Biax. compression ($-\sigma$)	-2σ	σ	Slope: -0.5
Triax. tension (σ)	3σ	0	Horiz. axis
Triax. compression ($-\sigma$)	-3σ	0	Horiz. axis
Pure shear (τ)	0	$\sqrt{3}\,\tau$	Vertical axis

Table 3.8 Definition of basic tests in the J_1°-$\sqrt{J_2'}$ invariant space

Case	J_1°	$\sqrt{J_2'}$	Comment
Uniax. tension (σ)	σ	$\frac{\sqrt{3}}{3}\sigma$	Slope: $\frac{\sqrt{3}}{3}$
Uniax. compression ($-\sigma$)	$-\sigma$	$-\frac{\sqrt{3}}{3}\sigma$	Slope: $-\frac{\sqrt{3}}{3}$
Biax. tension (σ)	2σ	$\frac{\sqrt{3}}{3}\sigma$	Slope: $\frac{\sqrt{3}}{6}$
Biax. compression ($-\sigma$)	-2σ	$-\frac{\sqrt{3}}{3}\sigma$	Slope: $-\frac{\sqrt{3}}{6}$
Triax. tension (σ)	3σ	0	Horiz. axis
Triax. compression ($-\sigma$)	-3σ	0	Horiz. axis
Pure shear (τ)	0	τ	Vertical axis

$$\sqrt{3J_2'} = \sigma = \frac{1}{2}J_1^{\circ}. \tag{3.38}$$

Further load paths for basic experiments in the J_1°-$\sqrt{3J_2'}$ invariant space are summarized in Table 3.7.

As an example, the curve for biaxial tension in the J_1°-$\sqrt{J_2'}$ invariant space is obtained as follows (Fig. 3.4; Table 3.8):

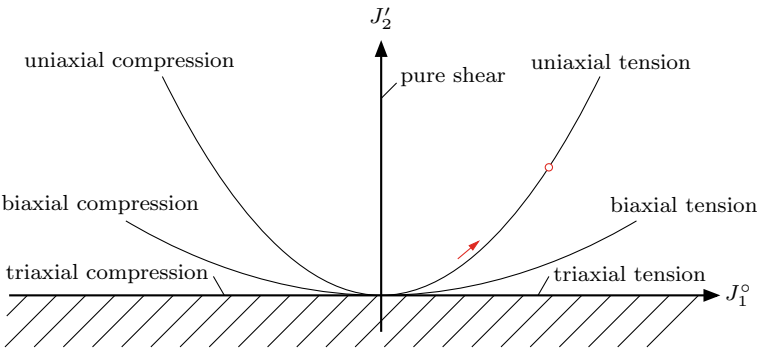

Fig. 3.6 Schematic representation of basic mechanical tests in the J_1°-J_2' invariant space

Table 3.9 Definition of basic tests in the J_1°-J_2' invariant space

Case	J_1°	J_2'	Comment
Uniax. tension (σ)	σ	$\frac{1}{3}\sigma^2$	Parabola
Uniax. compression ($-\sigma$)	$-\sigma$	$-\frac{1}{3}\sigma^2$	Parabola
Biax. tension (σ)	2σ	$\frac{1}{3}\sigma^2$	Parabola
Biax. compression ($-\sigma$)	-2σ	$-\frac{1}{3}\sigma^2$	Parabola
Triax. tension (σ)	3σ	0	Horiz. axis
Triax. compression ($-\sigma$)	-3σ	0	Horiz. axis
Pure shear (τ)	0	τ^2	Vertical axis

$$\sqrt{J_2'} = \frac{\sqrt{3}}{3}\sigma = \frac{\sqrt{3}}{6}J_1^\circ. \tag{3.39}$$

In a similar way, one obtains the curve for biaxial tension in the J_1°-J_2' invariant space:

$$J_2' = \frac{1}{3}\sigma^2 = \frac{1}{3}\left(\frac{1}{2}J_1^\circ\right)^2 = \frac{1}{12}\left(J_1^\circ\right)^2 \tag{3.40}$$

The experimental realization of multiaxial stress states is quite difficult and requires specialized testing equipment, which is not available in many laboratories. One possibility is a so-called biaxial testing machine [17] as shown in Fig. 3.7a. Such

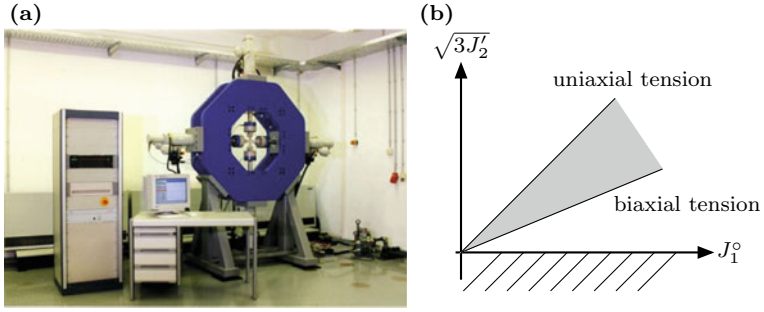

Fig. 3.7 Biaxial stress states: **a** experimental realization [17] and **b** representation in the J_1°-$\sqrt{3J_2'}$ invariant space

a sophisticated testing machine allows to investigate a certain part of the J_1°-$\sqrt{3J_2'}$ invariant space as indicated in Fig. 3.7b. As an alternative, one may use hollow cylinders under internal and/or external pressure where in addition a tensile of compressive load is superimposed along the longitudinal tube axis [18].

3.3 Yield Conditions

The yield condition can generally be expressed as

$$F(\boldsymbol{\sigma}, \boldsymbol{q}) \leq 0, \tag{3.41}$$

where $\boldsymbol{q} = \left[\kappa \ \boldsymbol{\alpha}\right]^{\mathrm{T}}$ is the column matrix of internal variables describing the hardening behavior of the material. Parameter κ relates to isotropic hardening while the matrix $\boldsymbol{\alpha}$ contains the kinematic hardening parameters. The mechanical meaning of F remains as indicated by Eqs. (3.30)–(3.32).

Restricting to isotropic hardening, Eq. (3.41) can be expressed as

$$F(\boldsymbol{\sigma}, \kappa) \leq 0. \tag{3.42}$$

3.3.1 Mises Yield Condition

The total deformation energy per unit volume of a three-dimensional body can be generally expressed as (see [14]):

$$w = \frac{1}{2}\left(\sigma_{xx}\varepsilon_{xx} + \sigma_{yy}\varepsilon_{yy} + \sigma_{zz}\varepsilon_{zz} + \tau_{xy}\gamma_{xy} + \tau_{xz}\gamma_{xz} + \tau_{yz}\gamma_{yz}\right). \tag{3.43}$$

Following the decomposition of the stress matrix in its spherical and deviatoric part as indicated in Fig. 3.2, this deformation energy can be split in its volumetric (w°) and distortional (w^s) part as:

$$w = \underbrace{\frac{1-2\nu}{6E}\left(\sigma_{xx}+\sigma_{yy}+\sigma_{zz}\right)^2}_{w^\circ} + \underbrace{\frac{1+\nu}{6E}\left[(\sigma_{xx}-\sigma_{yy})^2+(\sigma_{yy}-\sigma_{zz})^2+(\sigma_{zz}-\sigma_{xx})^2+6(\tau_{xy}^2+\tau_{yz}^2+\tau_{xz}^2)\right]}_{w^\mathrm{s}}. \tag{3.44}$$

The von Mises yield condition states now that plastic deformation starts as soon as the distortional deformation energy per unit volume, i.e.

$$w^\mathrm{s} = \frac{1+\nu}{6E}\left[(\sigma_{xx}-\sigma_{yy})^2+(\sigma_{yy}-\sigma_{zz})^2+(\sigma_{zz}-\sigma_{xx})^2+6(\tau_{xy}^2+\tau_{yz}^2+\tau_{xz}^2)\right], \tag{3.45}$$

reaches a critical value ($k_\mathrm{t}^2/(6G)$) (see [19, 20]). This yield condition is commonly applied for ductile metals. The expression in units of stress is given for a general three-dimensional stress state as

$$F(\sigma_{ij}) = \underbrace{\sqrt{\frac{1}{2}\left((\sigma_x-\sigma_y)^2+(\sigma_y-\sigma_z)^2+(\sigma_z-\sigma_x)^2\right)+3\left(\sigma_{xy}^2+\sigma_{yz}^2+\sigma_{xz}^2\right)}}_{\sigma_\mathrm{eff}} - k_\mathrm{t} = 0, \tag{3.46}$$

or in the principal stress space ($\sigma_1, \sigma_2, \sigma_3$) with $\sigma_{xy} = \sigma_{yz} = \sigma_{xz} = 0$:

$$F(\sigma_{ij}) = \underbrace{\sqrt{\frac{1}{2}\left((\sigma_1-\sigma_2)^2+(\sigma_2-\sigma_3)^2+(\sigma_3-\sigma_1)^2\right)}}_{\sigma_\mathrm{eff}} - k_\mathrm{t} = 0. \tag{3.47}$$

The graphical representation in the principal stress space is given in Fig. 3.8 where a cylinder with its longitudinal axis equal to the hydrostatic axis is obtained.

Expressed with the second invariant of the stress deviator (see Table 3.4), one can write the following formulation (Fig. 3.9):

$$F(J_2') = \sqrt{3J_2'} - k_\mathrm{t} = 0. \tag{3.48}$$

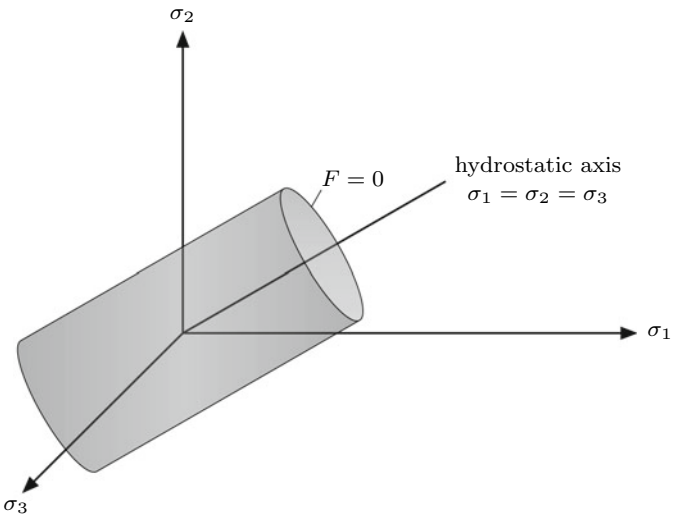

Fig. 3.8 Graphical representation of the yield condition according to von Mises in the principal stress space

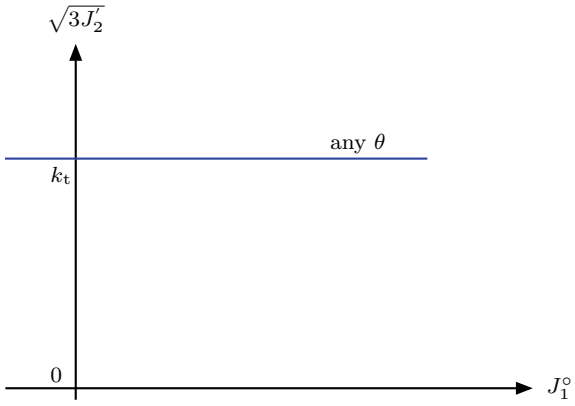

Fig. 3.9 Graphical representation of the yield condition according to von Mises in the $\sqrt{3J_2'}$-J_1° space

The representation in the $\sqrt{3J_2'}$-J_1° space (see Fig. 3.10) shows that the yield condition is independent of the hydrostatic stress.

The view along the hydrostatic axis is shown in Fig. 3.10 where it can be seen that there is no difference under tension and compression for uniaxial stress states.

A representation in the two-component principal σ_1-σ_2 space is obtained by substituting the particular basic invariant formulations from Table 3.5 (σ_1-σ_2 space) into Eq. (3.48) as (see Fig. 3.11):

$$F_{\sigma_1-\sigma_2} = \sigma_1^2 + \sigma_2^2 - \sigma_1\sigma_2 - k_t^2 = 0, \tag{3.49}$$

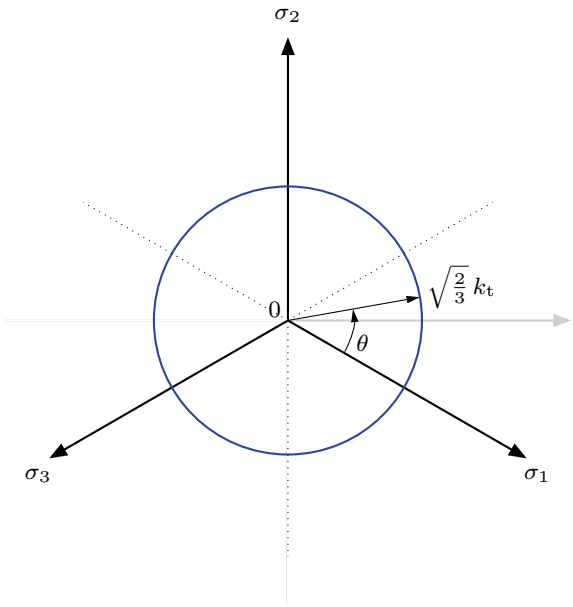

Fig. 3.10 Graphical representation of the yield condition according to von Mises in the octahedral plane

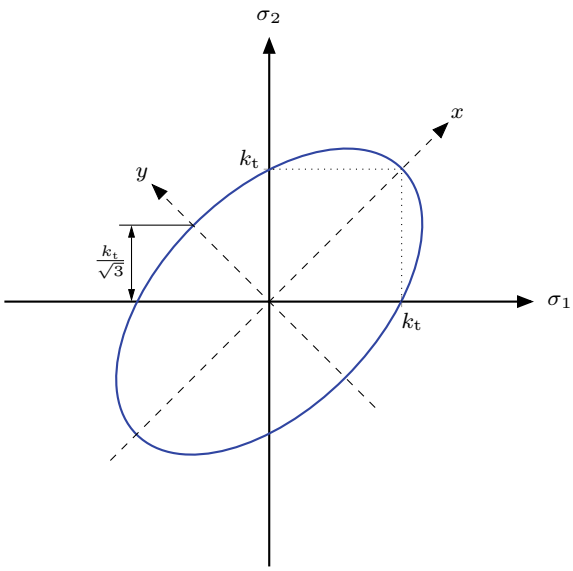

Fig. 3.11 Graphical representation of the yield condition according to von Mises in the σ_1-σ_2 space

or represented in a standard form to easier identify an ellipse (see Fig. 3.11) as

$$F_{\sigma_1-\sigma_2} = \left(\frac{x}{\sqrt{2}\,k_\mathrm{t}}\right)^2 + \left(\frac{y}{\sqrt{2}\,k_\mathrm{s}}\right)^2 - 1 = 0, \tag{3.50}$$

where $x = (\sigma_1 + \sigma_2)/\sqrt{2}$ and $y = (\sigma_2 - \sigma_1)/\sqrt{2}$.

The transformation of Eq. (3.49) into Eq. (3.50) can be obtained in the following way:

$$\sigma_1^2 + \sigma_2^2 - \sigma_1\sigma_2 = k_\mathrm{t}^2, \tag{3.51}$$

$$4\sigma_1^2 + 4\sigma_2^2 - 4\sigma_1\sigma_2 = 4k_\mathrm{t}^2, \tag{3.52}$$

$$\sigma_1^2 + 2\sigma_1\sigma_2 + \sigma_2^2 + 3(\sigma_1^2 - 2\sigma_1\sigma_2 + \sigma_2^2) = 4k_\mathrm{t}^2, \tag{3.53}$$

$$\frac{1}{4}(\sigma_1 + \sigma_2)^2 + \frac{3}{4}(\sigma_2 - \sigma_1)^2 = k_\mathrm{t}^2, \tag{3.54}$$

$$\left(\frac{\sigma_1 + \sigma_2}{2\,k_\mathrm{t}}\right)^2 + \left(\frac{\sigma_2 - \sigma_1}{2\,\frac{k_\mathrm{s}}{\sqrt{3}}}\right)^2 = 1. \tag{3.55}$$

A representation in the two-component normal/shear σ-τ space is obtained by substituting the particular basic invariant formulations from Table 3.5 into Eq. (3.48) to finally give the following ellipse (see Fig. 3.12):

$$F_{\sigma-\tau} = \left(\frac{\sigma}{k_\mathrm{t}}\right)^2 + \left(\frac{\sqrt{3}\,\tau}{k_\mathrm{t}}\right)^2 - 1 = 0. \tag{3.56}$$

The last formulation allows to identify the relationship between the shear and tensile yield stress. Setting $\sigma = 0$, which means then $\tau \to k_\mathrm{s}$, gives:

$$k_\mathrm{s} = \frac{k_\mathrm{t}}{\sqrt{3}}. \tag{3.57}$$

Based on this relation, it is possible to express the yield condition in terms of the shear yield stress, for example, as:

$$F(J_2') = \sqrt{J_2'} - k_\mathrm{s} = 0. \tag{3.58}$$

Table 3.10 illustrates the fact that it is not the right approach to look on single stress components if one has to judge if the stress state is in the elastic or already in the plastic domain. Only the equivalent stress based on a yield condition can answer this question in the case of multiaxial stress states.

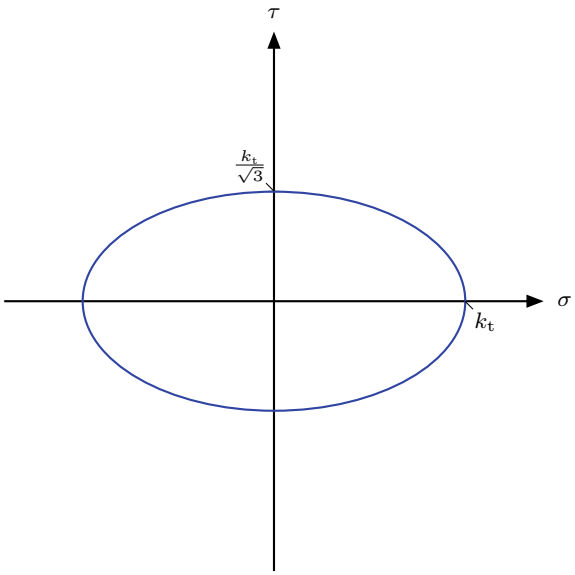

Fig. 3.12 Graphical representation of the yield condition according to von Mises in the σ-τ space

3.3.2 Tresca Yield Condition

The Tresca yield condition, also known as the maximum shear stress theory, postulates yielding as soon as the maximum shear stress reaches an experimental value. This yield condition is commonly applied for ductile metals. The expression is given for the principal stresses as

$$\max\left(\frac{1}{2}|\sigma_1-\sigma_2|\,,\frac{1}{2}|\sigma_2-\sigma_3|\,,\frac{1}{2}|\sigma_3-\sigma_1|\right)=k_s, \tag{3.59}$$

or

$$F(\sigma_i)=\max\left(\frac{1}{2}|\sigma_1-\sigma_2|\,,\frac{1}{2}|\sigma_2-\sigma_3|\,,\frac{1}{2}|\sigma_3-\sigma_1|\right)-k_s=0. \tag{3.60}$$

Expressed with the second and third invariant of the stress deviator, the following formulation is obtained:

$$F(J_2',J_3')=4\left(J_2'\right)^3-27\left(J_3'\right)^2-36k_s^2\left(J_2'\right)^2+96k_s^4J_2'-64k_s^6=0. \tag{3.61}$$

The graphical representation in the principal stress space is given in Fig. 3.13 where a prism of six sides with its longitudinal axis equal to the hydrostatic axis is obtained.

Table 3.10 Equivalent von Mises stress for different stress states

Stress matrix σ_{ij}	von Mises stress Eq. (3.47)	Domain ($k_t^{init} = 150$)
$\begin{bmatrix} 100 & 0 & 0 \\ 0 & 100 & 0 \\ 0 & 0 & 0 \end{bmatrix}$	100	Elastic
$\begin{bmatrix} 100 & 0 & 0 \\ 0 & -100 & 0 \\ 0 & 0 & 0 \end{bmatrix}$	173.2	Plastic
$\begin{bmatrix} 200 & 0 & 20 \\ 0 & 80 & 20 \\ 20 & 20 & 90 \end{bmatrix}$	125.3	Elastic
$\begin{bmatrix} 200 & 0 & 20 \\ 0 & 80 & 20 \\ 20 & 20 & 200 \end{bmatrix}$	129.3	Elastic
$\begin{bmatrix} 100 & 0 & 20 \\ 0 & 80 & 20 \\ 20 & 20 & -80 \end{bmatrix}$	177.8	Plastic

The view along the hydrostatic axis is shown in Fig. 3.14 where a hexagon can be seen. In addition, it can be concluded that the tensile and compressive yield stresses have the same magnitude.

The representation in the $\sqrt{3J_2'}$-J_1° space (see Fig. 3.15) shows that the yield condition is independent of the hydrostatic stress.

For a representation in the two-component principal σ_1-σ_2 space, the following six straight-line equations can be derived from Eq. (3.59) (see Fig. 3.16):

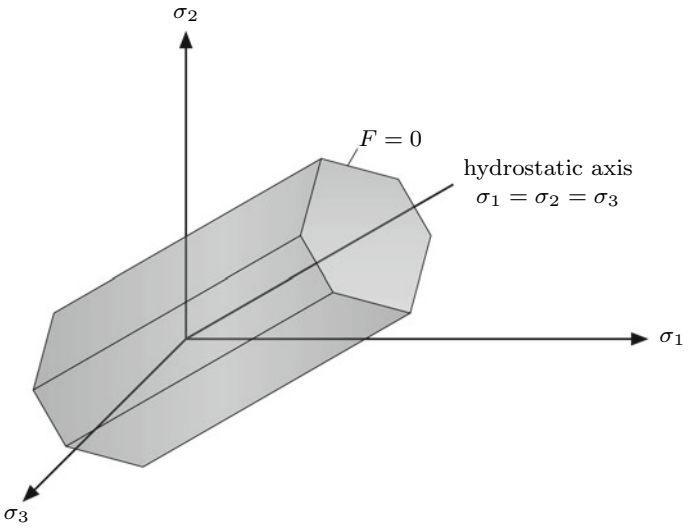

Fig. 3.13 Graphical representation of the yield condition according to Tresca in the principal stress space

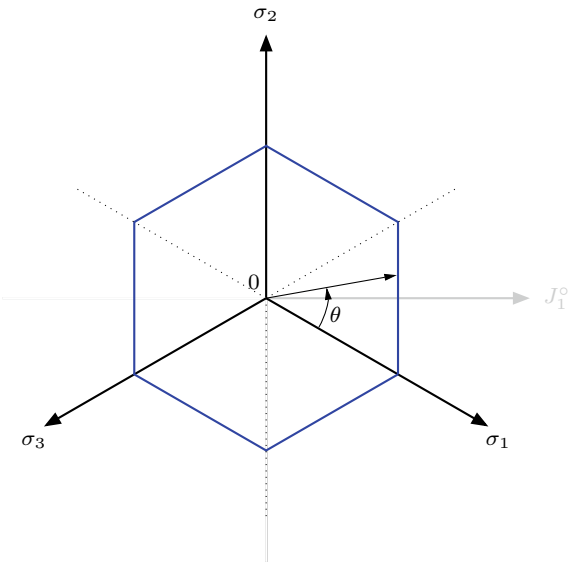

Fig. 3.14 Graphical representation of the yield condition according to Tresca in the octahedral plane

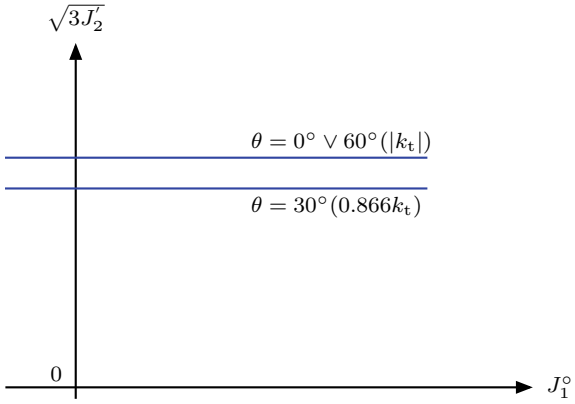

Fig. 3.15 Graphical representation of the yield condition according to Tresca in the $\sqrt{3J_2'}$-J_1° space

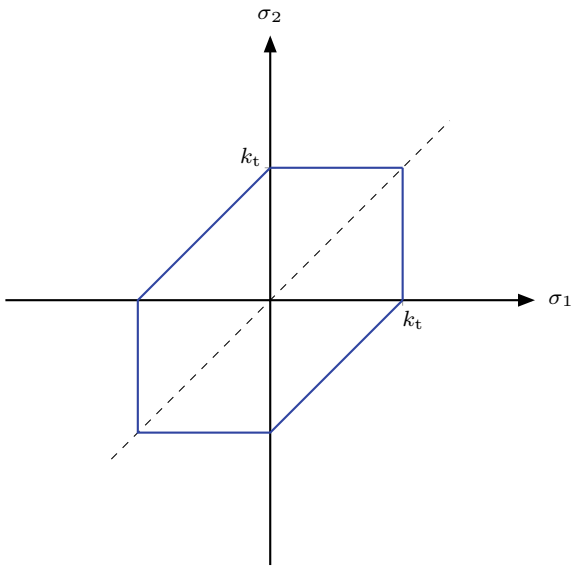

Fig. 3.16 Graphical representation of the yield condition according to Tresca in the σ_1-σ_2 space

$$
\begin{aligned}
\sigma_2^{(1)} &= \sigma_1 - 2k_s = \sigma_1 - k_t, \\
\sigma_2^{(2)} &= \sigma_1 + 2k_s = \sigma_1 + k_t, \\
\sigma_2^{(3)} &= 2k_s = k_t, \\
\sigma_2^{(4)} &= -2k_s = -k_t, \\
\sigma_1^{(5)} &= 2k_s = k_t, \\
\sigma_1^{(6)} &= -2k_s = -k_t,
\end{aligned}
\tag{3.62}
$$

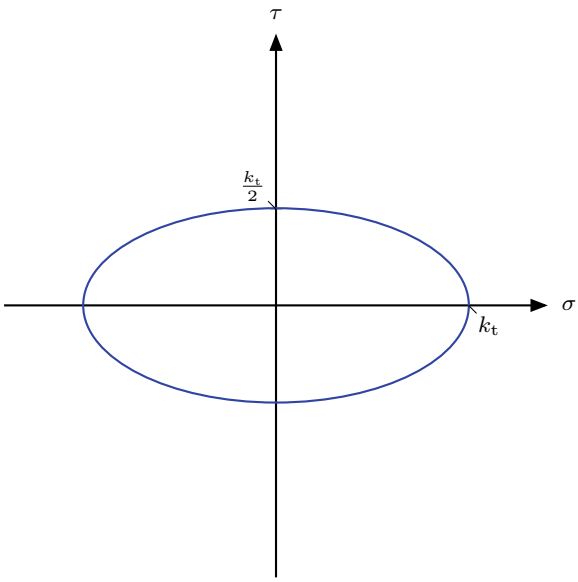

Fig. 3.17 Graphical representation of the yield condition according to Tresca in the σ-τ space

The principal stresses[5] σ_1 and σ_2 result from Mohr's circle as

$$\sigma_1 = \frac{\sigma}{2} + \sqrt{\left(\frac{\sigma}{2}\right)^2 + \tau^2} \quad ; \quad \sigma_2 = \frac{\sigma}{2} - \sqrt{\left(\frac{\sigma}{2}\right)^2 + \tau^2}. \tag{3.63}$$

Substituting Eq. (3.63) into Eq. $(3.59)_1$ yields the yield condition in the σ-τ space as (see Fig. 3.17)

$$F_{\sigma-\tau} = \left(\frac{\sigma}{2}\right)^2 + \tau^2 = k_s^2 \tag{3.64}$$

or:

$$F_{\sigma-\tau} = \left(\frac{\sigma}{k_t}\right)^2 + \left(\frac{2\tau}{k_t}\right)^2 - 1 = 0. \tag{3.65}$$

The last formulation allows to identify the relationship between the shear and tensile yield stress as:

$$k_s = \frac{k_t}{2}. \tag{3.66}$$

[5] Mohr's circle gives $\sigma_1 > 0$ and $\sigma_3 < 0$ with $\sigma_2 = 0$.

3.3.3 *Drucker-Prager Yield Condition*

The Drucker-Prager yield condition is an extension of the formulation according to von Mises (see Eq. (3.58)), which considers the influence of the weighted (factor α) hydrostatic stress (J_1°):

$$F(J_1^{\circ}, J_2') = \alpha J_1^{\circ} + \sqrt{J_2'} - k_s = 0, \tag{3.67}$$

where the α and k_s are the material parameters. It should be noted here that the von Mises yield condition is included in Eq. (3.67) for $\alpha = 0$. This condition is usually applied as a failure condition for soils, rocks, and concrete.

The representation in the $\sqrt{J_2'}$-J_1° space (see Fig. 3.18) shows that the yield condition is linearly dependent on the hydrostatic stress. This behavior would represent in the principal stress space a right-circular cone.

The view along the hydrostatic axis is shown in Fig. 3.19 where it can be seen that, as in the case of von Mises, a circle is obtained. However, the radius is now a function of the hydrostatic stress, i.e. $r = \sqrt{2}(k_s - \alpha J_1^{\circ})$. This radius reduces in the π-plane, meaning for $J_1^{\circ} = 0$ or $\sigma_m = 0$, to $r = \sqrt{2}k_s$, which is identical to the constant radius of the von Mises yield condition, see Fig. 3.10 and relation (3.57).

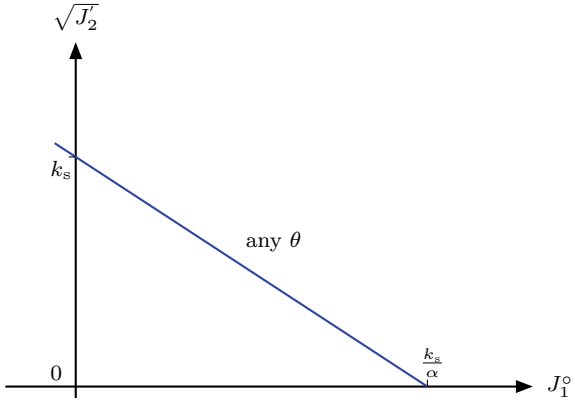

Fig. 3.18 Graphical representation of the yield condition according to Drucker-Prager in the $\sqrt{J_2'}$-J_1° space

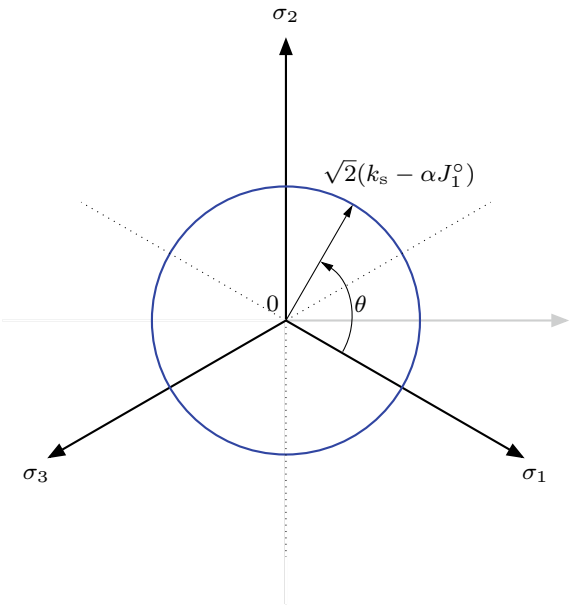

Fig. 3.19 Graphical representation of the yield condition according to Drucker-Prager in an octahedral plane ($\sigma_m = \text{const.}$)

Substituting the equations from Table 3.5 for the basic invariants (σ_1-σ_2 space) into Eq. (3.67), the representation in the two-component principal σ_1-σ_2 space is obtained as

$$F_{\sigma_1-\sigma_2} = \left(1 - 3\alpha^2\right)\left(\sigma_1^2 + \sigma_2^2\right) - \left(1 + 6\alpha^2\right)\sigma_1\sigma_2 + 6\alpha k_s\left(\sigma_1 + \sigma_2\right) - 3k_s^2, \quad (3.68)$$

or after some transformations the equation of a shifted and rotated ellipse in the σ_1-σ_2 space is obtained as (see Fig. 3.20):

$$F_{\sigma_1-\sigma_2} = \left(\frac{x + \frac{6\sqrt{2}k_s\alpha}{1-12\alpha^2}}{\frac{\sqrt{6}k_s}{1-12\alpha^2}}\right)^2 + \left(\frac{y}{\frac{\sqrt{2}k_s}{\sqrt{1-12\alpha^2}}}\right)^2 - 1 = 0, \quad (3.69)$$

where

$$x = \frac{1}{\sqrt{2}}\left(\sigma_1 + \sigma_2\right), \quad y = \frac{1}{\sqrt{2}}\left(\sigma_2 - \sigma_1\right). \quad (3.70)$$

The transformation of Eq. (3.68) into Eq. (3.69) can be obtained in the following way:

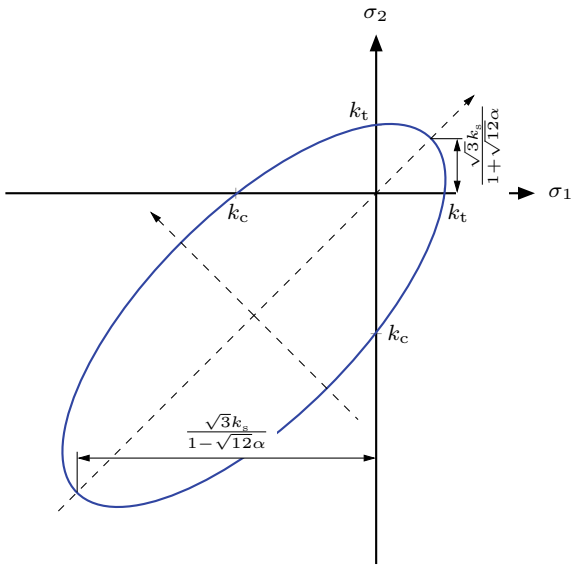

Fig. 3.20 Graphical representation of the yield condition according to Drucker-Prager in the σ_1-σ_2 space

$$
\begin{aligned}
&\frac{1}{3}\left(\sigma_1^2+\sigma_2^2-\sigma_1\sigma_2\right)=k_s^2-2k_s\alpha\left(\sigma_1+\sigma_2\right)+\alpha^2\left(\sigma_1+\sigma_2\right)^2 \mid \times 12,\\
&4\left(\sigma_1^2+\sigma_2^2-\sigma_1\sigma_2\right)=12k_s^2-24k_s\alpha\left(\sigma_1+12\sigma_2\right)+12\alpha^2\left(\sigma_1+\sigma_2\right)^2,\\
&\sigma_1^2+2\sigma_1\sigma_2+\sigma_2^2+3\left(\sigma_1^2-2\sigma_1\sigma_2+\sigma_2^2\right)=12k_s^2-24k_s\alpha\left(\sigma_1+12\sigma_2\right)\\
&\quad+12\alpha^2\left(\sigma_1+\sigma_2\right)^2,\\
&\left(\sigma_1+\sigma_2\right)^2+3\left(\sigma_1-\sigma_2\right)^2=12k_s^2-24k_s\alpha\left(\sigma_1+12\sigma_2\right)+12\alpha^2\left(\sigma_1+\sigma_2\right)^2,\\
&\left(\sigma_1+\sigma_2\right)^2+3\left(\sigma_1-\sigma_2\right)^2+24k_s\alpha\left(\sigma_1+12\sigma_2\right)-12\alpha^2\left(\sigma_1+\sigma_2\right)^2\\
&\quad=\left(\frac{12k_s^2}{1-12\alpha^2}-\frac{12\alpha^2k_s^2}{1-12\alpha^2}\right),\\
&3\left(1-12\alpha^2\right)\left(\sigma_1-\sigma_2\right)^2+\left(1-12\alpha^2\right)^2\left(\sigma_1+\sigma_2\right)^2\\
&\quad+2\times12k_s\alpha\left(1-12\alpha^2\right)\left(\sigma_1+\sigma_2\right)+12^2\alpha^2k_s^2=12k_s^2,\\
&3\left(1-12\alpha^2\right)\left(\sigma_1-\sigma_2\right)^2+\left(\left(1-12\alpha^2\right)\left(\sigma_1+\sigma_2\right)+12k_s\alpha\right)^2=12k_s^2,\\
&\frac{\left(1-12\alpha^2\right)\left(\sigma_1-\sigma_2\right)^2}{4k_s^2}+\frac{\left(\left(1-12\alpha^2\right)\left(\sigma_1+\sigma_2\right)+12k_s\alpha\right)^2}{12k_s^2}=1.
\end{aligned}
\tag{3.71}
$$

The same procedure yields under consideration of $k_s^2=\frac{k_s^2}{1-3\alpha^2}-\frac{3\alpha^2k_s^2}{1-3\alpha^2}$ also to a shifted ellipse in the σ-τ space (see Fig. 3.21):

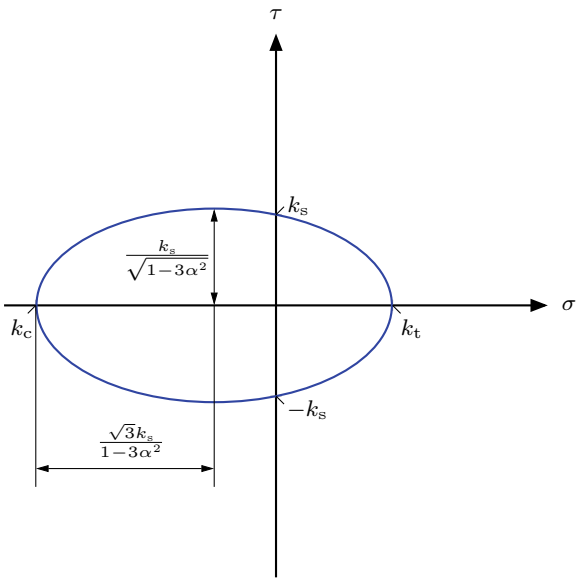

Fig. 3.21 Graphical representation of the yield condition according to Drucker-Prager in the σ-τ space

$$\left(\frac{\sigma + \frac{3k_s\alpha}{1-3\alpha^2}}{\frac{\sqrt{3}k_s}{1-3\alpha^2}}\right)^2 + \left(\frac{\tau}{\frac{k_s}{\sqrt{1-3\alpha^2}}}\right)^2 - 1 = 0. \tag{3.72}$$

Setting $\tau \to 0$ in the last relation allows to extract the relation between the tensile/compressive yield stress and the shear limit ($\sigma \to k_t \wedge \sigma \to k_c$) as:

$$k_t = \frac{\sqrt{3}}{1+\sqrt{3}\alpha}k_s, \quad k_c = \frac{\sqrt{3}}{1-\sqrt{3}\alpha}k_s. \tag{3.73}$$

Finally, it should be noted here that also the formulation

$$F(J_1^o, J_2') = \alpha J_1^o + \sqrt{J_2'} - \frac{\bar{\sigma}}{\sqrt{3}} = 0, \tag{3.74}$$

where

$$\bar{\sigma} = (1 + \alpha\sqrt{3})k_t \tag{3.75}$$

and the alternative expression linear Mohr-Coulomb can be found in literature.

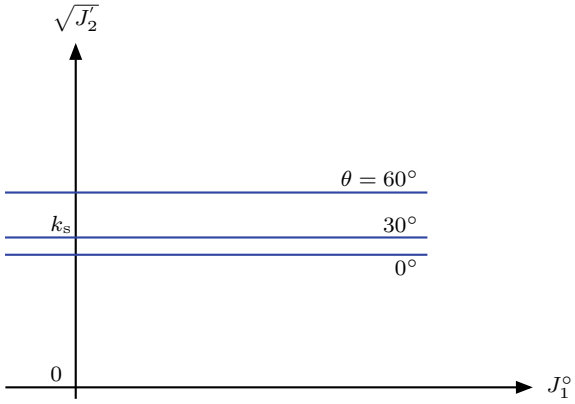

Fig. 3.22 Graphical representation of the yield condition according to Sayir ($\alpha = 1.25$) in the $\sqrt{3J_2'}$-J_1° space

3.3.4 Sayir Yield Condition

The yield condition proposed by Sayir [13, 21, 22] is a simple linear combination of the second and third deviator invariant in the form

$$F(J_2', J_3') = J_2' + \frac{\alpha}{k_t} J_3' - k_s^2 = 0, \tag{3.76}$$

which allows to consider a difference in the tensile and compressive yield stress for isotropic materials. Based on the requirement for convexity, it can be shown that the scalar parameter α must be in the following boundaries [21]:

$$-3 \leq \alpha \leq 1.5. \tag{3.77}$$

The representation in the $\sqrt{J_2'}$-J_1° space (see Fig. 3.22) shows that the yield condition is independent of the hydrostatic stress. However, different values are obtained for different Lode angles θ. This means that we must expect a clear deviation from a circular shape in an octahedral plane.

The view along the hydrostatic axis is shown in Fig. 3.23 where it can be seen that, the boundaries of the limit surfaces for $\alpha = 1.5$ or $\alpha = -3$, i.e. the convexity limits, are rather straight lines representing triangles.

Substituting the equations from Table 3.5 for the basic invariants (σ_1-σ_2 space) into Eq. (3.67), the representation in the two-component principal σ_1-σ_2 space is obtained as (see Fig. 3.24)

$$F_{\sigma_1-\sigma_2} = \frac{1}{3}\left(\sigma_1^2 + \sigma_2^2 - \sigma_1\sigma_2\right) + \frac{\alpha}{27k_t}\left(2\sigma_1^3 + 2\sigma_2^3 - 3\sigma_1\sigma_2(\sigma_1 + \sigma_2)\right) - k_s^2 = 0. \tag{3.78}$$

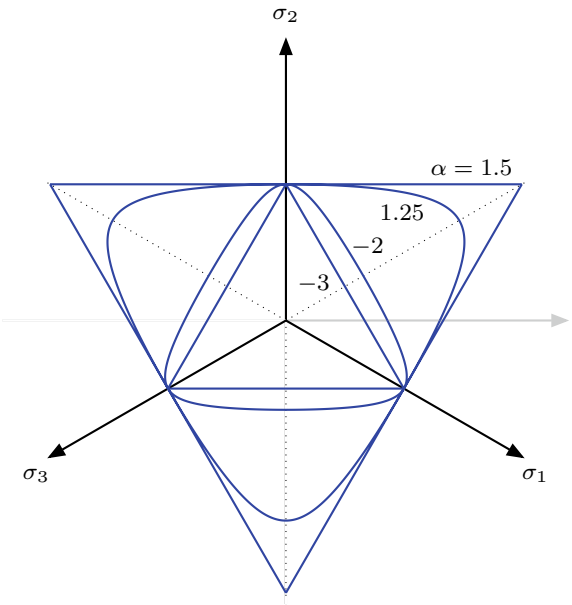

Fig. 3.23 Graphical representation of the yield condition according to Sayir in an octahedral plane ($\sigma_m = \text{const.}$)

A representation in the two-component normal/shear σ-τ space is obtained by substituting the particular basic invariant formulations (σ-τ space) from Table 3.5 into Eq. (3.76) to finally give the following representation (see Fig. 3.25):

$$F_{\sigma-\tau} = \frac{1}{3}\sigma^2 + \tau^2 + \frac{\alpha}{k_t}\left(\frac{2}{27}\sigma^3 + \frac{1}{3}\sigma\tau^2\right) - k_s^2 = 0. \tag{3.79}$$

Setting $\tau \to 0$ in the last relation allows to extract a simple relation between the tensile yield stress and the shear limit ($\sigma > 0 \to k_t$) as:

$$k_s = \sqrt{\frac{1}{3} + \frac{2}{27}\alpha} \cdot k_t. \tag{3.80}$$

Unfortunately does the setting $\tau \to 0$ together with ($\sigma < 0 \to k_c$) not provide such a simple relationship:

$$\frac{1}{3}k_c^2 + \frac{2}{27}\alpha\frac{k_c^3}{k_t} - k_s^2 = 0, \tag{3.81}$$

or under consideration of Eq. (3.80)

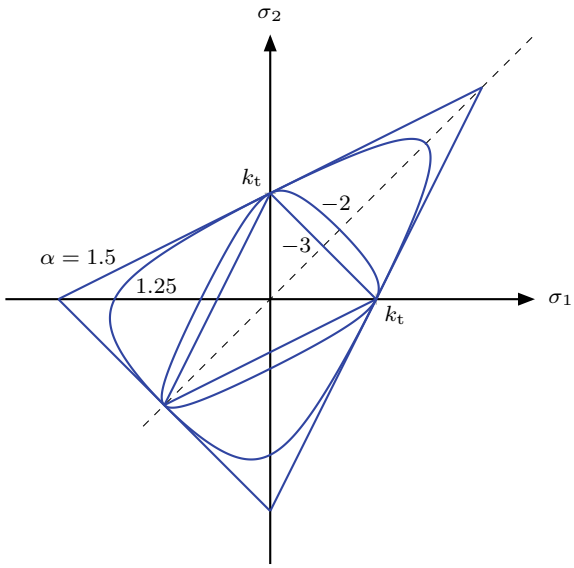

Fig. 3.24 Graphical representation of the yield condition according to Sayir in the σ_1-σ_2 space

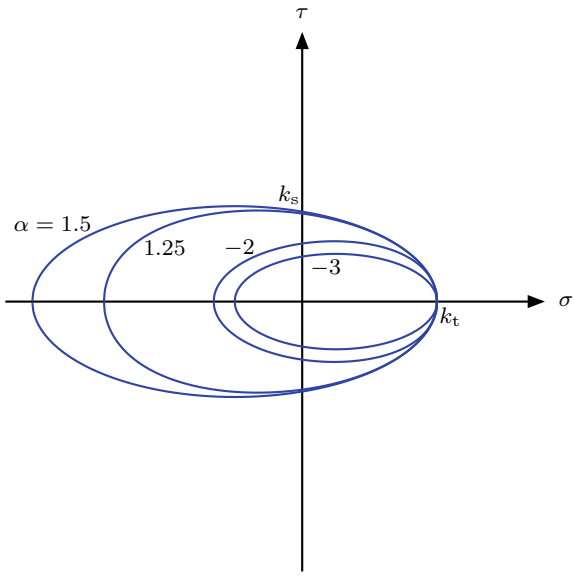

Fig. 3.25 Graphical representation of the yield condition according to Sayir in the σ-τ space

$$\frac{1}{3}k_c^2 + \frac{2}{27}\alpha\frac{k_c^3}{k_t} - \left(\frac{1}{3} + \frac{2}{27}\alpha\right)k_t^2 = 0, \tag{3.82}$$

which allows a numerical evaluation of the relationship between the compressive and shear yield stress.

3.4 Flow Rule

The flow rule, which allows the evaluation of the plastic strain increments, in its general form is given by

$$\mathrm{d}\varepsilon^{\mathrm{pl}} = \mathrm{d}\lambda\, \boldsymbol{r}(\boldsymbol{\sigma}, \boldsymbol{q}), \tag{3.83}$$

where $\mathrm{d}\lambda$ is a scalar called the plastic multiplier or consistency parameter and function $\boldsymbol{r}(\boldsymbol{\sigma}, \boldsymbol{q}) : (\mathbb{R}^6 \times \mathbb{R}^{\dim(q)} \to \mathbb{R}^6)$ is the plastic flow direction. The plastic flow direction is often stated in terms of a plastic potential function Q and the plastic strain increments are given by $\mathrm{d}\varepsilon^{\mathrm{pl}} = \mathrm{d}\lambda \frac{\partial Q}{\partial \boldsymbol{\sigma}}$. The flow is said to be associated if $Q = F$, otherwise non-associated.

The evolution equation for the internal variables $\boldsymbol{q}$ can be specified in its general form as

$$\mathrm{d}\boldsymbol{q} = \mathrm{d}\lambda\, \boldsymbol{h}(\boldsymbol{\sigma}, \boldsymbol{q}), \tag{3.84}$$

where the function $\boldsymbol{h} : (\mathbb{R}^6 \times \mathbb{R}^7 \to \mathbb{R}^7)$ describes the evolution of the hardening parameters.

3.5 Hardening Rule

The hardening rule allows the consideration of the influence of material hardening on the yield condition and the flow rule.

3.5.1 Isotropic Hardening

In the case of isotropic hardening, the yield stress is expressed as being dependent on an inner variable κ:

$$k = k(\kappa). \tag{3.85}$$

This results in the effect that the size of the yield surface is scaled but the origin remains unchanged. If the equivalent plastic strain[6] is used for the hardening variable ($\kappa = \varepsilon^{\mathrm{pl}}_{\mathrm{eff}}$), then one talks about strain hardening.

Another possibility is to describe the hardening being dependent on the specific[7] plastic work ($\kappa = w^{\mathrm{pl}} = \int \boldsymbol{\sigma}\, \mathrm{d}\varepsilon^{\mathrm{pl}}$). Then one talks about work hardening.

---

[6] The effective plastic strain is in the general three-dimensional case the function $\varepsilon^{\mathrm{pl}}_{\mathrm{eff}} : (\mathbb{R}^6 \to \mathbb{R}_+)$ with $\varepsilon^{\mathrm{pl}}_{\mathrm{eff}} = \sqrt{\frac{2}{3}\boldsymbol{\varepsilon}^{\mathrm{pl}}\boldsymbol{\varepsilon}^{\mathrm{pl}}}$.

[7] This is the volume-specific definition, meaning $\left[w^{\mathrm{pl}}\right] = \frac{\mathrm{N}}{\mathrm{m}^2}\frac{\mathrm{m}}{\mathrm{m}} = \frac{\mathrm{kg\,m}}{\mathrm{s}^2\mathrm{m}^2}\frac{\mathrm{m}}{\mathrm{m}} = \frac{\mathrm{kg\,m}^2}{\mathrm{s}^2\mathrm{m}^3} = \frac{\mathrm{J}}{\mathrm{m}^3}$.

Figure 2.3 shows different modeling approaches for the flow curve, meaning the graphical illustration of the yield stress being dependent on the inner variable for different hardening approaches.

3.5.2 Kinematic Hardening

In the case of pure kinematic hardening, the yield condition is expressed as being dependent on a set of inner variables:

$$F(\boldsymbol{\sigma}, \boldsymbol{\alpha}) = f(\boldsymbol{\sigma} - \boldsymbol{\alpha}) - k = 0, \tag{3.86}$$

where the material parameter k is constant and the kinematic hardening parameters $\boldsymbol{\alpha}$ are dependent on inner variables. These hardening parameters represent the center of the yield surface and result in the effect that the surface translates as a rigid body in the stress space.

References

1. Altenbach H, Altenbach J, Zolochevsky A (1995) Erweiterte Deformationsmodelle und Versagenskriterien der Werkstoffmechanik. Deutscher Verlag für Grundstoffindustrie, Stuttgart
2. Altenbach H (2012) Kontinuumsmechanik: Einführung in die materialunabhängigen und materialabhängigen Gleichungen. Springer, Berlin
3. Altenbach H, Öchsner A (eds) (2020) Encyclopedia of continuum mechanics. Springer, Berlin
4. Backhaus G (1983) Deformationsgesetze. Akademie-Verlag, Berlin
5. Betten J (1987) Tensorrechnung für Ingenieure. Teubner Verlag, Stuttgart
6. Chen WF, Han DJ (1988) Plasticity for structural engineers. Springer, New York
7. Itskov M (2009) Tensor algebra and tensor analysis for engineers: with applications to continuum mechanics. Springer, Berlin
8. Lurie AI, Belyaev A (2005) Theory of elasticity. Springer, Berlin
9. Betten J (2001) Kontinuumsmechanik. Springer, Berlin
10. Moore TA (2013) A general relativity workbook. University Science Books, Mill Valley
11. Suzuki H, Ninomiya T, Sumino K, Takeuchi (1985) Dislocation in solids: proceedings of the IX Yamada. VNU Science Press, Utrecht
12. Gurson AL (1977) Continuum theory of ductile rupture by void nucleation and growth: part I—yield criteria and flow rules for ductile media. J Eng Mater-T ASME 99:2–15
13. Betten J (1976) Plastische Anisotropie und Bauschinger-Effekt; allgemeine Formulierung und Vergleich mit experimentell ermittelten Fließortkurven. Acta Mech 25:79–94
14. Öchsner A (2016) Continuum damage and fracture mechanics. Springer, Singapore
15. Chen WF, Zhang H (1991) Structural plasticity: theory, problems, and CAE software. Springer, New York
16. Nayak GC, Zienkiewicz OC (1972) Convenient form of stress invariants for plasticity. J Struct Div-ASCE 98:1949–954
17. Öchsner A (2003) Experimentelle und numerische Untersuchung des elastoplastischen Verhaltens zellularer Modellwerkstoffe. VDI-Verlag, Düsseldorf
18. Bardenheier R (1982) Mechanisches Versagen von Polymerwerkstoffen: Anstrengungsbewertung mehrachsialer Spannungszustände. Carl Hanser Verlag, München

19. Asaro RJ, Lubarda VA (2006) Mechanics of solids and materials. Cambridge University Press, Cambridge
20. Nash WA (1998) Schaum's outline of theory and problems of strength of material. McGraw-Hill, New York
21. Betten J (1979) Über die Konvexität von Fließkörpern isotroper und anisotroper Stoffe. Acta Mech 32:233–247
22. Sayir M (1970) Zur Fließbedingung der Plastizitätstheorie. Ing Arch 39:414–432

Chapter 4
Elasto-plastic Finite Element Simulations

Abstract This chapter presents an introduction to the integration of the elasto-plastic constitutive law in the context of the finite element method. The different concepts are described in detail for one-dimensional problems and only afterwards generalized to the multiaxial stress state. In the context of numerical approximation methods, the so-called predictor-corrector methods are used to integrate the material equations.

4.1 Approach for One-Dimensional Problems

4.1.1 Integration of the Material Equations

The treatment of elasto-plastic finite element simulation is covered in many articles and book publications. Table 4.1 summarizes a few recommended textbooks on this topic.

In comparison to a finite element calculation with pure linear-elastic material behavior, the calculation at a simulation of plastic material behavior cannot be conducted in one step any longer, since at this point in general no obvious connection between stress and strain exists.[1] The load is instead applied incrementally, whereupon in each increment a nonlinear system of equations has to be solved (for example with the Newton-Raphson algorithm). The principal finite element equation therefore has to be set in the following incremental form:

$$\boldsymbol{K}(\Delta \boldsymbol{u})\Delta \boldsymbol{u} = \Delta \boldsymbol{f}, \tag{4.1}$$

where $\boldsymbol{K}$ is the global stiffness matrix, $\boldsymbol{u}$ is the column matrix of nodal unknowns and $\boldsymbol{f}$ is the column matrix of external loads.

Additionally, the state variables—as for example the stress σ_{n+1}—have to be calculated for each increment $(n+1)$ in each integration point (Gauss point), based

[1] In the general case with six stress and strain components (under consideration of the symmetry of the stress and strain tensor) an obvious relation only exists between effective stress and effective plastic strain. In the one-dimensional case however these parameters reduce to: $\sigma_{\text{eff}} = |\sigma|$ and $\varepsilon^{\text{pl}}_{\text{eff}} = |\varepsilon^{\text{pl}}|$.

A. Öchsner, *Elements of Classical Plasticity Theory*,
https://doi.org/10.1007/978-3-031-14201-7_4

Table 4.1 Recommended textbooks for the treatment of elasto-plastic finite element simulations

Year (1st ed.)	Author	Title	Reference
1980	D. R. J. Owen, E. Hinton	Finite Elements in Plasticity: Theory and Practice	[1]
1991	M. A. Crisfield	Non-Linear Finite Element Analysis of Solids and Structures. Volume 1: Essentials	[2]
1997	M. A. Crisfield	Non-Linear Finite Element Analysis of Solids and Structures. Volume 2: Advanced Topics	[3]
1998	J. C. Simo, T. J. R. Hughes	Computational Inelasticity	[4]
2000	T. Belytschko, W. K. L. Liu, B. Moran	Nonlinear Finite Elements for Continua and Structures	[5]
	I. Doltsinis	Elements of Plasticity: Theory and Computation	[6]
2004	J. N. Reddy	An Introduction to Nonlinear Finite Element Analysis	[7]
2005	F. Dunne, N. Petrinic	Introduction to Computational Plasticity	[8]
2008	P. Wriggers	Nonlinear Finite Element Methods	[9]
2008	N. E. A. de Souza, D. Perić, D. R. J. Owen	Computational Methods for Plasticity	[10]
2010	A. Anandarajah	Computational Methods in Elasticity and Plasticity: Solids and Porous Media	[11]
2013	R. I. Borja	Plasticity: Modeling & Computation	[12]
2013	A. Öchsner, M. Merkel	One-Dimensional Finite Elements: An Introduction to the FE Method	[13]
2018	M. Trapp, A. Öchsner	Computational Plasticity for Finite Elements: A Fortran-Based Introduction	[14]

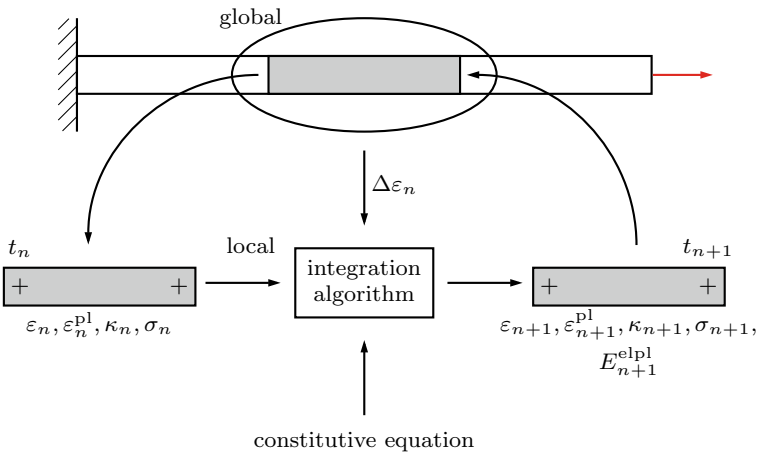

Fig. 4.1 Schematic illustration of the integration algorithm for plastic material behavior in the FEM; adopted from [9]. Integration points are marked schematically through the symbol '**+**'

on the stress state at the end of the previous increment (n) and the given strain increment ($\Delta\varepsilon_n$) (see Fig. 4.1).

To that, the explicit material law in infinitesimal form given has to be integrated numerically according to Eqs. (2.2) and (2.41). Explicit integration methods, as for example the Euler procedure[2] however are inaccurate and possibly unstable, since a global error could accumulate [2]. Within the FEM one uses so-called predictor-corrector methods (see Fig. 4.2), in which, first a so-called predictor is explicitly determined and afterwards implicitly corrected instead of explicit integration procedures. In a first step, a test stress state (the so-called trial stress condition) is calculated under the assumption of pure linear-elastic material behavior via an elastic predictor:[3]

$$\sigma_{n+1}^{\mathrm{trial}} = \sigma_n + \underbrace{E\Delta\varepsilon_n}_{\text{predictor } \Delta\sigma_n^{\mathrm{el}}} \quad . \tag{4.2}$$

The given hardening condition in this test stress state equals the condition at the end of the previous increment. Therefore, it is assumed that the load step occurs pure elastically, meaning without plastic deformation and therefore without hardening:

[2] The explicit Euler procedure or polygon method (also Euler-Cauchy method) is the most simple procedure for the numerical solution of an initial value problem. The new stress state results according to this procedure in $\sigma_{n+1} = \sigma_n + E_n^{\mathrm{elpl}}\Delta\varepsilon$, whereupon the initial value problem can be named as $\frac{\mathrm{d}\sigma}{\mathrm{d}\varepsilon} = E^{\mathrm{elpl}}(\sigma, \varepsilon)$ with $\sigma(\varepsilon_0) = \sigma_0$.

[3] In the general three-dimensional case the relation is applied on the stress matrix and the increment of the strain matrix: $\boldsymbol{\sigma}_{n+1}^{\mathrm{trial}} = \boldsymbol{\sigma}_n + \boldsymbol{C}\Delta\boldsymbol{\varepsilon}_n$.

$$\kappa_{n+1}^{\text{trial}} = \kappa_n. \tag{4.3}$$

Based on the location of the test stress state in the stress space two elementary conditions can be distinguished with the help of the yield condition:

(a) The stress state is in the elastic area (see Fig. 4.2a) or on the yield surface boundary (valid stress state):

$$F(\sigma_{n+1}^{\text{trial}}, \kappa_{n+1}^{\text{trial}}) \leq 0. \tag{4.4}$$

In this case, the test state can be taken on as the new stress/hardening state, since it equals the real state:

$$\sigma_{n+1} = \sigma_{n+1}^{\text{trial}}, \tag{4.5}$$

$$\kappa_{n+1} = \kappa_{n+1}^{\text{trial}}. \tag{4.6}$$

In conclusion, one proceeds to the next increment.

(b) The stress state is outside the yield surface boundary (invalid stress state), see Fig. 4.2b, c:

$$F(\sigma_{n+1}^{\text{trial}}, \kappa_{n+1}^{\text{trial}}) > 0. \tag{4.7}$$

If this case occurs, a valid state ($F(\sigma_{n+1}, \kappa_{n+1}) = 0$) on the yield surface boundary is calculated in the second part of the procedure from the invalid test state. Therefore, the necessary stress difference

$$\Delta\sigma^{\text{pl}} = \sigma_{n+1}^{\text{trial}} - \sigma_{n+1} \tag{4.8}$$

is referred to as the plastic corrector.

For the calculation of the plastic corrector, the terms back projection, return mapping or catching up are used. Figure 4.3 compares the predictor-corrector approaches schematically in the one-dimensional stress space.

In the following the back projection is considered closely. Detailed descriptions can be found in [2–5, 8, 10].

The stress difference between initial and final state (stress increment)

$$\Delta\sigma_n = \sigma_{n+1} - \sigma_n \tag{4.9}$$

results, according to Hooke's law from the elastic part of the strain increment, which results as the difference from the total strain increment and its plastic part:

$$\Delta\sigma_n = E\Delta\varepsilon_n^{\text{el}} = E(\Delta\varepsilon_n - \Delta\varepsilon_n^{\text{pl}}). \tag{4.10}$$

Figure 4.4 shows that the total strain increment in dependence on the trial stress state can be illustrated as follows:

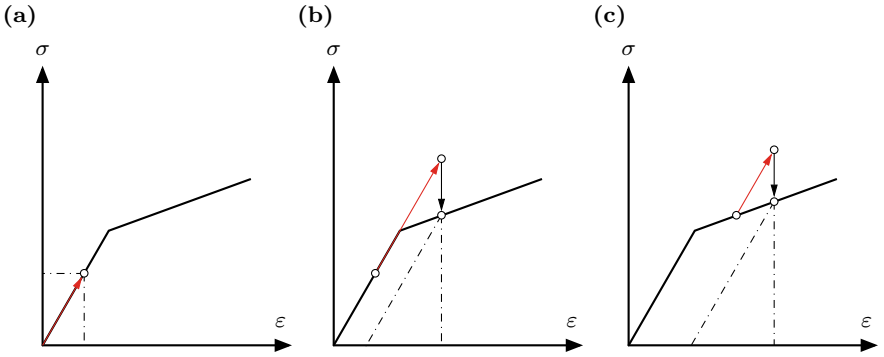

Fig. 4.2 Schematic illustration of the predictor-corrector method in the stress-strain diagram: **a** elastic predictor in the elastic area; **b**, **c** elastic predictor outside the yield surface boundary

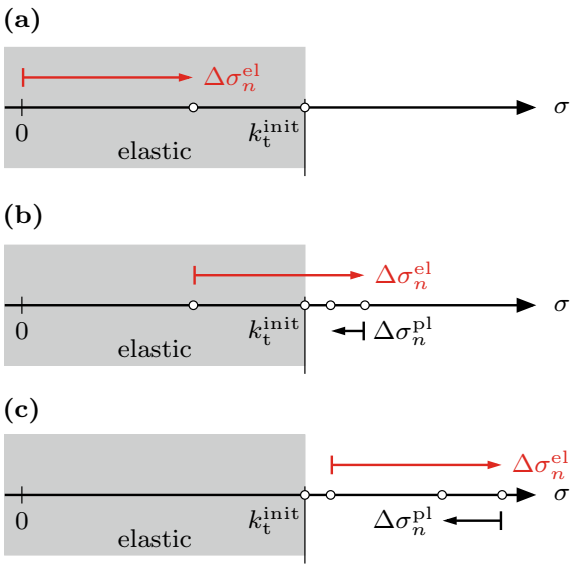

Fig. 4.3 Schematic illustration of the predictor-corrector method in the one-dimensional stress space: **a** elastic predictor in the elastic area; **b**, **c** elastic predictor outside of the initial yield surface

$$\Delta\varepsilon_n = \varepsilon_{n+1} - \varepsilon_n = \frac{1}{E}\left(\sigma_{n+1}^{\mathrm{trial}} - \sigma_n\right). \tag{4.11}$$

If the last equation as well as the flow rule[4] according to Eq. (2.14) are inserted in Eq. (4.10), the final stress state σ_{n+1} in dependence on the trial stress state $\sigma_{n+1}^{\mathrm{trial}}$ results in:

[4] At this point within the notation it is formally switched from $\mathrm{d}\lambda$ to $\Delta\lambda$. Therefore the transition from the differential to the incremental notation occurs.

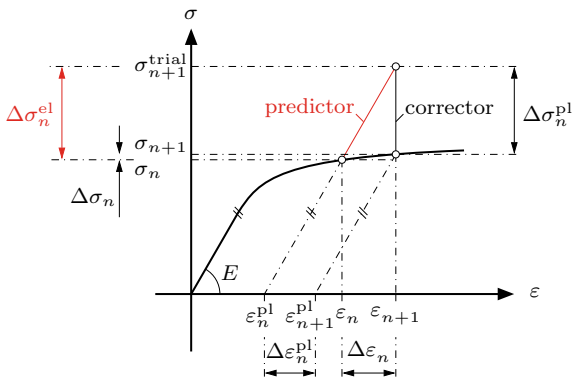

Fig. 4.4 Schematic illustration of the back projection in the stress-strain diagram. Adapted from [4]

$$\sigma_{n+1} = \sigma_{n+1}^{\text{trial}} - \Delta\lambda_{n+1} E \operatorname{sgn}(\sigma). \tag{4.12}$$

Dependent on the location of the evaluation of the function $\operatorname{sgn}(\sigma)$ different methods result in the general case (see Table 4.2) to calculate the initial value for the plastic corrector or alternatively to define the final stress state iteratively. To obtain an initial value for the plastic corrector, $\operatorname{sgn}(\sigma)$ can either be evaluated in the trial stress state (backward-Euler) or on the yield surface (forward-Euler; at the transition from the elastic to the plastic area this is the initial yield surface, see Fig. 4.2b). If the function $\operatorname{sgn}(\sigma)$ is evaluated in the final state at the iterative calculation, the normal rule (see Sect. 2.3) is fulfilled in the final state. For this fully implicit backward-Euler algorithm (also referred to as the closest point projection (CPP)) [4] however in the general three-dimensional case derivatives of higher order must be calculated. In the so-called cutting-plane algorithm [15] the function $\operatorname{sgn}(\sigma)$ is calculated in the stress state of the i-th iteration step. The normal rule is not exactly fulfilled in the final state, however no calculations of derivatives of higher order are necessary. At the so-called mid-point rule [16] the function $\operatorname{sgn}(\sigma)$ is evaluated in the final state and on the yield surface as well as weighted in equal parts. If the function $\operatorname{sgn}(\sigma)$ is only evaluated on the yield surface, this leads to the semi-implicit backward-Euler algorithm [17], for which only derivatives of first order are necessary.

If one considers the dependency of the yield condition from the hardening variable, one needs another equation, which describes the hardening. From the evolution equation of the hardening variables (2.17) the following incremental relation results

$$\kappa_{n+1} = \kappa_n + \Delta\lambda_{n+1} \tag{4.13}$$

for the definition of the hardening variable.

Finally it can be remarked that three of the listed integration rules in Table 4.2 can be summarized via the following equation

Table 4.2 Overview over the predictor-corrector methods

Location of the evaluation of sgn(n)	Equation (4.12)
Initial value for corrector	
Trial condition	$\sigma_{n+1} = \sigma_{n+1}^{\text{trial}} - \Delta\lambda_{n+1} E \operatorname{sgn}(\sigma_{n+1}^{\text{trial}})$
On the flow curve	$\sigma_{n+1} = \sigma_{n+1}^{\text{trial}} - \Delta\lambda_{n+1} E \operatorname{sgn}(\sigma_n)$
During the iteration	
In the final stress state (fully impl. backward-Euler alg.) (closest point projection)	$\sigma_{n+1} = \sigma_{n+1}^{\text{trial}} - \Delta\lambda_{n+1} E \operatorname{sgn}(\sigma_{n+1})$
On the flow curve (semi-impl. backward-Euler alg.)	$\sigma_{n+1} = \sigma_{n+1}^{\text{trial}} - \Delta\lambda_{n+1} E \operatorname{sgn}(\sigma_n)$
In the final state and on the flow curve (mid-point rule)	$\sigma_{n+1} = \sigma_{n+1}^{\text{trial}} - \Delta\lambda_{n+1} E \frac{1}{2} \times (\operatorname{sgn}(\sigma_{n+1}) + \operatorname{sgn}(\sigma_n))$
Stress state of i-th iteration step (cutting-plane algorithm)	$\sigma_{n+1} = \sigma_{n+1}^{\text{trial}} - \Delta\lambda_{n+1} E \operatorname{sgn}(\sigma^{(i)})$

$$\sigma_{n+1} = \sigma_{n+1}^{\text{trial}} - \Delta\lambda_{n+1} E \left([1-\eta]\operatorname{sgn}(\sigma_n) + \eta \operatorname{sgn}(\sigma_{n+1})\right). \tag{4.14}$$

The parameter η then becomes 1, 0 or $\frac{1}{2}$.

4.1.2 Derivation of the Fully Implicit Backward-Euler Algorithm for Isotropic Hardening

4.1.2.1 Mathematical Derivation

In this back projection method, the stress location on the yield surface, which is energetically closest to the test state (see Sect. 4.1.2.2) is calculated. Therefore this does not involve, as the name suggests, a calculation of the closest geometric point. The assumption that the plastic work takes on a maximum at a given strain serves as a basis for the method. Together with the elementary demand that the calculated stress state has to lie on the flow curve (yield surface), the CPP method can be interpreted in the mathematical sense as a solution of an extremal value problem (maximum of the plastic work) with side-conditions (the unknown stress condition has to be on the

yield surface) [4]. The method is hereby implicit in the calculation of the function $\operatorname{sgn}(\sigma)$ since the evaluation occurs in the final state $n+1$. Because of this, the CPP algorithm is also referred to as the fully implicit backward-Euler algorithm. In the final state the following equations are therefore fulfilled:

$$\sigma_{n+1} = \sigma_{n+1}^{\text{trial}} - \Delta\lambda_{n+1} E \operatorname{sgn}(\sigma_{n+1}), \tag{4.15}$$

$$\kappa_{n+1} = \kappa_n + \Delta\lambda_{n+1}, \tag{4.16}$$

$$F = F(\sigma_{n+1}, \kappa_{n+1}) = 0. \tag{4.17}$$

Outside of the final state, however, at each of these equations a residual[5] r remains:

$$\begin{aligned} r_\sigma(\sigma, \kappa, \Delta\lambda) &= \sigma - \sigma_{n+1}^{\text{trial}} + \Delta\lambda E \operatorname{sgn}(\sigma) \neq 0 \quad \text{or} \\ &= E^{-1}\sigma - E^{-1}\sigma_{n+1}^{\text{trial}} + \Delta\lambda \operatorname{sgn}(\sigma) \neq 0, \end{aligned} \tag{4.18}$$

$$\begin{aligned} r_\kappa(\kappa, \Delta\lambda) &= \kappa - \kappa_n - \Delta\lambda \neq 0 \quad \text{or} \\ &= -\kappa + \kappa_n + \Delta\lambda \neq 0, \end{aligned} \tag{4.19}$$

$$r_F(\sigma, \kappa) = F(\sigma, \kappa) = |\sigma| - k(\kappa) \neq 0. \tag{4.20}$$

The unknown stress/hardening state therefore represents the root of a vector function $\boldsymbol{m}$, which consists of the single residual functions. Furthermore, it seems to make sense to also summarize the arguments for a single vector argument $\boldsymbol{v}$:

$$\boldsymbol{m}(\boldsymbol{v}) \in (\mathbb{R}^3 \to \mathbb{R}^3) = \begin{bmatrix} r_\sigma(\boldsymbol{v}) \\ r_\kappa(\boldsymbol{v}) \\ r_F(\boldsymbol{v}) \end{bmatrix}, \quad \boldsymbol{v} = \begin{bmatrix} \sigma \\ \kappa \\ \Delta\lambda \end{bmatrix}. \tag{4.21}$$

The Newton method (iteration index: i) is commonly used for the determination of the root:[6]

$$\boldsymbol{v}^{(i+1)} = \boldsymbol{v}^{(i)} - \left(\frac{\mathrm{d}\boldsymbol{m}}{\mathrm{d}\boldsymbol{v}}(\boldsymbol{v}^{(i)}) \right)^{-1} \boldsymbol{m}(\boldsymbol{v}^{(i)}), \tag{4.22}$$

whereupon the following

$$\boldsymbol{v}^{(0)} = \begin{bmatrix} \sigma^{(0)} \\ \kappa^{(0)} \\ \Delta\lambda^{(0)} \end{bmatrix} = \begin{bmatrix} \sigma_{n+1}^{\text{trial}} \\ \kappa_n \\ 0 \end{bmatrix} \tag{4.23}$$

has to be used as the initial value. The Jacobian matrix $\frac{\partial \boldsymbol{m}}{\partial \boldsymbol{v}}$ of the residual functions results from the partial derivatives of the Eqs. (4.66) up to (4.69) to:

---

[5] From the Latin 'residuus' for left or remaining.

[6] The Newton method is usually used as follows for a one-dimensional function: $x^{(i+1)} = x^{(i)} - \left(\frac{\mathrm{d}f}{\mathrm{d}x}(x^{(i)}) \right)^{-1} \times f(x^{(i)})$.

$$\frac{\partial \boldsymbol{m}}{\partial \boldsymbol{v}}(\sigma, \kappa, \Delta\lambda) = \begin{bmatrix} \frac{\partial r_\sigma}{\partial \sigma} & \frac{\partial r_\sigma}{\partial \kappa} & \frac{\partial r_\sigma}{\partial \Delta\lambda} \\ \frac{\partial r_\kappa}{\partial \sigma} & \frac{\partial r_\kappa}{\partial \kappa} & \frac{\partial r_\kappa}{\partial \Delta\lambda} \\ \frac{\partial r_F}{\partial \sigma} & \frac{\partial r_F}{\partial \kappa} & \frac{\partial r_F}{\partial \Delta\lambda} \end{bmatrix} = \begin{bmatrix} E^{-1} & 0 & \operatorname{sgn}(\sigma) \\ 0 & -1 & 1 \\ \operatorname{sgn}(\sigma) & -\frac{\partial k(\kappa)}{\partial \kappa} & 0 \end{bmatrix}. \tag{4.24}$$

Next to the fulfillment of Eqs. (4.62) up to (4.65), which are given due to plasticity, in each integration point also the global force equilibrium hast to be fulfilled. In order to make use of the Newton method, it is even necessary at small strains in the general three-dimensional case to define the elasto-plastic stiffness matrix,[7] which is consistent to the integration algorithm [9]. The consistent elasto-plastic modulus results from the following in the one-dimensional case:

$$E_{n+1}^{\text{elpl}} = \frac{\partial \sigma_{n+1}}{\partial \varepsilon_{n+1}} = \frac{\partial \Delta\sigma_n}{\partial \varepsilon_{n+1}}. \tag{4.25}$$

With the inversion of the Jacobian matrix $\frac{\partial \boldsymbol{m}}{\partial \boldsymbol{v}}$, which has to be evaluated in the converged condition of the above listed Newton iteration,

$$\left[\left(\frac{\partial \boldsymbol{m}}{\partial \boldsymbol{v}}\right)_{n+1}\right]^{-1} = \begin{bmatrix} \tilde{m}_{11} & \tilde{m}_{12} & \tilde{m}_{13} \\ \tilde{m}_{21} & \tilde{m}_{22} & \tilde{m}_{23} \\ \tilde{m}_{31} & \tilde{m}_{32} & \tilde{m}_{33} \end{bmatrix}_{n+1} \tag{4.26}$$

$$= \frac{E}{E + \frac{\partial k}{\partial \kappa}} \begin{bmatrix} \frac{\partial k}{\partial \kappa} & -\operatorname{sgn}(\sigma)\frac{\partial k}{\partial \kappa} & \operatorname{sgn}(\sigma) \\ \operatorname{sgn}(\sigma) & -1 & -E^{-1} \\ \operatorname{sgn}(\sigma) & E^{-1}\frac{\partial k}{\partial \kappa} & -E^{-1} \end{bmatrix}_{n+1} \tag{4.27}$$

the elasto-plastic modulus can be defined from

$$E_{n+1}^{\text{elpl}} = \tilde{m}_{11}. \tag{4.28}$$

For this consider Eq. (2.41) and note that under the assumption of Eq. (2.7) the relation $\frac{\partial F}{\partial \kappa} = -\frac{\partial k}{\partial \kappa}$ results. As can be seen from Eq. (4.72), the consistent elasto-plastic modulus in the *one-dimensional* case does not depend on the chosen integration algorithm and equals the continuum form given in Eq. (2.41). However at this point it needs be considered that this identity does not have to exist at higher dimensions any longer.

For the special case of linear hardening, meaning $\frac{\partial k}{\partial \kappa} = E^{\text{pl}} = \text{const.}$, Eq. (4.22) is not to be solved iteratively and the unknown solution vector $\boldsymbol{v}_{n+1}$ results directly with the help of the initial value (4.23) in:

$$\boldsymbol{v}_{n+1} = \boldsymbol{v}^{(0)} - \left(\frac{\mathrm{d}\boldsymbol{m}}{\mathrm{d}\boldsymbol{v}}(\boldsymbol{v}^{(0)})\right)^{-1} \boldsymbol{m}(\boldsymbol{v}^{(0)}), \tag{4.29}$$

[7] Also referred to as consistent elasto-plastic tangent modulus matrix, consistent tangent stiffness matrix or algorithmic stiffness matrix.

or in components as:

$$\begin{bmatrix} \sigma_{n+1} \\ \kappa_{n+1} \\ \Delta\lambda_{n+1} \end{bmatrix} = \begin{bmatrix} \sigma_{n+1}^{\text{trial}} \\ \kappa_n \\ 0 \end{bmatrix} - \frac{E}{E + E^{\text{pl}}} \times \begin{bmatrix} E^{\text{pl}} & -\text{sgn}(\sigma_{n+1}^{\text{trial}})E^{\text{pl}} & \text{sgn}(\sigma_{n+1}^{\text{trial}}) \\ \text{sgn}(\sigma_{n+1}^{\text{trial}}) & -1 & -E^{-1} \\ \text{sgn}(\sigma_{n+1}^{\text{trial}}) & E^{-1}E^{\text{pl}} & -E^{-1} \end{bmatrix} \begin{bmatrix} 0 \\ 0 \\ F_{n+1}^{\text{trial}} \end{bmatrix}. \tag{4.30}$$

The third equation of (4.30) yields the consistency parameter in the case of the linear hardening to:

$$\Delta\lambda_{n+1} = \frac{F_{n+1}^{\text{trial}}}{E + E^{\text{pl}}}. \tag{4.31}$$

The insertion of the consistency parameter into the first equation of (4.30) yields the stress in the final stress state to:

$$\sigma_{n+1} = \left(1 - \frac{F_{n+1}^{\text{trial}}}{E + E^{\text{pl}}} \times \frac{E}{|\sigma_{n+1}^{\text{trial}}|}\right)\sigma_{n+1}^{\text{trial}}. \tag{4.32}$$

From the second equation of (4.30) the isotropic hardening variable in the final stress state is given in the following with the last two results:

$$\kappa_{n+1} = \kappa_n + \frac{F_{n+1}^{\text{trial}}}{E + E^{\text{pl}}} = \kappa_n + \Delta\lambda_{n+1}. \tag{4.33}$$

Finally, the plastic strain results into the following via the flow rule

$$\varepsilon_{n+1}^{\text{pl}} = \varepsilon_n^{\text{pl}} + \Delta\lambda_{n+1}\,\text{sgn}(\sigma_{n+1}), \tag{4.34}$$

and the consistent elasto-plastic modulus can be defined according to Eq. (2.41).

To conclude, the calculation steps of the CPP algorithm are presented in compact form:

I. **Calculation of the Test State**

$$\begin{aligned} \sigma_{n+1}^{\text{trial}} &= \sigma_n + E\Delta\varepsilon_n \\ \kappa_{n+1}^{\text{trial}} &= \kappa_n \end{aligned}$$

II. **Test of Validity of the Stress State**

$F(\sigma_{n+1}^{\text{trial}}, \kappa_{n+1}^{\text{trial}}) \leq 0$	
Y	N
$\sigma_{n+1} = \sigma_{n+1}^{\text{trial}}$ $\kappa_{n+1} = \kappa_{n+1}^{\text{trial}}$ End CPP	Back Projection necessary ($\Rightarrow$ Step III)

III. **Back Projection**

Initial Values:

$$\boldsymbol{v}^{(0)} = \begin{bmatrix} \sigma^{(0)} \\ \kappa^{(0)} \\ \Delta\lambda^{(0)} \end{bmatrix} = \begin{bmatrix} \sigma_{n+1}^{\text{trial}} \\ \kappa_n \\ 0 \end{bmatrix}$$

Root Finding with the Newton Method:

$$\boldsymbol{v}^{(i+1)} = \boldsymbol{v}^{(i)} - \left(\frac{\mathrm{d}\boldsymbol{m}}{\mathrm{d}\boldsymbol{v}} (\boldsymbol{v}^{(i)}) \right)^{-1} \boldsymbol{m}(\boldsymbol{v}^{(i)})$$

As long as $\|\boldsymbol{v}^{(i+1)} - \boldsymbol{v}^{(i)}\| < t_{\text{end}}^{v}$

In the termination criterion the vector norm (or length) of a vector has been used, which results in the following $\|\boldsymbol{x}\| = \left(\sum_{i=1}^{n} x_i^2 \right)^{0.5}$ for an arbitrary vector $\boldsymbol{x}$.

IV. **Actualization of the Parameters**

$$\begin{aligned} \sigma_{n+1} &= \sigma^{(i+1)} \\ \kappa_{n+1} &= \kappa^{(n+1)} \\ E_{n+1}^{\text{elpl}} &= \tilde{m}_{11} \end{aligned}$$

The internally used calculation precision in the FE system appears perfect as termination precision t_{end}^{v} in the Newton method.

Figure 4.4 shows that the entire strain increment in dependence on the test stress state can be illustrated as

$$\Delta\varepsilon_n = \varepsilon_{n+1} - \varepsilon_n = E^{-1}(\sigma_{n+1}^{\text{trial}} - \sigma_n). \tag{4.35}$$

If one inserts the last equation and the flow rule[8] according to Eq. (2.14) in Eq. (4.10), the final stress state σ_{n+1} in dependence on the test stress state $\sigma_{n+1}^{\text{trial}}$

[8] At this point it is switched from $\mathrm{d}\lambda$ to $\Delta\lambda$.

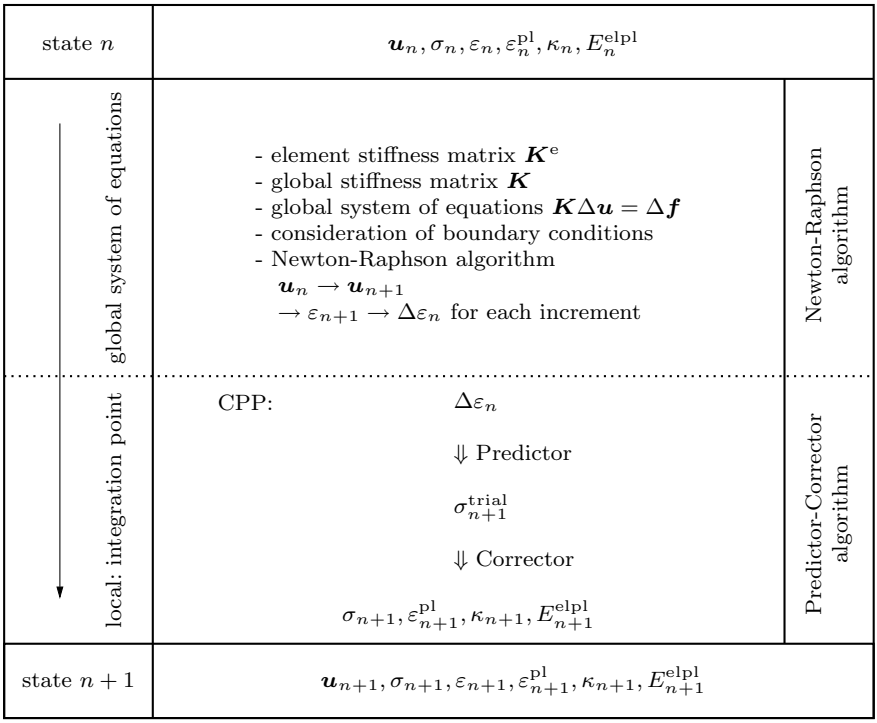

Fig. 4.5 General procedure of an elasto-plastic finite element calculation

results in:

$$\sigma_{n+1} = \sigma_{n+1}^{\mathrm{trial}} - \Delta\lambda_{n+1} E \operatorname{sgn}(\sigma_{n+1}^{\mathrm{trial}}). \tag{4.36}$$

The general procedure of an elasto-plastic finite element calculation is illustrated in Fig. 4.5.

One can see that the solution of an elasto-plastic problem occurs on two levels. On the global level, meaning for the global system of equations under consideration of the boundary conditions, the Newton-Raphson iteration scheme is made use of to define the incremental global displacement vector $\Delta\boldsymbol{u}_n$. By summing the displacement increments, the total global displacement vector $\boldsymbol{u}_{n+1}$ of the unknown nodal displacement of a structure consisting of finite elements results. Via the strain-displacement relation the strain ε_{n+1} or, alternatively the strain increment $\Delta\varepsilon_n$ per element, can be determined from the nodal displacement.[9] The strain increment of

[9] At this point for the considered linear bar elements a constant strain distribution per element results. In general, the strain results as a function of the element coordinates which is usually evaluated on the integration points. Therefore, one would in the general case normally define a strain *matrix* $\boldsymbol{\varepsilon}$ per element, which combines the different strain values on the integration points. This however is unnecessary for a linear bar element. A scalar strain or alternative stress value is enough for the description.

an element is now used on the level of the integration points, to define the remaining state variables iteratively with the help of a predictor-corrector method.

4.1.2.2 Interpretation as Convex Optimization Problem

The fully implicit backward-Euler algorithm can also be understood as a solution of a convex optimization problem. A general derivation of the following is given in [4]. As an objective function the complementary energy has to be minimized hereby under the side-condition that the yield condition is fulfilled.

In the following, the derivation of the optimization problem for the example of isotropic strain hardening is illustrated. The complementary energy[10] between the test stress state and an arbitrary state $(\sigma, |\varepsilon^{\mathrm{pl}}|)$ at an increment of the back projection can be split into its elastic and plastic parts according to

$$\bar{\pi}(\sigma, |\varepsilon^{\mathrm{pl}}|) = \bar{\pi}^{\mathrm{el}}(\sigma, |\varepsilon^{\mathrm{pl}}|) + \bar{\pi}^{\mathrm{pl}}(\sigma, |\varepsilon^{\mathrm{pl}}|). \tag{4.37}$$

At this point in the case of the considered *linear* elasticity, the complementary energy $\bar{\pi}^{\mathrm{el}}$ and the potential energy π^{el} are the same. Due to the assumption of the *linear isotropic* hardening accordingly it is valid that $\bar{\pi}^{\mathrm{pl}} = \pi^{\mathrm{pl}}$ (see Fig. 4.6). Therefore, the following occurs for the complementary energy

$$\begin{aligned} \bar{\pi} &= \pi^{\mathrm{el}} + \bar{\pi}^{\mathrm{pl}} \\ &= \int \left(\sigma_{n+1}^{\mathrm{trial}} - \sigma\right) \mathrm{d}\varepsilon^{\mathrm{el}} + \int \left(|\varepsilon^{\mathrm{pl}}| - |\varepsilon_n^{\mathrm{pl}}|\right) \mathrm{d}\sigma. \end{aligned} \tag{4.38}$$

The assumption of linearity in the elastic and plastic area, meaning $\mathrm{d}\sigma = E\mathrm{d}\varepsilon^{\mathrm{el}}$ and $\mathrm{d}\sigma = E^{\mathrm{pl}}\mathrm{d}\varepsilon^{\mathrm{pl}}$, can be used in Eq. (4.38) so that the following finally results for the complementary energy

$$\bar{\pi}(\sigma, |\varepsilon^{\mathrm{pl}}|) = \frac{1}{2}(\sigma_{n+1}^{\mathrm{trial}} - \sigma)\frac{1}{E}(\sigma_{n+1}^{\mathrm{trial}} - \sigma) + \frac{1}{2}(|\varepsilon_n^{\mathrm{pl}}| - |\varepsilon^{\mathrm{pl}}|)E^{\mathrm{pl}}(|\varepsilon_n^{\mathrm{pl}}| - |\varepsilon^{\mathrm{pl}}|). \tag{4.39}$$

The fractions of $\bar{\pi}$ result as triangular areas in Fig. 4.6, which can also be used directly for the definition of the complementary energy. For the case that the flow curve k exhibits a certain course, the plastic energy parts for an arbitrary state $(\sigma, |\varepsilon^{\mathrm{pl}}|)$ can be calculated via

$$\pi^{\mathrm{pl}} = \int_{|\varepsilon_n^{\mathrm{pl}}|}^{|\varepsilon^{\mathrm{pl}}|} \left(k(|\varepsilon^{\mathrm{pl}}|) - \sigma_n\right) \mathrm{d}|\varepsilon^{\mathrm{pl}}|, \tag{4.40}$$

$$\bar{\pi}^{\mathrm{pl}} = \int_{|\varepsilon_n^{\mathrm{pl}}|}^{|\varepsilon^{\mathrm{pl}}|} \left(\sigma - k(|\varepsilon^{\mathrm{pl}}|)\right) \mathrm{d}|\varepsilon^{\mathrm{pl}}|. \tag{4.41}$$

[10] Hereby the energy per unit volume is considered.

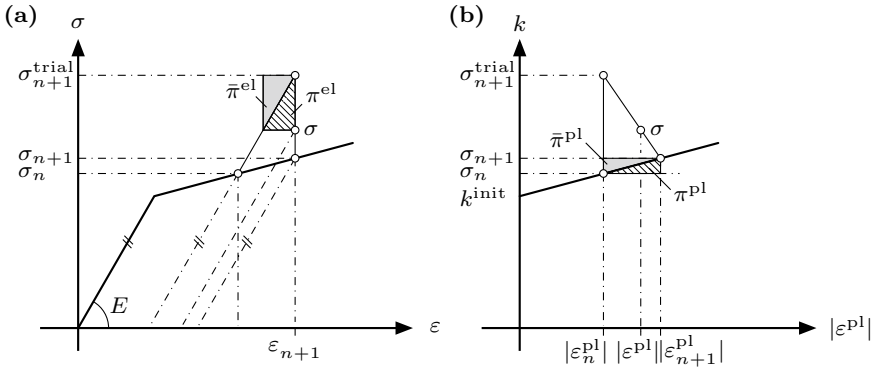

Fig. 4.6 Illustration of the elastic potential and plastic dissipative energy and the corresponding complementary energy between two states of the back projection in the case of the linear hardening

The side-condition of the optimization problem is given through the yield condition and states that the final stress state has to be within or on the boundary of the elastic area. From Eq. (2.9) a limiting line results in a ε^{pl}-σ coordinate system:

$$\varepsilon^{\text{pl}} \geq \frac{1}{E^{\text{pl}}}\left(|\sigma| - k^{\text{init}}\right) \quad \text{and} \quad \varepsilon^{\text{pl}} \geq 0. \tag{4.42}$$

Generally, the side-condition, meaning the elastic area, can also be specified as

$$\mathbb{E}_\sigma := \left\{(\sigma, |\varepsilon^{\text{pl}}|) \in \mathbb{R} \times \mathbb{R}_+ | F(\sigma, |\varepsilon^{\text{pl}}|) \leq 0\right\} \tag{4.43}$$

and the convex optimization problem can be formulated as follows:

$$\begin{aligned} &\text{Define}(\sigma_{n+1}, |\varepsilon_{n+1}^{\text{pl}}|) \in \mathbb{E}_\sigma, \text{ so that} \\ \bar{\pi}(\sigma_{n+1}, |\varepsilon_{n+1}^{\text{pl}}|) &= \min\left\{\bar{\pi}(\sigma, |\varepsilon^{\text{pl}}|)\right\}\Big|_{(\sigma, |\varepsilon^{\text{pl}}|) \in \mathbb{E}_\sigma}. \end{aligned}$$

Since $E > 0$—and under the assumption $E^{\text{pl}} > 0$—it results that $\bar{\pi}$ is a convex function. The side-condition, meaning $F \leq 0$, also represents a convex function,[11] and the application of the Lagrange multiplier method leads to

$$\mathcal{L}(\sigma, |\varepsilon^{\text{pl}}|, \mathrm{d}\lambda) := \bar{\pi}(\sigma, |\varepsilon^{\text{pl}}|) + \mathrm{d}\lambda F(\sigma, |\varepsilon^{\text{pl}}|). \tag{4.44}$$

The gradients of the Lagrange function $\mathcal{L}$ result in:

[11] The convexity of a yield condition can be derived from the Drucker's stability postulate [18, 19].

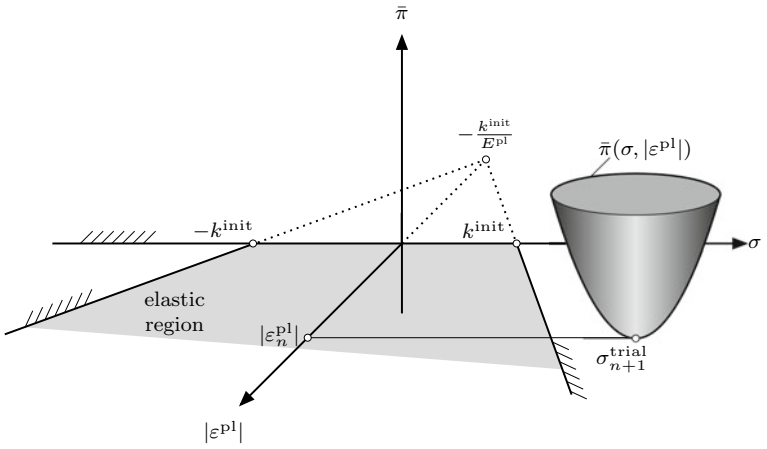

Fig. 4.7 Interpretation of the fully implicit backward-Euler algorithm as a convex optimization problem. Adapted from [4]

$$\frac{\partial}{\partial \sigma} \mathcal{L}\left(\sigma_{n+1}, |\varepsilon_{n+1}^{\text{pl}}|, \mathrm{d}\lambda\right) = 0, \tag{4.45}$$

$$\frac{\partial}{\partial |\varepsilon^{\text{pl}}|} \mathcal{L}\left(\sigma_{n+1}, |\varepsilon_{n+1}^{\text{pl}}|, \mathrm{d}\lambda\right) = 0. \tag{4.46}$$

For Eqs. (4.45) and (4.46) the following results

$$\frac{\partial \mathcal{L}}{\partial \sigma} = (\sigma_{n+1}^{\text{trial}} - \sigma)\left(-\frac{1}{E}\right) + \mathrm{d}\lambda \,\mathrm{sgn}(\sigma) = 0, \tag{4.47}$$

$$\frac{\partial \mathcal{L}}{\partial |\varepsilon^{\text{pl}}|} = (|\varepsilon_n^{\text{pl}}| - |\varepsilon^{\text{pl}}|)(-E^{\text{pl}}) + \mathrm{d}\lambda(-E^{\text{pl}}) = 0. \tag{4.48}$$

The last two equations comply with the rules (4.33) and (4.12) of the previous section. A graphical interpretation of the implicit backward-Euler algorithm in the sense of a convex optimization problem is given in Fig. 4.7. If an invalid test state ($F > 0$) results, the ellipsoid of the complementary energy lies outside of the valid area of the elastic energy. It needs to be remarked at this point that the absolute minimum (without side-condition) of the complementary energy lies in the σ-$|\varepsilon^{\text{pl}}|$ plane and therefore results in $\bar{\pi}(\sigma_{n+1}^{\text{trial}}, |\varepsilon_n^{\text{pl}}|) = 0$.

The minimum of the complementary energy under consideration of the side-condition, meaning $F \leq 0$, therefore has to be localized on the cutting curve between

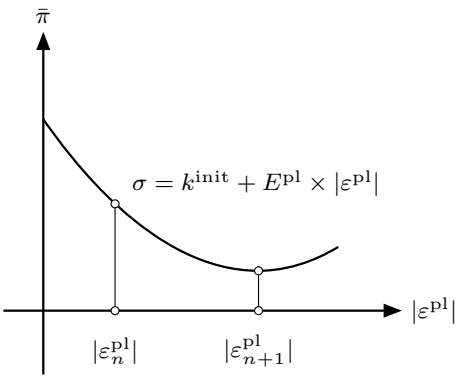

Fig. 4.8 Illustration of the complementary energy in a cutting plane along the flow curve

the ellipsoid of the complementary energy and the plane along the flow curve[12] (see Eq. (4.42)). If Eq. (4.42) in the complementary energy according to Eq. (4.39) is considered, the following results

$$\bar{\pi}(\sigma, |\varepsilon^{\text{pl}}|) = \frac{1}{2E}(\sigma_{n+1}^{\text{trial}} - \sigma)^2 + \frac{1}{2}E^{\text{pl}}\left(|\varepsilon_n^{\text{pl}}| - \frac{1}{E^{\text{pl}}}\left(\sigma - k^{\text{init}}\right)\right)^2, \tag{4.49}$$

this means a polynomial of 2nd order in the variable σ. The minimum of this function—and therefore the state $n+1$—results via partial derivative for $\sigma > 0$ (meaning for a tensile test) in:

$$\frac{\partial \bar{\pi}}{\partial \sigma} = -\frac{\sigma_{n+1}^{\text{trial}} - \sigma_{n+1}}{E} - \left(|\varepsilon_n^{\text{pl}}| - \frac{\sigma_{n+1} - k^{\text{init}}}{E^{\text{pl}}}\right) \tag{4.50}$$

or

$$\sigma_{n+1} = \underbrace{\frac{EE^{\text{pl}}}{E + E^{\text{pl}}}}_{E^{\text{elpl}}}\left(\frac{k^{\text{init}}}{E^{\text{pl}}} + \frac{\sigma_{n+1}^{\text{trial}}}{E} + |\varepsilon_n^{\text{pl}}|\right). \tag{4.51}$$

Via Eq. (4.42) the plastic strain in the final stress state results in:

$$\varepsilon_{n+1}^{\text{pl}} = \underbrace{\frac{EE^{\text{pl}}}{E + E^{\text{pl}}}}_{E^{\text{elpl}}}\left(\frac{k^{\text{init}}}{EE^{\text{pl}}} + \frac{\sigma_{n+1}^{\text{trial}}}{EE^{\text{pl}}} + \frac{|\varepsilon_n^{\text{pl}}|}{E^{\text{pl}}}\right) - \frac{k^{\text{init}}}{E^{\text{pl}}}. \tag{4.52}$$

[12] This plane has to stand vertically on the σ-$|\varepsilon^{\text{pl}}|$ plane. For a tensile test the plane has to go through the limit curve in the area $\sigma > 0$. For a compression test the according straight line from the area $\sigma < 0$ has to be chosen.

A graphical illustration of the cutting curve is given in Fig. 4.8. One can consider at this point that $|\varepsilon_n^{\mathrm{pl}}|$ equals the test stress state.

4.1.3 Derivation of the Fully Implicit Backward-Euler Algorithm for Kinematic Hardening

The derivation for pure kinematic hardening is quite similar to the approach for isotropic hardening, see Sect. 4.1.2. Replacing the equation for the isotropic hardening variable by the expression for the kinematic hardening variable according to Prager gives the following set of three equations in the final state:

$$\sigma_{n+1} = \sigma_{n+1}^{\mathrm{trial}} - \Delta\lambda_{n+1} E \operatorname{sgn}(\sigma_{n+1} - \alpha_{n+1}), \tag{4.53}$$

$$\alpha_{n+1} = \alpha_n + \Delta\lambda_{n+1} H \operatorname{sgn}(\sigma_{n+1} - \alpha_{n+1}), \tag{4.54}$$

$$F_{n+1} = |\sigma_{n+1} - \alpha_{n+1}| - k = 0. \tag{4.55}$$

Outside of the final state, at each of these equations a residual r remains again:

$$\begin{aligned} r_\sigma(\sigma, \Delta\lambda, \alpha) &= \sigma - \sigma_{n+1}^{\mathrm{trial}} + \Delta\lambda E \operatorname{sgn}(\sigma - \alpha) \neq 0 \quad \text{or} \\ &= E^{-1}\sigma - E^{-1}\sigma_{n+1}^{\mathrm{trial}} + \Delta\lambda \operatorname{sgn}(\sigma - \alpha) \neq 0, \end{aligned} \tag{4.56}$$

$$\begin{aligned} r_\alpha(\alpha, \Delta\lambda, \sigma) &= \alpha - \alpha_n - \Delta\lambda H \operatorname{sgn}(\sigma - \alpha) \neq 0 \quad \text{or} \\ &= -\alpha + \alpha_n + \Delta\lambda H \operatorname{sgn}(\sigma - \alpha) \neq 0, \end{aligned} \tag{4.57}$$

$$r_F(\sigma, \alpha) = F(\sigma, \alpha) = |\sigma - \alpha| - k \neq 0. \tag{4.58}$$

We define again a vector function $\boldsymbol{m}$, a vector argument $\boldsymbol{v}$ and initial values $\boldsymbol{v}^{(0)}$:

$$\boldsymbol{m}(\boldsymbol{v}) \in (\mathbb{R}^3 \to \mathbb{R}^3) = \begin{bmatrix} r_\sigma(\boldsymbol{v}) \\ r_\alpha(\boldsymbol{v}) \\ r_F(\boldsymbol{v}) \end{bmatrix}, \quad \boldsymbol{v} = \begin{bmatrix} \sigma \\ \alpha \\ \Delta\lambda \end{bmatrix}, \quad \boldsymbol{v}^{(0)} = \begin{bmatrix} \sigma_{n+1}^{\mathrm{trial}} \\ \alpha_n \\ 0 \end{bmatrix}, \tag{4.59}$$

to perform a Newton iteration as given in Eq. (4.22). The Jacobian matrix $\frac{\partial \boldsymbol{m}}{\partial \boldsymbol{v}}$ of the residual functions reads for this case:

$$\begin{aligned} \frac{\partial \boldsymbol{m}}{\partial \boldsymbol{v}}(\sigma, \alpha, \Delta\lambda) &= \begin{bmatrix} \dfrac{\partial r_\sigma}{\partial \sigma} & \dfrac{\partial r_\sigma}{\partial \alpha} & \dfrac{\partial r_\sigma}{\partial \Delta\lambda} \\ \dfrac{\partial r_\alpha}{\partial \sigma} & \dfrac{\partial r_\alpha}{\partial \alpha} & \dfrac{\partial r_\alpha}{\partial \Delta\lambda} \\ \dfrac{\partial r_F}{\partial \sigma} & \dfrac{\partial r_F}{\partial \alpha} & \dfrac{\partial r_F}{\partial \Delta\lambda} \end{bmatrix} \\ &= \begin{bmatrix} E^{-1} & 0 & \operatorname{sgn}(\sigma - \alpha) \\ 0 & -1 & H \operatorname{sgn}(\sigma - \alpha) \\ \operatorname{sgn}(\sigma - \alpha) & -\operatorname{sgn}(\sigma - \alpha) & 0 \end{bmatrix}. \end{aligned} \tag{4.60}$$

Thus, the inversion of the Jacobian matrix $\frac{\partial \boldsymbol{m}}{\partial \boldsymbol{v}}$, which has to be evaluated in the converged condition of the Newton iteration (see Eq. (4.22)), takes the following form:

$$\left[\left(\frac{\partial \boldsymbol{m}}{\partial \boldsymbol{v}}\right)_{n+1}\right]^{-1} = \begin{bmatrix} \tilde{m}_{11} & \tilde{m}_{12} & \tilde{m}_{13} \\ \tilde{m}_{21} & \tilde{m}_{22} & \tilde{m}_{23} \\ \tilde{m}_{31} & \tilde{m}_{32} & \tilde{m}_{33} \end{bmatrix}_{n+1} = \frac{1}{E+H} \times \begin{bmatrix} HE & -E & E\,\mathrm{sgn}(\sigma-\alpha) \\ HE & -E & -H\,\mathrm{sgn}(\sigma-\alpha) \\ E\,\mathrm{sgn}(\sigma-\alpha) & \mathrm{sgn}(\sigma-\alpha) & -1 \end{bmatrix}_{n+1}. \quad (4.61)$$

4.1.4 Derivation of the Fully Implicit Backward-Euler Algorithm for Combined Hardening

The derivation of the algorithm for combined hardening requires the combination of the approaches from the two previous sections. Thus, the following set of four equations is obtained in the final state:

$$\sigma_{n+1} = \sigma_{n+1}^{\mathrm{trial}} - \Delta\lambda_{n+1} E\,\mathrm{sgn}(\sigma_{n+1} - \alpha_{n+1}), \quad (4.62)$$

$$\kappa_{n+1} = \kappa_n + \Delta\lambda_{n+1}, \quad (4.63)$$

$$\alpha_{n+1} = \alpha_n + \Delta\lambda_{n+1} H\,\mathrm{sgn}(\sigma_{n+1} - \alpha_{n+1}), \quad (4.64)$$

$$F_{n+1} = F(\sigma_{n+1}, \kappa_{n+1}, \alpha_{n+1}) = 0. \quad (4.65)$$

The corresponding four residual equations read now:

$$\begin{aligned} r_\sigma(\sigma, \Delta\lambda, \alpha) &= \sigma - \sigma_{n+1}^{\mathrm{trial}} + \Delta\lambda E\,\mathrm{sgn}(\sigma-\alpha) \neq 0 \quad \text{or} \\ &= E^{-1}\sigma - E^{-1}\sigma_{n+1}^{\mathrm{trial}} + \Delta\lambda\,\mathrm{sgn}(\sigma-\alpha) \neq 0, \quad (4.66) \\ r_\kappa(\kappa, \Delta\lambda) &= \kappa - \kappa_n - \Delta\lambda \neq 0 \quad \text{or} \\ &= -\kappa + \kappa_n + \Delta\lambda \neq 0, \quad (4.67) \\ r_\alpha(\alpha, \Delta\lambda, \sigma) &= \alpha - \alpha_n - \Delta\lambda H\,\mathrm{sgn}(\sigma-\alpha) \neq 0 \quad \text{or} \\ &= -\alpha + \alpha_n + \Delta\lambda H\,\mathrm{sgn}(\sigma-\alpha) \neq 0, \quad (4.68) \\ r_F(\sigma, \alpha, \kappa) &= F(\sigma, \alpha, \kappa) = |\sigma-\alpha| - (k^{\mathrm{init}} + E^{\mathrm{pl}}\kappa) \neq 0. \quad (4.69) \end{aligned}$$

We define again a vector function $\boldsymbol{m}$, a vector argument $\boldsymbol{v}$ and initial values $\boldsymbol{v}^{(0)}$

$$\boldsymbol{m}(\boldsymbol{v}) \in (\mathbb{R}^4 \to \mathbb{R}^4) = \begin{bmatrix} r_\sigma(\boldsymbol{v}) \\ r_\kappa(\boldsymbol{v}) \\ r_\alpha(\boldsymbol{v}) \\ r_F(\boldsymbol{v}) \end{bmatrix}, \quad \boldsymbol{v} = \begin{bmatrix} \sigma \\ \kappa \\ \alpha \\ \Delta\lambda \end{bmatrix}, \quad \boldsymbol{v}^{(0)} = \begin{bmatrix} \sigma_{n+1}^{\text{trial}} \\ \kappa_n \\ \alpha_n \\ 0 \end{bmatrix}, \tag{4.70}$$

to perform the Newton iteration as given in Eq. (4.22). The Jacobian matrix $\frac{\partial \boldsymbol{m}}{\partial \boldsymbol{v}}$ of the residual functions reads for this case:

$$\begin{aligned} \frac{\partial \boldsymbol{m}}{\partial \boldsymbol{v}}(\sigma, \kappa, \alpha, \Delta\lambda) &= \begin{bmatrix} \frac{\partial r_\sigma}{\partial \sigma} & \frac{\partial r_\sigma}{\partial \kappa} & \frac{\partial r_\sigma}{\partial \alpha} & \frac{\partial r_\sigma}{\partial \Delta\lambda} \\ \frac{\partial r_\kappa}{\partial \sigma} & \frac{\partial r_\kappa}{\partial \kappa} & \frac{\partial r_\kappa}{\partial \alpha} & \frac{\partial r_\kappa}{\partial \Delta\lambda} \\ \frac{\partial r_\alpha}{\partial \sigma} & \frac{\partial r_\alpha}{\partial \kappa} & \frac{\partial r_\alpha}{\partial \alpha} & \frac{\partial r_\alpha}{\partial \Delta\lambda} \\ \frac{\partial r_F}{\partial \sigma} & \frac{\partial r_F}{\partial \kappa} & \frac{\partial r_F}{\partial \alpha} & \frac{\partial r_F}{\partial \Delta\lambda} \end{bmatrix} \\ &= \begin{bmatrix} E^{-1} & 0 & 0 & \operatorname{sgn}(\sigma - \alpha) \\ 0 & -1 & 0 & 1 \\ 0 & 0 & -1 & H \operatorname{sgn}(\sigma - \alpha) \\ \operatorname{sgn}(\sigma - \alpha) & -E^{\text{pl}} & -\operatorname{sgn}(\sigma - \alpha) & 0 \end{bmatrix}, \end{aligned} \tag{4.71}$$

and its inverse can be stated as:

$$\begin{aligned} \left[\left(\frac{\partial \boldsymbol{m}}{\partial \boldsymbol{v}}\right)_{n+1}\right]^{-1} &= \begin{bmatrix} \tilde{m}_{11} & \tilde{m}_{12} & \tilde{m}_{13} & \tilde{m}_{14} \\ \tilde{m}_{21} & \tilde{m}_{22} & \tilde{m}_{23} & \tilde{m}_{24} \\ \tilde{m}_{31} & \tilde{m}_{32} & \tilde{m}_{33} & \tilde{m}_{34} \\ \tilde{m}_{41} & \tilde{m}_{42} & \tilde{m}_{43} & \tilde{m}_{44} \end{bmatrix}_{n+1} = \frac{1}{E + E^{\text{pl}} + H} \\ &\times \begin{bmatrix} (E^{\text{pl}} + H)E & -E^{\text{pl}} E \operatorname{sgn}(\sigma - \alpha) & -E & E \operatorname{sgn}(\sigma - \alpha) \\ E \operatorname{sgn}(\sigma - \alpha) & -(E + H) & \operatorname{sgn}(\sigma - \alpha) & -1 \\ HE & E^{\text{pl}} H \operatorname{sgn}(\sigma - \alpha) & -(E + E^{\text{pl}}) & -H \operatorname{sgn}(\sigma - \alpha) \\ E \operatorname{sgn}(\sigma - \alpha) & E^{\text{pl}} & \operatorname{sgn}(\sigma - \alpha) & -1 \end{bmatrix}_{n+1}. \end{aligned} \tag{4.72}$$

It should be noted here that some authors introduce an auxiliary variable, the so-called *relative stress* $\xi = \sigma - \alpha$. Then, the partial derivatives in Eq. (4.71) can be obtained by respecting the derivative of the transformed coordinate, for example, as:

$$\frac{\partial r_F}{\partial \alpha} = \frac{\partial r_F}{\partial \xi} \frac{\partial \xi}{\partial \alpha} = \operatorname{sgn}(\xi) \times (-1) = -\operatorname{sgn}(\sigma - \alpha). \tag{4.73}$$

The complete iteration scheme for the case of combined hardening reads finally:

$$\begin{bmatrix} \sigma_{n+1} \\ \kappa_{n+1} \\ \alpha_{n+1} \\ \mathrm{d}\lambda_{n+1} \end{bmatrix} = \begin{bmatrix} \sigma_{n+1}^{\mathrm{trial}} \\ \kappa_n \\ \alpha_n \\ 0 \end{bmatrix} - \frac{1}{E + E^{\mathrm{pl}} + H} \times \begin{bmatrix} (E^{\mathrm{pl}} + H)E & -E^{\mathrm{pl}} E \operatorname{sgn}(\sigma - \alpha) & -E & E \operatorname{sgn}(\sigma - \alpha) \\ E \operatorname{sgn}(\sigma - \alpha) & -(E + H) & \operatorname{sgn}(\sigma - \alpha) & -1 \\ HE & E^{\mathrm{pl}} H \operatorname{sgn}(\sigma - \alpha) & -(E + E^{\mathrm{pl}}) & -H \operatorname{sgn}(\sigma - \alpha) \\ E \operatorname{sgn}(\sigma - \alpha) & E^{\mathrm{pl}} & \operatorname{sgn}(\sigma - \alpha) & -1 \end{bmatrix}_{n+1} \begin{bmatrix} 0 \\ 0 \\ 0 \\ F_{n+1}^{\mathrm{trial}} \end{bmatrix}. \tag{4.74}$$

4.1.5 Derivation of the Semi-implicit Backward-Euler Algorithm for Isotropic Hardening

To avoid the higher derivatives in the Jacobian matrix $\frac{\partial \boldsymbol{m}}{\partial \boldsymbol{v}}$ of the residual functions in the general three-dimensional case, the so-called semi-implicit backward-Euler algorithm can be made use of. This procedure is implicit in the consistency parameter (state $n + 1$), however explicit in the function $\operatorname{sgn}(\sigma)$ since the calculation occurs in the initial state n. Because of that, the normal rule in the final state $n + 1$ is not fulfilled exactly. To avoid a drift away from the flow curve, the yield condition in the final state $n + 1$ is fulfilled exactly. Therefore, the integration scheme results in:

$$\sigma_{n+1} = \sigma_{n+1}^{\mathrm{trial}} - \Delta\lambda_{n+1} E \operatorname{sgn}(\sigma_n), \tag{4.75}$$

$$\kappa_{n+1} = \kappa_n + \Delta\lambda_{n+1}, \tag{4.76}$$

$$F = F(\sigma_{n+1}, \kappa_{n+1}) = 0. \tag{4.77}$$

Outside of the final state also at this point a residual r remains at each of these equations:

$$\begin{aligned} r_\sigma(\sigma, \kappa, \Delta\lambda) &= E^{-1}\sigma - E^{-1}\sigma_{n+1}^{\mathrm{trial}} + \Delta\lambda \operatorname{sgn}(\sigma_n) \neq 0, \\ r_\kappa(\kappa, \Delta\lambda) &= -\kappa + \kappa_n + \Delta\lambda \neq 0, \\ r_F(\sigma, \kappa) &= F(\sigma, \kappa) = |\sigma| - k(\kappa) \neq 0. \end{aligned} \tag{4.78}$$

The partial derivatives of the residual functions finally lead to the following Jacobian matrix:

$$\frac{\partial \boldsymbol{m}}{\partial \boldsymbol{v}}(\sigma, \kappa, \Delta\lambda) = \begin{bmatrix} E^{-1} & 0 & \operatorname{sgn}(\sigma_n) \\ 0 & -1 & 1 \\ \operatorname{sgn}(\sigma) & -\frac{\partial k(\kappa)}{\partial \kappa} & 0 \end{bmatrix}. \tag{4.79}$$

If one compares the Jacobian matrix according to Eqs. (4.79) and (4.71) one can see that the integration requirements for the fully implicit and semi-implicit

algorithm are identical for the considered one-dimensional case at this point, as long as the stress state σ and σ_n lie in the same quadrant, meaning exhibiting the same algebraic sign. Similar conclusions can be drawn for the, in Table 4.2 summarized integration requirements.

To conclude, it can be remarked that the concept of the plastic material behavior, which was originally developed for the permanent deformation of metals, is also applied for other classes of material. Typically the macroscopic stress-strain diagram is regarded at this point, which exhibits a similar course as for classic metals. As an example, the following materials and disciplines can be listed herefor:

- Plastics [20],
- Fibre-reinforced plastics [21],
- Soil mechanics [22, 23],
- Concrete [24].

4.1.6 Sample Problems and Supplementary Problems

4.1.6.1 Sample Problems

4.1 Back Projection at Linear Hardening—Continuum Bar
Figure 4.9a shows an idealized stress-strain diagram as it can, for example, be derived experimentally from an uniaxial tensile test. With the help of this material behavior the deformation of a tension bar (see Fig. 4.9b) can be simulated. Thereby the right-hand end is displaced by $u = 8 \times 10^{-3}$ m in total, whereupon the deformation is applied in 10 equal increments. The bar needs to be regarded as a continuum hereby and should not be discretized with finite elements.

(a) Calculate the stress state with the help of the CPP algorithm in each increment and mark all values, which have to be updated.
(b) Graphically illustrate the stress distribution.

Solution 4.1

(a) For the back projection various material properties of the elastic and plastic regime are needed. The modulus of elasticity E results as the quotient from the stress and strain increment in the elastic regime in:

$$E = \frac{\Delta\sigma}{\Delta\varepsilon} = \frac{350 \text{ MPa}}{0.005} = 70{,}000 \text{ MPa}. \tag{4.80}$$

The plastic modulus E^{pl} results as the quotient from the yield stress and the plastic strain increment in:

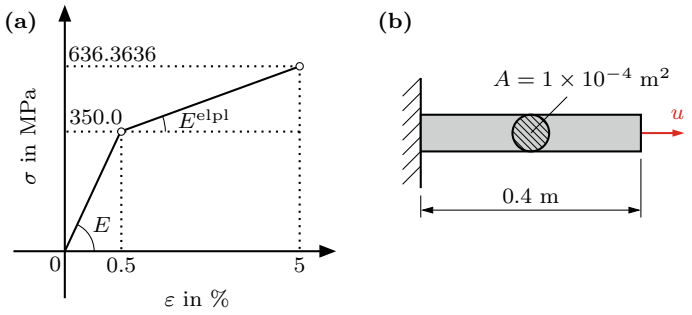

Fig. 4.9 Sample problem back projection at linear hardening: **a** stress-strain distribution; **b** geometry and boundary conditions

$$E^{\text{pl}} = \frac{\Delta k}{\Delta \varepsilon^{\text{pl}}} = \frac{636.3636 \text{ MPa} - 350 \text{ MPa}}{(0.05 - 636.3636 \text{ MPa}/E) - (0.005 - 350 \text{ MPa}/E)}$$
$$= 7000 \text{ MPa}. \tag{4.81}$$

Therefore, the elasto-plastic material modulus can be calculated via Eq. (2.46) in

$$E^{\text{elpl}} = \frac{E \times E^{\text{pl}}}{E + E^{\text{pl}}} = \frac{70{,}000 \text{ MPa} \times 7000 \text{ MPa}}{70{,}000 \text{ MPa} + 7000 \text{ MPa}} = 6363.636 \text{ MPa}. \tag{4.82}$$

Finally, the equation of the flow curve results in the following via the initial yield stress:

$$k(\kappa) = 350 \text{ MPa} + 7000 \text{ MPa} \times \kappa. \tag{4.83}$$

A graphical illustration of the flow curve is given in Fig. 4.10.
For the integration algorithm the strain increment is additionally necessary. At a total displacement of 8 mm and 10 equidistant steps, the strain increment can be determined via:

$$\Delta\varepsilon = \frac{1}{10} \times \frac{8 \text{ mm}}{400 \text{ mm}} = 0.002. \tag{4.84}$$

For the first two increments, trial stress states result in the elastic regime ($F < 0$), and the resulting stress can be calculated via Hooke's law (4.2). From the third increment on an invalid test stress state ($F > 0$) results for the first time and the stress has to be calculated via Eq. (4.30), whereupon the constant matrix expression results in:

$$\begin{bmatrix} 7000 & -7000 & 1 \\ 1 & -1 & -(70{,}000)^{-1} \\ 1 & 0,1 & -(70{,}000)^{-1} \end{bmatrix}. \tag{4.85}$$

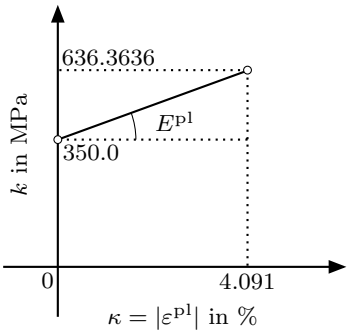

Fig. 4.10 Flow curve for a continuum bar

Table 4.3 Numerical values of the back projection for a continuum bar with linear hardening (10 increments, $\Delta\varepsilon = 0.002$)

Inc	ε	σ^{trial}	σ	κ	dλ	E^{elpl}
–	–	MPa	MPa	10^{-3}	10^{-3}	MPa
1	0.002	140.0	140.0	0.0	0.0	0.0
2	0.004	280.0	280.0	0.0	0.0	0.0
3	0.006	420.0	356.364	0.909091	0.909091	6363.636
4	0.008	496.364	369.091	2.727273	1.818182	6363.636
5	0.010	509.091	381.818	4.545455	1.818182	6363.636
6	0.012	521.818	394.545	6.363636	1.818182	6363.636
7	0.014	534.545	407.273	8.181818	1.818182	6363.636
8	0.016	547.273	420.000	10.000000	1.818182	6363.636
9	0.018	560.000	432.727	11.818182	1.818182	6363.636
10	0.020	572.727	445.455	13.636364	1.818182	6363.636

Table 4.3 summarizes the numerical results for the 10 increments.

(b) A graphical illustration of the stress distribution is given in Fig. 4.11. Due to the *linear* hardening behavior, the back projection for each increment occurs in one step.
Finally, it needs to be remarked at this point that for the special case of *linear* hardening at *uniaxial* stress states, the stress in the plastic area (inc ≥ 3) can directly be calculated via (see Fig. 2.1b)

$$\begin{aligned}\sigma(\varepsilon) &= k_{\mathrm{t}}^{\mathrm{init}} + E^{\mathrm{elpl}} \times (\varepsilon - \varepsilon_{\mathrm{t}}^{\mathrm{init}}) \\ &= E\varepsilon_{\mathrm{t}}^{\mathrm{init}} + E^{\mathrm{elpl}}\varepsilon - E^{\mathrm{elpl}}\varepsilon_{\mathrm{t}}^{\mathrm{init}} \\ \sigma(\varepsilon) &= (E - E^{\mathrm{elpl}}) \times \varepsilon_{\mathrm{t}}^{\mathrm{init}} + E^{\mathrm{elpl}} \times \varepsilon. \end{aligned} \tag{4.86}$$

The intention of this example however is to illustrate the concept of the back projection and not to define the stress according to the simplest method.

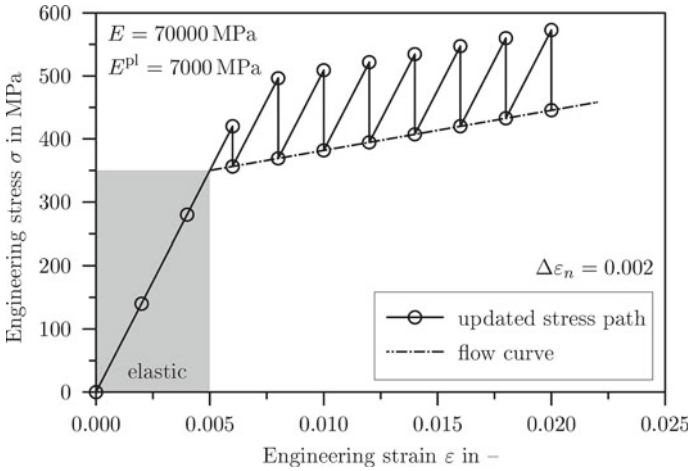

Fig. 4.11 Stress distribution in the case of the back projection for a continuum bar with linear hardening (10 increments, $\Delta\varepsilon = 0.002$)

Fig. 4.12 Sample problem back projection in the case of linear hardening: **a** displacement boundary condition; **b** force boundary condition

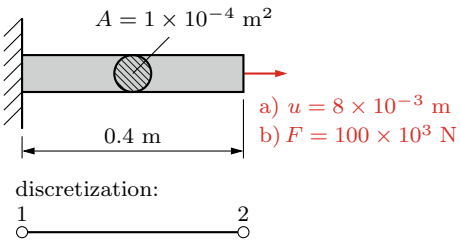

4.2 Back Projection at Linear Hardening—Discretization via One Finite Element, Displacement and Force Boundary Condition

The continuum bar from Example 4.1 can be discretized within the frame of this example via one single finite element, see Fig. 4.12. The material behavior can be defined as shown in Fig. 4.9a. The load on the right-hand end of the bar can be applied in 10 equal increments, whereupon

(a) $u = 8\,\text{mm}$,
(b) $F = 100\,\text{kN}$

can be applied. Calculate the stress state in each increment with the help of the CPP algorithm and mark all values, which have to be updated. As convergence criteria an absolute displacement difference of 1×10^{-5} mm can be assigned.

Solution 4.2

When using solely one element, the global system of equations results in the following—without the consideration of the boundary conditions:

$$\frac{A\tilde{E}}{L}\begin{bmatrix} 1 & -1 \\ -1 & 1 \end{bmatrix}\begin{bmatrix} \Delta u_1 \\ \Delta u_2 \end{bmatrix} = \begin{bmatrix} \Delta F_1 \\ \Delta F_2 \end{bmatrix}. \tag{4.87}$$

Table 4.4 Numerical values of the displacement and strain for displacement boundary condition (10 increments, $\Delta\varepsilon = 0.002$)

Inc	Δu_2	$\Delta\varepsilon$	u_2	ε
–	10^{-4} m	–	10^{-4} m	–
1	8.0	0.002	8.0	0.002
2	8.0	0.002	16.0	0.004
3	8.0	0.002	24.0	0.006
4	8.0	0.002	32.0	0.008
5	8.0	0.002	40.0	0.010
6	8.0	0.002	48.0	0.012
7	8.0	0.002	56.0	0.014
8	8.0	0.002	64.0	0.016
9	8.0	0.002	72.0	0.018
10	8.0	0.002	80.0	0.020

Since in general this is a nonlinear system of equations, an incremental form has been assigned. The modulus $\tilde{E}$ equals the elasticity modulus E in the elastic range and the elasto-plastic material modulus E^{elpl} in the plastic range. Since a fixed support is given on the left-hand node ($\Delta u_1 = 0$), Eq. (4.87) can be simplified to

$$\frac{A\tilde{E}}{L} \times \Delta u_2 = \Delta F_2. \tag{4.88}$$

Case (a) Displacement boundary condition $u = 8$ mm on the right-hand node:
In the case of the displacement boundary condition Eq. (4.88) must not be solved, since for each increment $\Delta u_2 = 8\,\text{mm}/10 = 0.8$ mm is known. Via the equation for the strain in the element, meaning $\varepsilon = \frac{1}{L}(u_2 - u_1)$, the strain increment results in the following in the case of the fixed support on the left-hand node:

$$\Delta\varepsilon = \frac{1}{L} \times \Delta u_2 = \frac{0.8\,\text{mm}}{400\,\text{mm}} = 0.002. \tag{4.89}$$

The entire displacement or alternatively strain can be calculated through the summation of the incremental displacement or alternatively strain values, see Table 4.4. It can be remarked at this point that for this case of displacement boundary condition at one element, the calculation of the displacement or alternatively the strain for all increments can be done without a stress calculation.

To calculate the stress and plastic strain in each increment, the calculation via the CPP algorithm for each increment has to be conducted via the strain increment $\Delta\varepsilon$ from Table 4.4. This is exactly what is calculated in Example 4.1 and the numerical results can be taken from Table 4.3.
Case (b) Force boundary condition $F = 100$ kN on the right-hand node:
In the case of the force boundary condition, Eq. (4.88) can be solved via the Newton-Raphson method. To do so, this equation has to be written in the form of a residual r as

$$r = \frac{A\tilde{E}}{L} \times \Delta u_2 - \Delta F_2 = \tilde{E}(u_2) \times \frac{A}{L} \times \Delta u_2 - \Delta F_2 = 0. \tag{4.90}$$

If one develops the last equation into a Taylor's series and neglects the terms of higher order, the following form results

$$r(\Delta u_2^{(i+1)}) = r(\Delta u_2^{(i)}) + \left(\frac{\partial r}{\partial \Delta u_2}\right)^{(i)} \times \delta(\Delta u_2) + \cdots, \tag{4.91}$$

whereupon

$$\delta(\Delta u_2) = \Delta u_2^{(i+1)} - \Delta u_2^{(i)} \tag{4.92}$$

is valid and

$$\left(\frac{\partial r}{\partial \Delta u_2}\right)^{(i)} = K_{\mathrm{T}}^{(i)} \tag{4.93}$$

represents the tangent stiffness matrix[13] in the i-th iteration step. Then Eq. (4.91) can also be written as

$$\delta(\Delta u_2) K_{\mathrm{T}}^{(i)} = -r\left(\Delta u_2^{(i)}\right) = \Delta F^{(i)} - \frac{\tilde{E}A}{L} \Delta u_2^{(i)}. \tag{4.94}$$

Multiplication via $(K_{\mathrm{T}}^{(i)})^{-1}$ and the use of Eq. (4.92) finally leads to

$$\Delta u_2^{(i+1)} = \Delta F^{(i)} \times \frac{L}{\tilde{E}A}, \tag{4.95}$$

whereupon $\tilde{E} = E$ is valid in the elastic range (increment 1–3) and $\tilde{E} = E^{\mathrm{elpl}}$ in the plastic range (increment 4–10).

Application of Eq. (4.95) leads to a value of $\Delta u_2 = 0.571429$ mm in the elastic range (increment 1–3) and in the plastic range (increment 4–10) a displacement increment of $\Delta u_2 = 6.285715$ mm occurs. It can be remarked at this point that the calculation of the displacement increments (increments 1–3 and 4–10) does not need an iteration and the application of Eq. (4.95) directly yields the desired result. As soon as the displacement increments (Δu_2) are calculated, the entire displacement on node 2 results via summation of the incremental values. Subsequently the strain in the element can be calculated via the relation $\varepsilon = \frac{1}{L}(u_2 - u_1)$, and the strain increments result through subtraction of two consecutive strain values (see Table 4.5).

[13] In the considered example with linear hardening, $\tilde{E}$ is constant in the elastic range (increment 1–3) and in the plastic range (increment 4–10) and therefore not a function of u_2. In the general case however $\tilde{E}$ has to be differentiated as well.

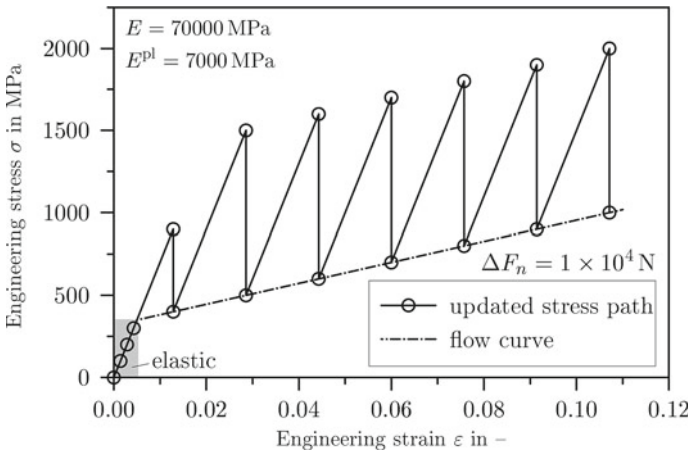

Fig. 4.13 Stress distribution in the case of the back projection for a continuum bar with linear hardening (10 increments, $\Delta F = 1 \times 10^4$)

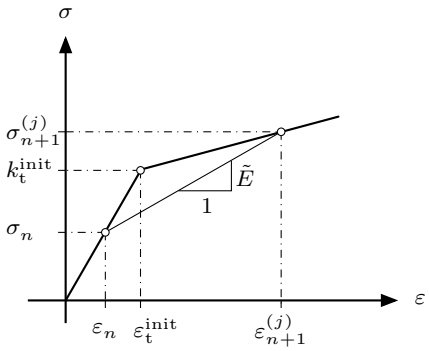

Fig. 4.14 Definition of the intermediate modulus $\tilde{E}$ in the case of the transition from the elastic to the plastic range

The calculation of the stress and the plastic strain now requires that the CPP algorithm is used in each increment, based on the strain increment $\Delta\varepsilon$. The graphical illustration of the back projection is given in Fig. 4.13. One can see clearly that the strain increments at a force boundary condition differ in the elastic and plastic range. As a consequence, quite high values result for the test stress state in the plastic range. Thus for the increments 5–10 $\sigma_{n+1}^{\text{trial}} = \sigma_{n+1} + 1000$ MPa is valid (Fig. 4.13).

Particular attention is required at the transition from the elastic to the plastic regime, meaning from increment 3–4. Here the modulus $\tilde{E}$ is not defined clearly and Eq. (4.95) has to be solved iteratively. For the first cycle of the calculation (cycle $j = 0$) the arithmetic mean between the modulus of elasticity E and the elasto-plastic material modulus E^{elpl} can be applied. For the further cycles (cycle $j \geq 1$) $\tilde{E}$ can be approximated via an intermediate modulus (secant modulus, see Fig. 4.14). Therefore the following relation results as a calculation requirement for the intermediate modulus $\tilde{E}$ in the elasto-plastic transition regime (at this point in the considered example at the transition from increment 3–4):

Table 4.5 Numerical values for one element in the case of linear hardening (10 increments; $\Delta F = 1 \times 10^4$ N)

Inc	Ex. force	Δu_2	u_2	ε	$\Delta\varepsilon$	σ	$\varepsilon^{\mathrm{pl}}$
–	10^4 N	mm	mm	10^{-2}	10^{-2}	MPa	10^{-2}
1	1.0	0.5714	0.5714	0.1429	0.1429	100.0	0.0
2	2.0	0.5714	1.1427	0.2857	0.1429	200.0	0.0
3	3.0	0.5714	1.7143	0.4286	0.1429	300.0	0.0
4	4.0	3.4286	5.1429	1.2857	0.8571	400.0	0.7143
5	5.0	6.2857	11.4286	2.8571	1.5714	500.0	2.1429
6	6.0	6.2857	17.7143	4.4286	1.5714	600.0	3.5714
7	7.0	6.2857	24.0000	6.0000	1.5714	700.0	5.0000
8	8.0	6.2857	30.2857	7.5714	1.5714	800.0	6.4286
9	9.0	6.2857	36.5714	9.1429	1.5714	900.0	7.8571
10	10.0	6.2857	42.8571	10.7143	1.5714	1000.0	9.2857

$$\tilde{E} = \begin{cases} \frac{E+E^{\mathrm{elpl}}}{2} & \text{for } j = 0 \\ \frac{\sigma_{n+1}^{(j)} - \sigma_n}{\varepsilon_{n+1}^{(j)} - \varepsilon_n} & \text{for } j > 0 \end{cases} . \tag{4.96}$$

The numerical values of the intermediate modulus $\tilde{E}$ at the transition from increment 3–4 and the differences of the displacement, which result herefrom on node 2 are summarized in Table 4.6. Since an absolute displacement difference of 1×10^{-5} mm was required as convergence criteria, 18 cycles are necessary to iterate the difference between the new and the old displacement on node 2 under these values. It can be considered at this point that the difference between the displacements on node 2 in the first cycle (cycle 0) result in $u_2^{\mathrm{new}} - u_2^{\mathrm{old}} = u_2^{(j=0)} - u_2|_{\mathrm{inc3}}$ and for the following cycles of the iteration via $u_2^{(j+1)} - u_2^{(j)}$ (Table 4.6).

The convergence behavior of the iteration rule is illustrated graphically in Fig. 4.15. An equidistant division was chosen in Fig. 4.15a and a logarithmic division (to be base 10) in Fig. 4.15b. One can see that quite a high convergence rate occurs at the beginning of the iteration, which flattens throughout the different cycles. At the chosen convergence criteria here of 10^{-5} the 18 iteration steps are therefore necessary, to finally reach the required absolute displacement difference. If one would require an absolute difference of 10^{-6} as convergence criteria, 21 iteration steps would be necessary.

4.3 Back Projection for a Bimaterial Bar

Two different material behaviors (see Fig. 4.16a) can be considered in the following to model a bimaterial bar (see Fig. 4.16b) via the FE method. The right-hand end is displaced by $u = 8$ mm hereby, whereupon the deformation is applied in 10 equal increments. The bar can be discretized with two finite elements hereby. Examine the following material combinations:

(a) Material I: pure elastic; Material II: pure elastic,

Table 4.6 Numerical values for the transition from increment 3–4

Cycle	$\tilde{E}^{(i)}$	$u_2^{\text{new}} - u_2^{\text{old}}$
–	MPa	mm
0	38,181.84	1.048×10^{-0}
1	23,719.00	6.388×10^{-1}
2	17,145.00	6.466×10^{-1}
3	14,157.16	4.925×10^{-1}
4	12,798.56	2.999×10^{-1}
5	12,181.16	1.584×10^{-1}
6	11,900.52	7.744×10^{-2}
7	11,772.96	3.642×10^{-2}
8	11,715.00	1.682×10^{-2}
9	11,688.64	7.699×10^{-3}
10	11,676.64	3.511×10^{-3}
11	11,671.20	1.598×10^{-3}
12	11,668.72	7.270×10^{-4}
13	11,667.60	3.305×10^{-4}
14	11,667.08	1.503×10^{-4}
15	11,666.88	6.831×10^{-5}
16	11,666.76	3.105×10^{-5}
17	11,666.72	1.411×10^{-5}
18	11,666.68	6.416×10^{-6}

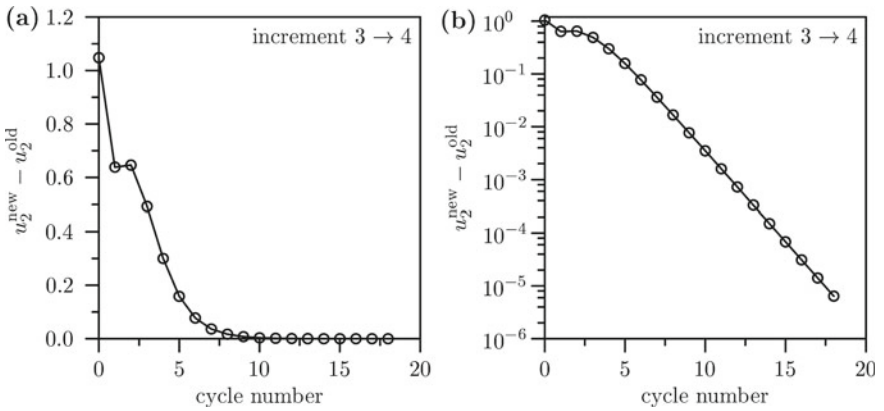

Fig. 4.15 Convergence behavior in the case of the transition from increment 3–4: **a** equidistant division; **b** logarithmic division of the absolute displacement difference

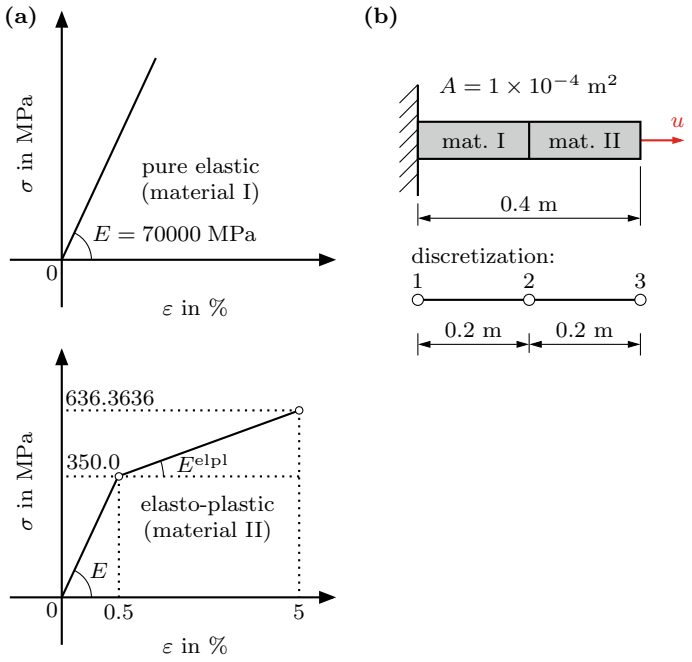

Fig. 4.16 Sample problem back projection in the case of a bar with different materials: **a** stress-strain distributions, **b** geometry, boundary conditions, and discretization

(b) Material I: elasto-plastic; Material II: elasto-plastic,
(c) Material I: pure elastic; Material II: elasto-plastic,

to calculate the displacement of the middle node. Furthermore, calculate the stress state in each element with the help of the CPP algorithm and mark all values, which have to be updated.

Solution 4.3
When using two finite elements, the global system of equations, without consideration of the boundary conditions, results in the following incremental form for this example:

$$\frac{A}{L} \times \begin{bmatrix} \tilde{E}^{\mathrm{I}} & -\tilde{E}^{\mathrm{I}} & 0 \\ -\tilde{E}^{\mathrm{I}} & \tilde{E}^{\mathrm{I}} + \tilde{E}^{\mathrm{II}} & -\tilde{E}^{\mathrm{II}} \\ 0 & -\tilde{E}^{\mathrm{II}} & \tilde{E}^{\mathrm{II}} \end{bmatrix} \begin{bmatrix} \Delta u_1 \\ \Delta u_2 \\ \Delta u_3 \end{bmatrix} = \begin{bmatrix} \Delta F_1 \\ \Delta F_2 \\ \Delta F_3 \end{bmatrix}. \tag{4.97}$$

The consideration of the boundary condition on the left-hand side, meaning $u_1 = 0$, yields the following reduced global system of equations:

$$\frac{A}{L} \times \begin{bmatrix} \tilde{E}^{\mathrm{I}} + \tilde{E}^{\mathrm{II}} & -\tilde{E}^{\mathrm{II}} \\ -\tilde{E}^{\mathrm{II}} & \tilde{E}^{\mathrm{II}} \end{bmatrix} \begin{bmatrix} \Delta u_2 \\ \Delta u_3 \end{bmatrix} = \begin{bmatrix} \Delta F_2 \\ \Delta F_3 \end{bmatrix}. \tag{4.98}$$

The consideration of the displacement boundary condition on the right-hand side, meaning $u_3 = u(t)$, and that $\Delta F_2 = \Delta F_3 = 0$ is valid, yields:

$$\frac{A}{L} \times (\tilde{E}^{\mathrm{I}} + \tilde{E}^{\mathrm{II}}) \Delta u_2 = \frac{\tilde{E}_2 A}{L} \Delta u_3, \tag{4.99}$$

or

$$\left(\frac{\tilde{E}^{\mathrm{I}}}{\tilde{E}^{\mathrm{II}}} + 1 \right) \Delta u_2 = \Delta u_3. \tag{4.100}$$

For the application of the Newton-Raphson method, Eq. (4.100) is written as a residual equation:

$$r = \left(\frac{\tilde{E}^{\mathrm{I}}}{\tilde{E}^{\mathrm{II}}} + 1 \right) \Delta u_2 - \Delta u_3 = 0. \tag{4.101}$$

If one develops the last equation into a Taylor's series and neglects the terms of higher order according to the procedure in Example 4.2, finally the following iteration rule results for the definition of the displacement of the middle node:

$$\Delta u_2^{(i+1)} = \left(\frac{\tilde{E}^{\mathrm{I}}}{\tilde{E}^{\mathrm{II}}} + 1 \right)^{-1} \times \Delta u_3^{(i)}. \tag{4.102}$$

In Eq. (4.102) in the elastic regime the elasticity modulus E has to be used for $\tilde{E}$ and in the plastic regime the elasto-plastic material modulus E^{elpl}.

Case (a) Material I: pure elastic; Material II: pure elastic:

For the case that both sections exhibit pure elastic material behavior with $E^{\mathrm{I}} = E^{\mathrm{II}}$, Eq. (4.102) simplifies in:

$$\Delta u_2^{(i+1)} = (1+1)^{-1} \times \Delta u_3^{(i)} = \frac{1}{2} \times \Delta u_3^{(i)} = 4\,\mathrm{mm}. \tag{4.103}$$

The strain in the left-hand element—which is identical with the strain in the right-hand element—can easily be defined via $\Delta\varepsilon = \frac{1}{200\,\mathrm{mm}} \times \Delta u_2$, and the stress results from the strain through multiplication with the modulus of elasticity. The results of this pure elastic calculation are summarized in Table 4.7.

In addition to the displacement, strain and stress values[14] Table 4.7 also contains the reaction forces on node 3. These reaction forces result due to multiplication of the stiffness matrix with the resultant vector of the displacements and have to be in equilibrium with the resulting forces from the stress: $F_{\mathrm{r},3} = \sigma A$.

Case (b) Material I: elasto-plastic; Material II: elasto-plastic:

For the case that both sections exhibit the same elasto-plastic material behavior, $\tilde{E}^{\mathrm{I}} = \tilde{E}^{\mathrm{II}}$ is always valid, and Eq. (4.102) also at this point yields a displacement

[14] One considers that in both sections or alternatively elements, the stress and strain are identical.

Table 4.7 Numerical values for a bimaterial bar in the case of pure linear-elastic behavior (10 increments; $\Delta u_3 = 0.8$ mm; $A = 100$ mm^2)

Inc	Δu_2	u_2	$\Delta\varepsilon$	ε	σ	$F_{\mathrm{r},3}$
–	mm	mm	–	–	MPa	10^4 N
1	0.4	0.4	0.002	0.002	140.0	1.4
2	0.4	0.8	0.002	0.004	280.0	2.8
3	0.4	1.2	0.002	0.006	420.0	4.2
4	0.4	1.6	0.002	0.008	560.0	5.6
5	0.4	2.0	0.002	0.010	700.0	7.0
6	0.4	2.4	0.002	0.012	840.0	8.4
7	0.4	2.8	0.002	0.014	980.0	9.8
8	0.4	3.2	0.002	0.016	1120.0	11.2
9	0.4	3.6	0.002	0.018	1260.0	12.6
10	0.4	4.0	0.002	0.020	1400.0	14.0

Table 4.8 Numerical values for a bimaterial bar in the case of elasto-plastic behavior (10 increments; $\Delta u_3 = 0.8$ mm; $A = 100$ mm^2)

Inc	Δu_2	u_2	$\Delta\varepsilon$	ε	σ	$\varepsilon^{\mathrm{pl}}$	$F_{\mathrm{r},3}$
–	mm	mm	–	–	MPa	10^{-3}	10^4 N
1	0.4	0.4	0.002	0.002	140.0	0.0	1.4
2	0.4	0.8	0.002	0.004	280.0	0.0	2.8
3	0.4	1.2	0.002	0.006	356.364	0.909091	3.56364
4	0.4	1.6	0.002	0.008	369.091	2.727273	3.69091
5	0.4	2.0	0.002	0.010	381.818	4.545455	3.81818
6	0.4	2.4	0.002	0.012	394.545	6.363636	3.94545
7	0.4	2.8	0.002	0.014	407.273	8.181818	4.07273
8	0.4	3.2	0.002	0.016	420.000	10.000000	4.20000
9	0.4	3.6	0.002	0.018	432.727	11.818182	4.32727
10	0.4	4.0	0.002	0.020	445.455	13.636364	4.45455

increment on the middle node from $\Delta u_2^{(i+1)} = \frac{1}{2} \times \Delta u_3^{(i)} = 4$ mm or alternatively a strain increment of $\Delta\varepsilon = 0.002$. For the calculation of the stress and the plastic strain for element II in the non-linear regime, the CPP algorithm has to be made use of, as in Example 4.1. The corresponding values are summarized in Table 4.8.

Table 4.9 Numerical values for a bimaterial bar in the case of different material behavior (10 increments; $\Delta u_3 = 0.8$ mm; $A = 100$ mm^2)

Inc	Δu_2	u_2	ε^{I}	$\varepsilon^{\mathrm{II}}$	σ^{I}	σ^{II}	$\varepsilon^{\mathrm{pl,I}}$	$\varepsilon^{\mathrm{pl,II}}$	$F_{\mathrm{r},3}$
–	mm	mm	10^{-3}	10^{-3}	MPa	MPa	10^{-3}	10^{-3}	10^4 N
1	0.4	0.4	2.0	2.0	140.0	140.0	0.0	0.0	1.4
2	0.4	0.8	4.0	4.0	280.0	280.0	0.0	0.0	2.8
3	0.23333	1.03333	5.16667	6.83333	361.667	361.667	0.0	1.66667	3.61667
4	0.06667	1.10000	5.50000	10.50000	385.000	385.000	0.0	5.00000	3.85000
5	0.06667	1.16667	5.83333	14.16667	408.333	408.333	0.0	8.33333	4.08333
6	0.06667	1.23333	6.16667	17.83333	431.667	431.667	0.0	11.66667	4.31667
7	0.06667	1.30000	6.50000	21.50000	455.000	455.000	0.0	15.00000	4.55000
8	0.06667	1.36667	6.83333	25.16667	478.333	478.333	0.0	18.33333	4.78333
9	0.06667	1.43333	7.16667	28.83333	501.667	501.667	0.0	21.66667	5.01667
10	0.06667	1.50000	7.50000	32.50000	525.000	525.000	0.0	25.00000	5.25000

Case (c) Material I: pure elastic; Material II: elasto-plastic:
At this point in the elastic regime of both elements also it occurs that the displacement at the middle node amounts to half of the displacement, which occurred on the right-hand node. As soon as the plastic material behavior occurs in the right-hand half of the bar, $\tilde{E}^{\mathrm{I}} \neq \tilde{E}^{\mathrm{II}}$ occurs and for the right-hand half of the bar, the elasto-plastic material modulus has to be made use of. Therefore, the calculation requirement for the displacement increment can be summarized as follows:

$$\Delta u_2^{(i+1)} = \begin{cases} \frac{1}{2} \times \Delta u_3^{(i)} & \text{in the elastic region} \\ \left(\frac{E^{\mathrm{I}}}{E^{\mathrm{elpl,II}}} + 1 \right)^{-1} \times \Delta u_3^{(i)} & \text{in the plastic region} \end{cases} . \tag{4.104}$$

The total displacement at the middle node results from the displacement increments through summation and the strain for each element can be defined via $\varepsilon = \frac{1}{L}(-u_{\mathrm{l}} + u_{\mathrm{r}})$ (index 'l' for left-hand and index 'r' for right-hand node of the bar element). As soon as the right-hand part of the bar enters the plastic region, the predictor-corrector method has to be made use of to be able to calculate the state variables. The numerical values of the incremental solution method are summarized in Table 4.9. At this point it can be remarked that in the plastic region a similar relation as in the elastic region can be set to calculate the stress increment from the strain increment (see Eq. (4.105)). However thereby it has to be considered that the modulus of elasticity has to be substituted by the elasto-plastic material modulus:

$$\Delta\sigma = \begin{cases} \Delta\varepsilon \times E & \text{in the elastic region} \\ \Delta\varepsilon \times E^{\mathrm{elpl}} & \text{in the plastic region} \end{cases} . \tag{4.105}$$

The transition from the elastic to the plastic region, meaning from increment 2–3, demands a special consideration at this point. The intermediate modulus $\tilde{E}^{\mathrm{II}}$ hereby has to be calculated according to Eq. (4.96), to be able to define the displacement

Table 4.10 Numerical values for transition from increment 2–3

Cycle	$\tilde{E}^{\mathrm{II},(i)}$	$\Delta u_2^{(i)}$	$u_2^{(i)}$	$\lvert u_2^{\mathrm{new}} - u_2^{\mathrm{old}} \rvert$	$\varepsilon^{\mathrm{II},(i)}$	$\Delta\varepsilon^{\mathrm{II},(i)}$	$\sigma^{\mathrm{II},(i)}$
–	MPa	mm	mm	10^{-2} mm	10^{-3}	10^{-3}	MPa
0	38181.82	0.282353	1.082353	28.235294	6.588235	2.588235	360.1070
1	30950.41	0.245272	1.045272	3.708073	6.773639	2.773639	361.2868
2	29306.91	0.236092	1.036092	0.918059	6.819542	2.819542	361.5789
3	28933.39	0.233962	1.033963	0.212904	6.830187	2.830187	361.6466
4	28848.50	0.233476	1.033476	0.0486115	6.832618	2.832618	61.6621
5	28829.20	0.233366	1.033366	0.0110598	6.833171	2.833171	361.6656
6	28824.82	0.233341	1.033341	0.0025142	6.833296	2.833296	361.6664
7	28823.82	0.233335	1.033335	0.0005714	6.833325	2.833325	361.6666

increment subsequently according to Eq. (4.104)$_2$. The absolute displacement on the middle node results from the summation, meaning $u_2^{(i)} = \Delta u_2^{(i)} + u_2|_{\mathrm{inc}2}$. The difference of the displacement on the middle node has to be determined in the first cycle (cycle 0) via $|u_2^{(i=0)} - u_2|_{\mathrm{inc}\,2}$ and for each further cycle (i) via $|u_2^{(i)} - u_2^{(i-1)}|$. The calculation of the strain in the right-hand half of the bar can occur via the given boundary condition u_3 via $\varepsilon^{\mathrm{II},(i)} = \frac{1}{L}(-u_2^{(i)} + u_3)$. Finally, the stress results via the CPP algorithm, based on the strain increment $\Delta\varepsilon^{\mathrm{II},(i)} = \varepsilon^{\mathrm{II},(i)} - \varepsilon^{\mathrm{II}}|_{\mathrm{inc}2}$. If the stress and strains are known, the new intermediate modulus can be determined for the next cycle via Eq. (4.96). As convergence criteria for the absolute displacement difference a value of 10^{-5} was given within this example (Table 4.10).

4.2 Approach for Three-Dimensinal Problems

4.2.1 Differentiation of the Yield Conditions

The first and if necessary the second derivative of the yield condition with respect to the stresses is required for return mapping algorithms. Is the yield condition expressed due to invariants, i.e. $F = F(J_1^{\circ}, J_2', J_3')$, considerable advantages arise from this formulation. Let us also mention that the stress matrix as given, for example, in Eq. (3.17) is rearranged in the context of the finite element method as a column matrix at which only the six independent components are stored:[15]

[15] The same holds for the corresponding hydrostatic and deviatoric parts as well as for the strain matrix.

$$\begin{bmatrix} \sigma_{xx} & \sigma_{xy} & \sigma_{xz} \\ \sigma_{xy} & \sigma_{yy} & \sigma_{yz} \\ \sigma_{xz} & \sigma_{yz} & \sigma_{zz} \end{bmatrix} \Rightarrow \begin{bmatrix} \sigma_x \\ \sigma_y \\ \sigma_x \\ \sigma_{xy} \\ \sigma_{yz} \\ \sigma_{zx} \end{bmatrix}. \tag{4.106}$$

The first derivative (gradient) of the yield surface with respect to the stress matrix is obtained due to the chain rule as:

$$\frac{\partial F}{\partial \boldsymbol{\sigma}} = \frac{\partial F}{\partial J_1^{\mathrm{o}}} \frac{\partial J_1^{\mathrm{o}}}{\partial \boldsymbol{\sigma}} + \frac{\partial F}{\partial J_2'} \frac{\partial J_2'}{\partial \boldsymbol{\sigma}} + \frac{\partial F}{\partial J_3'} \frac{\partial J_3'}{\partial \boldsymbol{\sigma}}. \tag{4.107}$$

Re-differentiation of Eq. (4.107) due to the product rule gives

$$\begin{aligned} \frac{\partial}{\partial \boldsymbol{\sigma}} \left(\frac{\partial F}{\partial \boldsymbol{\sigma}} \right) = \frac{\partial^2 F}{\partial \boldsymbol{\sigma} \partial \boldsymbol{\sigma}} &= \left[\frac{\partial^2 F}{\partial J_1^{\mathrm{o}} \partial \boldsymbol{\sigma}} \right] \frac{\partial J_1^{\mathrm{o}}}{\partial \boldsymbol{\sigma}} + \left[\frac{\partial^2 J_1^{\mathrm{o}}}{\partial \boldsymbol{\sigma} \partial \boldsymbol{\sigma}} \right] \frac{\partial F}{\partial J_1^{\mathrm{o}}} \\ &+ \left[\frac{\partial^2 F}{\partial J_2' \partial \boldsymbol{\sigma}} \right] \frac{\partial J_2'}{\partial \boldsymbol{\sigma}} + \left[\frac{\partial^2 J_2'}{\partial \boldsymbol{\sigma} \partial \boldsymbol{\sigma}} \right] \frac{\partial F}{\partial J_2'} \\ &+ \left[\frac{\partial^2 F}{\partial J_3' \partial \boldsymbol{\sigma}} \right] \frac{\partial J_3'}{\partial \boldsymbol{\sigma}} + \left[\frac{\partial^2 J_3'}{\partial \boldsymbol{\sigma} \partial \boldsymbol{\sigma}} \right] \frac{\partial F}{\partial J_3'} \\ &= \left[\frac{\partial^2 F}{\partial J_1^{\mathrm{o}} \partial J_1^{\mathrm{o}}} \frac{\partial J_1^{\mathrm{o}}}{\partial \boldsymbol{\sigma}} \right] \frac{\partial J_1^{\mathrm{o}}}{\partial \boldsymbol{\sigma}} + \left[\frac{\partial^2 J_1^{\mathrm{o}}}{\partial \boldsymbol{\sigma} \partial \boldsymbol{\sigma}} \right] \frac{\partial F}{\partial J_1^{\mathrm{o}}} \\ &+ \left[\frac{\partial^2 F}{\partial J_2' \partial J_2'} \frac{\partial J_2'}{\partial \boldsymbol{\sigma}} \right] \frac{\partial J_2'}{\partial \boldsymbol{\sigma}} + \left[\frac{\partial^2 J_2'}{\partial \boldsymbol{\sigma} \partial \boldsymbol{\sigma}} \right] \frac{\partial F}{\partial J_2'} \\ &+ \left[\frac{\partial^2 F}{\partial J_3' \partial J_3'} \frac{\partial J_3'}{\partial \boldsymbol{\sigma}} \right] \frac{\partial J_3'}{\partial \boldsymbol{\sigma}} + \left[\frac{\partial^2 J_3'}{\partial \boldsymbol{\sigma} \partial \boldsymbol{\sigma}} \right] \frac{\partial F}{\partial J_3'}, \end{aligned} \tag{4.108}$$

from which the second derivative of the yield criterion (Hesse matrix) can be obtained by application of the associative law as

$$\begin{aligned} \frac{\partial^2 F}{\partial \boldsymbol{\sigma} \partial \boldsymbol{\sigma}} &= \frac{\partial^2 F}{\partial J_1^{\mathrm{o}} \partial J_1^{\mathrm{o}}} \left[\frac{\partial J_1^{\mathrm{o}}}{\partial \boldsymbol{\sigma}} \left(\frac{\partial J_1^{\mathrm{o}}}{\partial \boldsymbol{\sigma}} \right)^{\mathrm{T}} \right] + \left[\frac{\partial^2 J_1^{\mathrm{o}}}{\partial \boldsymbol{\sigma} \partial \boldsymbol{\sigma}} \right] \frac{\partial F}{\partial J_1^{\mathrm{o}}} \\ &+ \frac{\partial^2 F}{\partial J_2' \partial J_2'} \left[\frac{\partial J_2'}{\partial \boldsymbol{\sigma}} \left(\frac{\partial J_2'}{\partial \boldsymbol{\sigma}} \right)^{\mathrm{T}} \right] + \left[\frac{\partial^2 J_2'}{\partial \boldsymbol{\sigma} \partial \boldsymbol{\sigma}} \right] \frac{\partial F}{\partial J_2'} \\ &+ \frac{\partial^2 F}{\partial J_3' \partial J_3'} \left[\frac{\partial J_3'}{\partial \boldsymbol{\sigma}} \left(\frac{\partial J_3'}{\partial \boldsymbol{\sigma}} \right)^{\mathrm{T}} \right] + \left[\frac{\partial^2 J_3'}{\partial \boldsymbol{\sigma} \partial \boldsymbol{\sigma}} \right] \frac{\partial F}{\partial J_3'}. \end{aligned} \tag{4.109}$$

The derivatives of the invariants with respect to the stresses are here independent of the yield criterion. Therefore, these functions need to implemented only once. If the yield criterion would be defined based on the stresses, each implementation of a new yield criterion would lead to a same high complexity for differentiation and programming. The first derivatives of the invariants with respect to the stress matrix result independently of the invariants as:

$$\frac{\partial J_1^{\mathrm{o}}}{\partial \boldsymbol{\sigma}} = \begin{Bmatrix} 1 \\ 1 \\ 1 \\ 0 \\ 0 \\ 0 \end{Bmatrix} = \mathbf{1}, \tag{4.110}$$

$$\frac{\partial J_2'}{\partial \boldsymbol{\sigma}} = \begin{Bmatrix} s_x \\ s_y \\ s_z \\ 2s_{xy} \\ 2s_{yz} \\ 2s_{zx} \end{Bmatrix} = \begin{Bmatrix} \frac{2}{3}\sigma_x - \frac{1}{3}(\sigma_y + \sigma_z) \\ \frac{2}{3}\sigma_y - \frac{1}{3}(\sigma_x + \sigma_z) \\ \frac{2}{3}\sigma_z - \frac{1}{3}(\sigma_x + \sigma_y) \\ 2\sigma_{xy} \\ 2\sigma_{yz} \\ 2\sigma_{zx} \end{Bmatrix} = \mathbf{L}\mathbf{s}, \tag{4.111}$$

$$\frac{\partial J_3'}{\partial \boldsymbol{\sigma}} = \begin{Bmatrix} s_y s_z - s_{yz}^2 \\ s_x s_z - s_{xz}^2 \\ s_x s_y - s_{xy}^2 \\ 2(s_{yz}s_{xz} - s_z s_{xy}) \\ 2(s_{xz}s_{xy} - s_x s_{yz}) \\ 2(s_{xy}s_{yz} - s_y s_{xz}) \end{Bmatrix} + \frac{1}{3} J_2' \begin{Bmatrix} 1 \\ 1 \\ 1 \\ 0 \\ 0 \\ 0 \end{Bmatrix}, \tag{4.112}$$

where the following diagonal scaling matrix was used: $\mathbf{L} = \lceil 1\ 1\ 1\ 2\ 2\ 2 \rfloor$.

Re-differentiation of Eqs. (4.110) till (4.112) gives finally the second-order derivative as:

$$\frac{\partial^2 J_1^{\mathrm{o}}}{\partial \boldsymbol{\sigma}\, \partial \boldsymbol{\sigma}} = \begin{bmatrix} 0 & 0 & 0 & 0 & 0 & 0 \\ 0 & 0 & 0 & 0 & 0 & 0 \\ 0 & 0 & 0 & 0 & 0 & 0 \\ 0 & 0 & 0 & 0 & 0 & 0 \\ 0 & 0 & 0 & 0 & 0 & 0 \\ 0 & 0 & 0 & 0 & 0 & 0 \end{bmatrix} = \mathbf{O}, \tag{4.113}$$

$$\frac{\partial^2 J_2'}{\partial \boldsymbol{\sigma}\, \partial \boldsymbol{\sigma}} = \frac{1}{3} \begin{bmatrix} 2 & -1 & -1 & 0 & 0 & 0 \\ -1 & 2 & -1 & 0 & 0 & 0 \\ -1 & -1 & 2 & 0 & 0 & 0 \\ 0 & 0 & 0 & 6 & 0 & 0 \\ 0 & 0 & 0 & 0 & 6 & 0 \\ 0 & 0 & 0 & 0 & 0 & 6 \end{bmatrix} = \mathbf{L}\left(\mathbf{I} - \frac{1}{3}\mathbf{1} \otimes \mathbf{1}\right), \tag{4.114}$$

Table 4.11 Derivatives of the yield conditions according to von Mises and Drucker-Prager with respect to the stress invariants

	Yield conditions according to	
	von Mises (3.48)	Drucker-Prager (3.67)
$\frac{\partial F}{\partial J_1^{\circ}}$	0	α
$\frac{\partial F}{\partial J_2'}$	$\frac{3}{2\sqrt{3}} \cdot (J_2')^{-\frac{1}{2}}$	$\frac{1}{2} \cdot (J_2')^{-\frac{1}{2}}$
$\frac{\partial^2 F}{\partial J_1^{\circ} \partial J_1^{\circ}}$	0	0
$\frac{\partial^2 F}{\partial J_2' \partial J_2'}$	$-\frac{\sqrt{3}}{4} \cdot (J_2')^{-\frac{3}{2}}$	$-\frac{1}{4} \cdot (J_2')^{-\frac{3}{2}}$

$$\frac{\partial^2 J_3'}{\partial \boldsymbol{\sigma} \partial \boldsymbol{\sigma}} = \frac{2}{3} \begin{bmatrix} s_x & s_z & s_y & s_{yx} & -2s_{zy} & s_{xz} \\ s_z & s_y & s_x & s_{yx} & s_{zy} & -2s_{xz} \\ s_y & s_x & s_z & -2s_{yx} & s_{zy} & s_{xz} \\ s_{yx} & s_{yx} & -2s_{yx} & -3s_z & 3s_{zx} & 3s_{yz} \\ -2s_{zy} & s_{zy} & s_{zy} & 3s_{zx} & -3s_x & 3s_{xy} \\ s_{xz} & -2s_{xz} & s_{xz} & 3s_{yz} & 3s_{xy} & -3s_y \end{bmatrix}. \tag{4.115}$$

Equation 4.114 contains the so-called dyadic product $\otimes$, which can be understood for two arbitrary column matrices as $\boldsymbol{a} \otimes \boldsymbol{b} = \boldsymbol{a}\boldsymbol{b}^{\mathrm{T}}$.

The derivatives of the yield conditions with respect to the invariants are in many cases quite simple, since they are based on the derivative of polynomials. The derivatives of the yield conditions according to von Mises and Drucker-Prager are summarised in Table 4.11.

4.2.2 Derivation of the Fully Implicit Backward Euler Algorithm for Isotropic Hardening

The derivation of the fully implicit backward Euler algorithm for isotropic hardening ($\boldsymbol{q} \rightarrow q$) follows the steps presented in Sect. 4.1.2 where based on the the previous

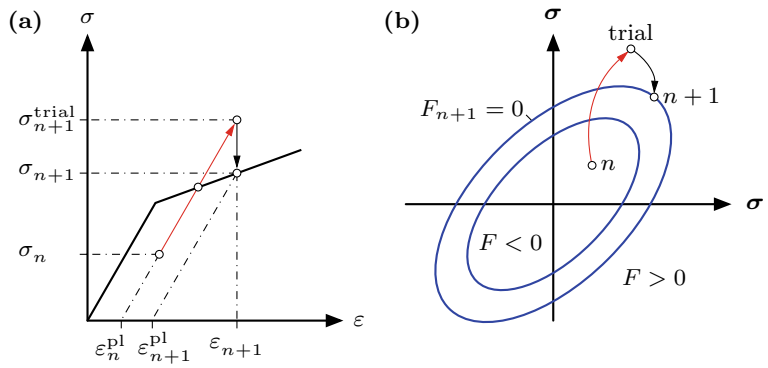

Fig. 4.17 Schematic representation of the integration algorithm: **a** uniaxial stress-strain diagram; **b** multidimensional stress space. The $\boldsymbol{\sigma}$-$\boldsymbol{\sigma}$ coordinate system represents the n-dimensional stress space

increment (n) the field variables must be calculated for the new state $(n+1)$ at each integration point.

Under the assumption of pure linear-elastic material behavior, an elastic predictor calculates the trial stress as:

$$\boldsymbol{\sigma}_{n+1}^{\text{trial}} = \boldsymbol{\sigma}_n + \underbrace{\boldsymbol{C}\Delta\boldsymbol{\varepsilon}_n}_{\text{predictor } \Delta\boldsymbol{\sigma}_n^{\text{el}}} . \tag{4.116}$$

The corresponding hardening state corresponds to the state of the previous increment since the load step is assumed to be pure elastic:

$$q_{n+1}^{\text{trial}} = q_n . \tag{4.117}$$

If the trial state is in the elastic range or on the yield surface ($F^{\text{trial}} \leq 0$), the real state at $n+1$ is equal to the calculated trial values of stress and hardening variables. However, if the stress state is outside the yield surface ($F^{\text{trial}} > 0$), the second part of the algorithm must calculate based on the plastic corrector $\boldsymbol{\sigma}_n^{\text{pl}}$ a valid state on the yield surface ($F_{n+1} = 0$), cf. Fig. 4.17.

The difference between the initial and target state (stress increment)

$$\Delta\boldsymbol{\sigma}_n = \boldsymbol{\sigma}_{n+1} - \boldsymbol{\sigma}_n \tag{4.118}$$

results according to Hooke's law from the elastic part of the strain increment which can be obtained as the difference between the total strain increment and the plastic part as:

$$\Delta\boldsymbol{\sigma}_n = \boldsymbol{C}\Delta\boldsymbol{\varepsilon}_n^{\text{el}} = \boldsymbol{C}\left(\Delta\boldsymbol{\varepsilon}_n - \Delta\boldsymbol{\varepsilon}_n^{\text{pl}}\right) . \tag{4.119}$$

The total strain increment $\Delta\boldsymbol{\varepsilon}_n$ can be expressed with the trial stress state according to Fig. 4.17 as:

$$\Delta\boldsymbol{\varepsilon}_n = \boldsymbol{\varepsilon}_{n+1} - \boldsymbol{\varepsilon}_n = \boldsymbol{C}^{-1}\left(\boldsymbol{\sigma}_{n+1}^{\text{trial}} - \boldsymbol{\sigma}_n\right) . \tag{4.120}$$

Introducing the last equation and the flow rule[16] in Eq. (4.119), the final state $\boldsymbol{\sigma}_{n+1}$ can be obtained in dependence of the trial stress state $\boldsymbol{\sigma}_{n+1}^{\text{trial}}$ as:

$$\boldsymbol{\sigma}_{n+1} = \boldsymbol{\sigma}_{n+1}^{\text{trial}} - \Delta\lambda_{n+1}\boldsymbol{C}\boldsymbol{r}(\boldsymbol{\sigma}). \tag{4.121}$$

Evaluating the function $\boldsymbol{r}(\boldsymbol{\sigma})$ during the iteration in the final state results in the implicit backward-Euler algorithm. Thus, the equations

$$\boldsymbol{\sigma}_{n+1} = \boldsymbol{\sigma}_{n+1}^{\text{trial}} - \Delta\lambda_{n+1}\boldsymbol{C}\boldsymbol{r}(\boldsymbol{\sigma}_{n+1}, q_{n+1}), \tag{4.122}$$

$$q_{n+1} = q_n + \Delta\lambda_{n+1}\boldsymbol{h}(\boldsymbol{\sigma}_{n+1}, q_{n+1}), \tag{4.123}$$

$$F = F(\boldsymbol{\sigma}_{n+1}, q_{n+1}), \tag{4.124}$$

are fulfilled in the final state $(n+1)$. However, a residual $\boldsymbol{r}$ remains for each of these equations outside the final state:

$$\begin{aligned} \boldsymbol{r}_{\boldsymbol{\sigma}}(\boldsymbol{\sigma}, q, \Delta\lambda) &= \boldsymbol{\sigma} - \boldsymbol{\sigma}_{n+1}^{\text{trial}} + \Delta\lambda\boldsymbol{C}\boldsymbol{r}(\boldsymbol{\sigma}, q) \neq \boldsymbol{0} \ \text{ or,} \\ &= \boldsymbol{C}^{-1}\boldsymbol{\sigma} - \boldsymbol{C}^{-1}\boldsymbol{\sigma}_{n+1}^{\text{trial}} + \Delta\lambda\boldsymbol{r}(\boldsymbol{\sigma}, q) \neq \boldsymbol{0}, \end{aligned} \tag{4.125}$$

$$\begin{aligned} r_q(\boldsymbol{\sigma}, q, \Delta\lambda) &= q - q_n - \Delta\lambda\boldsymbol{h}(\boldsymbol{\sigma}, q) \neq 0 \ \text{ or,} \\ &= -q + q_n + \Delta\lambda\boldsymbol{h}(\boldsymbol{\sigma}, q) \neq 0, \end{aligned} \tag{4.126}$$

$$r_F(\boldsymbol{\sigma}, q) = F(\boldsymbol{\sigma}, q) \neq 0. \tag{4.127}$$

Thus, the final stress and hardening state is the root of a matrix function $\boldsymbol{m}$ which is composed of the residual functions. Furthermore, it is useful to collect all variables in a single variable matrix $\boldsymbol{v}$:

$$\boldsymbol{m}(\boldsymbol{v}) \in \left(\mathbb{R}^8 \to \mathbb{R}^8\right) = \begin{bmatrix} \boldsymbol{r}_{\boldsymbol{\sigma}}(\boldsymbol{v}) \\ \boldsymbol{r}_q(\boldsymbol{v}) \\ r_F(\boldsymbol{v}) \end{bmatrix}, \quad \boldsymbol{v} = \begin{bmatrix} \boldsymbol{\sigma} \\ q \\ \Delta\lambda \end{bmatrix}. \tag{4.128}$$

The root is found by a Newton iteration (iteration index: i):

$$\boldsymbol{v}^{(i+1)} = \boldsymbol{v}^{(i)} - \left[\frac{\mathrm{d}\boldsymbol{m}}{\partial\boldsymbol{v}}\left(\boldsymbol{v}^{(i)}\right)\right]^{-1} \boldsymbol{m}\left(\boldsymbol{v}^{(i)}\right), \tag{4.129}$$

where

$$\boldsymbol{v}^{(0)} = \begin{bmatrix} \boldsymbol{\sigma}^{(0)} \\ q^{(0)} \\ \Delta\lambda^{(0)} \end{bmatrix} = \begin{bmatrix} \boldsymbol{\sigma}_{n+1}^{\text{trial}} \\ q_n \\ 0 \end{bmatrix}, \tag{4.130}$$

[16] At this point, we change again the notation from $\mathrm{d}\lambda$ to $\Delta\lambda$.

can be used as the initial value. The Jacobian matrix $\frac{\partial \boldsymbol{m}}{\partial \boldsymbol{v}}$ of the residual functions is obtained from the partial derivatives of Eqs. (4.125)–(4.127) as:

$$\frac{\partial \boldsymbol{m}}{\partial \boldsymbol{v}}(\boldsymbol{\sigma}, q, \Delta\lambda) = \begin{bmatrix} \frac{\partial r_{\boldsymbol{\sigma}}}{\partial \boldsymbol{\sigma}} & \frac{\partial r_{\boldsymbol{\sigma}}}{\partial q} & \frac{\partial r_{\boldsymbol{\sigma}}}{\partial \Delta\lambda} \\ \frac{\partial r_q}{\partial \boldsymbol{\sigma}} & \frac{\partial r_q}{\partial q} & \frac{\partial r_q}{\partial \Delta\lambda} \\ \frac{\partial r_F}{\partial \boldsymbol{\sigma}} & \frac{\partial r_F}{\partial q} & \frac{\partial r_F}{\partial \Delta\lambda} \end{bmatrix} (\boldsymbol{\sigma}, q, \Delta\lambda) \tag{4.131}$$

$$= \begin{bmatrix} \boldsymbol{C}^{-1} + \Delta\lambda \frac{\partial \boldsymbol{r}}{\partial \boldsymbol{\sigma}} & \Delta\lambda \frac{\partial \boldsymbol{r}}{\partial q} & \boldsymbol{r} \\ \Delta\lambda \frac{\partial \boldsymbol{h}}{\partial \boldsymbol{\sigma}} & -\mathbf{I} + \Delta\lambda \frac{\partial \boldsymbol{h}}{\partial q} & \boldsymbol{h} \\ \frac{\partial F}{\partial \boldsymbol{\sigma}} & \frac{\partial F}{\partial q} & 0 \end{bmatrix} (\boldsymbol{\sigma}, q, \Delta\lambda)\,. \tag{4.132}$$

In addition to the fulfillment of the plasticity Eqs. (4.122)–(4.124) in each integration point, the global equilibrium must be fulfilled. To be able to apply the Newton iteration for this task, it is required even for small strains in the general three-dimensional case to derive the appropriate elasto-plastic tangent modulus,[17] cf. [9]. The consistent elasto-plastic modulus results for the three-dimensional case as:

$$\boldsymbol{C}^{\text{elpl}}_{n+1} = \frac{\partial \boldsymbol{\sigma}_{n+1}}{\partial \boldsymbol{\varepsilon}_{n+1}} = \frac{\partial \Delta \boldsymbol{\sigma}_n}{\partial \boldsymbol{\varepsilon}_{n+1}}. \tag{4.133}$$

The inverse of the Jacobian matrix $\frac{\partial \boldsymbol{m}}{\partial \boldsymbol{v}}$ which has to be evaluated in the converged state of the above mentioned Newton iteration gives

$$\left[\left(\frac{\partial \boldsymbol{m}}{\partial \boldsymbol{v}}\right)_{n+1}\right]^{-1} = \begin{bmatrix} \tilde{\boldsymbol{m}}_{11} & \tilde{\boldsymbol{m}}_{12} & \tilde{\boldsymbol{m}}_{13} \\ \tilde{\boldsymbol{m}}_{21} & \tilde{\boldsymbol{m}}_{22} & \tilde{\boldsymbol{m}}_{23} \\ \tilde{\boldsymbol{m}}_{31} & \tilde{\boldsymbol{m}}_{32} & \tilde{\boldsymbol{m}}_{33} \end{bmatrix}_{n+1}, \tag{4.134}$$

from which the elasto-plastic tangent modulus results as [9]:

$$\boldsymbol{C}^{\text{elpl}}_{n+1} = \tilde{\boldsymbol{m}}_{11}. \tag{4.135}$$

Some basic simulations with implemented constitutive laws can be found, for example, in [25].

[17] Alternative notation is consistent tangent modulus or algorithmic modulus.

References

1. Owen DRJ, Hinton E (1980) Finite elements in plasticity: theory and practice. Pineridge Press Limited, Swansea
2. Crisfield MA (2001) Non-linear finite element analysis of solids and structures. Vol. 1: Essentials. Wiley, Chichester
3. Crisfield MA (2000) Non-linear finite element analysis of solids and structures. Vol. 2: Advanced topics. Wiley, Chichester
4. Simo JC, Hughes TJR (1998) Computational inelasticity. Springer, New York
5. Belytschko T, Liu WK, Moran B (2000) Nonlinear finite elements for continua and structures. Wiley, Chichester
6. Doltsinis I (2000) Elements of plasticity: theory and computation. WIT Press, Southampton
7. Reddy JN (2004) An introduction to nonlinear finite element analysis. Oxford University Press, Oxford
8. Dunne F, Petrinic N (2005) Introduction to computational plasticity. Oxford University Press, Oxford
9. Wriggers P (2008) Nonlinear finite element methods. Springer, Berlin
10. de Souza NEA, Perić D, Owen DRJ (2008) Computational methods for plasticity: theory and applications. Wiley, Chichester
11. Anandarajah A (2010) Computational methods in elasticity and plasticity: solids and porous media. Springer, New York
12. Borja RI (2013) Plasticity: modeling & computation. Springer, Berlin
13. Öchsner A, Merkel M (2013) One-dimensional finite elements: an introduction to the FE method. Springer, Berlin
14. Trapp M, Öchsner A (2018) Computational plasticity for finite elements: a Fortran-based introduction. Springer, Cham
15. Simo JC, Ortiz M (1985) A unified approach to finite deformation elastoplasticity based on the use of hyperelastic constitutive equations. Comput Method Appl Mech Eng 49:221–245
16. Ortiz M, Popov EP (1985) Accuracy and stability of integration algorithms for elastoplastic constitutive equations. Int J Num Meth Eng 21:1561–1576
17. Moran B, Ortiz M, Shih CF (1990) Formulation of implicit finite element methods for multiplicative finite deformation plasticity. Int J Num Meth Eng 29:483–514
18. Betten J (1979) Über die Konvexität von Fließkörpern isotroper und anisotroper Stoffe. Acta Mech 32:233–247
19. Lubliner J (1990) Plasticity theory. Macmillan Publishing Company, New York
20. Balankin AS, Bugrimov AL (1992) A fractal theory of polymer plasticity. Polym Sci 34:246–248
21. Spencer AJM (1992) Plasticity theory for fibre-reinforced composites. J Eng Math 26:107–118
22. Chen WF, Baladi GY (1985) Soil plasticity. Elsevier, Amsterdam
23. Chen WF, Liu XL (1990) Limit analysis in soil mechanics. Elsevier, Amsterdam
24. Chen WF (1982) Plasticity in reinforced concrete. McGraw-Hill, New York
25. Öchsner A (2003) Experimentelle und numerische untersuchung des elastoplastischen verhaltens zellularer Modellwerkstoffe. VDI-Verlag, Düsseldorf

Index

A. Öchsner, *Elements of Classical Plasticity Theory*,
https://doi.org/10.1007/978-3-031-14201-7